Institute for Space and Nuclear Power Studies

THE UNIVERSITY of NEW MEXICO

AN EFFECTIVE METHODOLOGY FOR THERMAL-HYDRAULICS ANALYSIS OF A VHTR CORE AND FUEL ELEMENTS

Boyce W. Travis and Mohamed S. El-Genk

Institute for Space and Nuclear Power Studies and Chemical and Nuclear Engineering Department
MSC01 1120, 1 University of New Mexico, Albuquerque, NM 87131-0001

Technical Report ISNPS-UNM-2-2012

Institute for Space and Nuclear Power Studies (ISNPS)

December 2012

Acknowledgements

This research is funded partially by Institute for Space and Nuclear Power Studies, the DOE NEUP contract No. 00044825 00002, Project No. 09-830 to the University of New Mexico and the U.S. NRC Graduate Fellowships grant number NRC-38-09-931.

ABSTRACT

The Very High Temperature Reactor (VHTR) is a Generation-IV design in the conceptual pre-licensing phase for potential construction by 2030-2050. It is graphite moderated, helium cooled reactor that operates at an exit temperature of up to 1273 K, making it ideal for generating electricity at a plant thermal efficiency upwards of 48% and the co-generation of process heat for hydrogen production and other industrial uses. Extensive thermal-hydraulics and safety analyses of VHTRs are being conducted using Computational Fluid Dynamics (CFD) and heat transfer codes, in conjunction with experiments and prototype demonstrations. These analyses are challenging, largely due to the 3-D simulation of the helium flow in the 10 m long coolant channels in the reactor core and the need to examine the effects of helium bypass flow in the interstitial gaps between the core fuel elements. This research, performed at the UNM-ISNPS, developed an effective thermal-hydraulics analyses methodology that markedly reduces the numerical meshing requirements and computational time. It couples the helium's 1-D convective flow and heat transfer in the channels to 3-D heat conduction in graphite and fuel compacts of VHTR fuel elements. Besides the helium local bulk temperature, the heat transfer coefficient is calculated using a Nusselt number correlation, developed and validated in this work. In addition to omitting the numerical meshing in the coolant channels, the simplified analysis methodology effectively decreases the total computation time by a factor of ~ 33 - 40 with little effect on the calculated temperatures (< 5 K), compared to a full 3-D thermal-hydraulics analysis.

The developed convective heat transfer correlation accounts for the effect of entrance mixing in the coolant channels, where $z/D < 25$. The correlation compares favorably, to

within $\pm$ 12%, with Taylor's (based on high temperature hydrogen heat transfer) and to within $\pm$ 2% of the calculated results for full 3-D analyses of a VHTR single channel module and multiple channels in the fuel elements. The simplified methodology is used to investigate the effects of helium bypass flow in interstitial gaps between fuel elements and of the helium bleed flow in control rod channels on calculated temperatures in the VHTR fuel elements. Thermal-hydraulics analysis of a one-element high and of a full height VHTR 1/6 core are also conducted. Results show that the interstitial bypass flow increases the temperatures near the center of the core fuel elements by 10-15 K, while reducing the temperatures along the edges of the elements by ~30 K. Without bypass flow, hotspots may occur at the location of burnable poison rods in the fuel elements, depending on the assumed volumetric heat generation rate in the rods. The helium bleed flow through the control rod channels reduces temperatures near them by 2-5 K, and only slightly increases the temperatures within the rest of the core fuel elements. In the VHTR 1/6 core thermal-hydraulics analysis, the helium bypass flow decreases the heat transfer from the core fuel elements to the adjacent radial graphite reflector blocks. Results demonstrate the effectiveness of the developed methodology and its potential use in future thermal-hydraulics design and in the safety analyses of VHTRs.

Table of Contents

List of Figures

List of Tables

Nomenclature

A	cross-section area of flow channel, m^2
C_p	specific heat, J/kg K
C	coolant channel
C_k	turbulence model constant (turbulence model Eq. (B.4))
C_μ	flow turbulence correction factor (turbulence model Eqs. (B.2-3))
D	coolant channel diameter, m
f	wall damping function (turbulence model (Eqs. (B.2-3))
F_i	wall distance function (turbulence model Eq. (B.7))
F	fuel region
FC	fuel compact
G	Graphite region
h	heat transfer coefficient, W/m^2 K
k	thermal conductivity, W/m K
k	turbulent kinetic energy transport variable (turbulence model Eqs. (B.1-7))
L	coolant channel total length, m
$\dot{m}$	mass flow rate, kg/s
n	Prandtl number exponent
Nu	Nusselt number, h D/k
P	Pressure, Pa
PD	fission power density, MW_{th}/m^3
PD^*	normalized power density, PD/PD_{max}
Pr	Prandtl number, $\mu C_p/k$

r	radial coordinate
Re	Reynolds number, $\dot{m}$ D/Aμ
R_g	helium gas constant, 2077 J/kg K
T	temperature, K
T_{ke}	kinetic energy transport variable, unit-less
T_{dr}	turbulent dissipation variable, unit-less
z	axial distance from heated channel entrance, m

Greek Symbols

ε	turbulent dissipation of kinetic energy (turbulence model Eqs. (B.1-3))
μ	dynamic viscosity, kg/m s
μ_t	eddy viscosity (turbulence model Eqs. (B.1-2, B.6-7))
φ	volume fraction (Eq. A.1)
φ	explicit wall turbulence factor (turbulence model Eqs. (1.2))
ρ	density, kg/m^3
σ_i	turbulence model constant (turbulence model Eqs. (B.1-2, B.4))
τ_{ij}	Reynolds stresses (turbulence model Eqs. (B.1-2))
Ω	vorticity (turbulence model Eq. (B.7)
ω	specific dissipation rate of turbulent kinetic energy (turbulence model Eq. (B.6-7))

Subscripts

b	bulk

FD	fully developed
Max	maximum
w	wall

Acronyms

BPR	Burnable Poison Rods
CBC	Closed Brayton Cycle
CFD	Computational Fluid Dynamics
GCR	Gas Cooled Reactor
HTGR	High Temperature Gas-cooled Reactor
HPC	high-pressure compressor
HPT	High Pressure Turbine
HTTR	High Temperature Test Reactor
IHX	Intermediate Heat Exchanger
INL	Idaho National Laboratory
ISNPS	Institute for Space and Nuclear Power Studies
LPC	low pressure compressor
LPT	Low-Pressure Turbine
LWR	Light Water Reactor
NGNP	Next Generation Nuclear Plant

PBMR	Pebble Bed Modular Reactor
PCS	Power Conversion System
SI	Sulfur-Iodine cycle
THTR	Thorium High Temperature Reactor
TRISO	TRistructural-ISOtropic
UNM	University of New Mexico
VHTR	Very High Temperature Reactor

Chapter 1 - Introduction

Throughout the world, demands for energy have escalated rapidly in recent years, and current projections indicate the need both to increase generation capacity and overhaul current energy infrastructures in order to keep pace with demand (MacDonald et al., 2004). Nuclear power plants present a potential solution to this issue. More specifically, the Generation-IV reactor designs currently being investigated could provide an economical and safe source of electricity and process heat for industrial uses as soon as 2030-2050 (Southworth, 2003). One promising Gen-IV design is the prismatic core, Very High Temperature Reactor (VHTR). This is a high temperature, gas cooled and graphite moderated reactor that combines the advantages of achieving high plant thermal efficiency and the co-generation of process heat for industrial applications due to its high operation temperatures (MacDonald et al., 2004). However, significant research and development remains to be done on the VHTR.

1.1 Historical perspective

The design and technologies underpinning the VHTR have a long history dating back almost six decades ago. Gas cooled reactors (GCRs) were first operated in the United Kingdom for the production of weapons-grade plutonium, but their design evolved into commercial generation by the 1960s (Beck et al., 2010). This early work on GCRs helped spur subsequent design and development of High Temperature Gas Cooled Reactors (HTGRs) in the UK, United States, Germany, Russia, Japan and China in the ensuing decades (Copinger and Moses, 2004; Zhang and Yu, 2002; Huang et al. 2004; Shiozawa et al. 2004; Kiryushin et al., 1997; IAEA, 2001). Particularly noteworthy HTGR designs include the Dragon reactor, the Peach Bottom reactor, and the Ft. St. Vrain reactor – each

used prismatic fuel element blocks and coated fuel particles dispersed in graphite (Beck et al., 2010; Copinger and Moses, 2004). Modern HTGRs are currently operating in Japan (the HTTR) and China (Shiozawa et al., 2004; Zhang et al., 2006). The HTTR provides valuable insights for future development of VHTRs, with its prismatic core design that operates at temperatures as high as 1223 K (950 °C) (Shiozawa et al., 2004). Such high temperatures, although they could increase plant thermal efficiencies to nearly 50%, can raise a host of material development issues and concerns. China's HTR-10 is a pebble-bed HTGR design used as a baseline for the development of commercial HTR-PM design currently being considered for construction and deployment (Zhang et al., 2006).

The developments of VHTRs are still in the pre-licensing design phase, and as such significant analyses need to be done to better understand its operational behavior and address critical safety concerns (MacDonald et al., 2003). One of the VHTR designs considered by the US is based on the GT-MHR from General Atomics (Kiryushin et al., 1997). A prototype demonstration plant for the next generation Nuclear Power Plant (NGNP) has been planned for construction at Idaho National Laboratory (Idaho National Laboratory, 2011). Such activities are currently on hold, and the focus of the NGNP project has been changed to address critical materials, operation and safety research.

An important component of these efforts on VHTR design is acquiring an extensive understanding of the reactor thermal-hydraulics behavior. Thermal-hydraulics analyses invariably involve computer simulation using Computational Fluid Dynamics (CFD) codes in conjunction with more simple system codes designed to optimize specific aspects of the reactor design and operation (such as the effect of pressure or bleed cooling

of the reactor vessel on reactor plant performance (MacDonald et al., 2004). CFD codes are very powerful tools to faithfully conduct thermal-hydraulics analyses of the entire VHTR core, a task that is desirable before advancing to the expensive step of building a test reactor prototype. Due to the large size of the VHTR core, which is approx. 8 meters in diameter and 10 m in height (neglecting the upper and lower plenums), even scaled down experiments to capture all of the thermal-hydraulics phenomena present would be very extensive, and therefore expensive. Some work has been done with scaled down experiments to understand flow behavior, such as the interstitial bypass gaps between hexagonal fuel elements in the VHTR core (Schultz et al., 2012). Although CFD models are not a direct substitute for large scale experimental work, they could provide valuable insight to help design and instrument planned experiments or prototypes. The inherent challenge with CFD use is the intense computation requirements (both in terms of hardware and time) to accurately model the heat transfer and flow turbulence within a VHTR core.

In prior work, CFD simulations of large sections of the VHTR (on the order of 1/6 or 1/12 of the core) have required supercomputer clusters that are very expensive (Pointer and Thomas, 2010; Sato et al., 2010; MacDonald et al., 2004). Pointer and Thomas (2010) indicated that while the use of CFD was viable to complete thermal-hydraulics analyses of the VHTR, developing a method of simplifying the numerical meshing approach to expedite simulations was desirable. Tak et al. (2008, 2010) presented a possible means of simplifying the thermal-hydraulics analysis of a VHTR via the use of a simplified 1-D method together with a Nusselt number correlation instead of explicitly simulating the helium flow in the reactor coolant channels. Aside from that, very few

efforts have been made to simplify the thermal hydraulics analysis of VHTRs. There is a need to develop and demonstrate the effectiveness of simplified methods of analyzing the thermal-hydraulics behavior of the VHTR core. Due to the complexity and size of the VHTR, these simplifying methods for the thermal-hydraulics modeling would reduce the computational requirements and running time of the analyses.

1.2 Objectives

The objectives of this research, performed at the University of New Mexico's (UNM) Institute for Space and Nuclear Power Studies (ISNPS), are to:

(a) Develop a simplified methodology for thermal-hydraulics analyses of a VHTR core and fuel elements as a surrogate to full 3-D analyses. This methodology entails thermally coupling a 1-D helium flow in the coolant channels to a 3-D thermal conduction in the graphite and fuel compacts. The desired outcome is to reduce the computation time and the numerical meshing requirements. Formulating the simplified analysis methodology required the development of an appropriate convective heat transfer correlation in the coolant channels.

(b) Develop and validate a convective heat transfer correlation based on a full 3-D thermal-hydraulics analysis of a VHTR single channel module and compare the correlation with others reported by other investigators based on experimental data for high-temperature gas flow in heated pipes;

(c) Demonstrate the effectiveness of the simplified analysis methodology for performing thermal-hydraulics analyses of a VHTR single channel module, single fuel element, and 1/6 full core;

(d) Investigate the effects of helium bypass flow in interstitial gaps between fuel elements and of helium bleed flow in the control rod channels on the calculated temperatures in a VHTR core; and

(e) Investigate the effect of varying the volumetric heat generation rate in the burnable poison rods in a fuel element, both with and without helium bypass and bleed flow, on the temperature distribution within the VHTR core.

Chapter 2 presents a background and history of gas cooled reactors, HTGRs, and VHTRs and their main operating and design parameters. This chapter also presents a review of existing literature on the VHTR analyzed in this work, including materials, the designs of the fuel compacts and fuel elements, and a review of prior work modeling the thermal-hydraulics of the VHTR.

Chapter 3 details the numerical meshing and procedures used in the performed thermal-hydraulic analyses of a VHTR single channel module, fuel element and 1/6 core. The software packages employed in this research and the motivations behind their usage are discussed in depth, including the numerical meshing and modeling approaches. The physical hardware used is also described.

Chapter 4 describes the turbulent convection heat transfer correlation developed for use in conjunction with 1-D helium flow in the coolant channels and 3-D conduction in the graphite and fuel compacts, as a surrogate for a full 3-D thermal-hydraulics analysis of the VHTR core and fuel elements.

Chapter 5 provides the results confirming the effectiveness of using the 1-D simplified methodology by comparing it to the results of a full 3-D CFD simulation of a

single fuel element. The results of the thermal-hydraulics analyses for a VHTR 1/6 core section using the developed simplified analysis methodology are also presented. In addition, results displaying the effects of helium interstitial bypass flow, bleed flow in the control rod channels, and the effect of varying the volumetric heat generation rate within the burnable poison rods in a single fuel element and a one fuel element tall, 1/6 core are investigated in this chapter.

Chapter 6 summarizes the results presented in the previous two chapters and draws conclusions on their impact in simplifying the thermal-hydraulics analysis of the VHTR, while Chapter 7 proposes potential directions for future work as extension to this research. The appendices at the end of this document provide supplemental information. Appendix A presents details on the material properties used in the performed analysis. Appendix B reviews the fluid modeling techniques used by others using CFD codes. In particular, it compares the accuracy and effect of the choice of turbulence model on the results of the thermal-hydraulics analysis of the VHTR.

Chapter 2 - Background

Gas cooled reactors have been operated and studied for more than half a century. Ongoing worldwide developments of gas cooled reactors that operate at high temperatures (800-1200 K) continue to capitalize on the advantages of achieving a high plant thermal efficiency (from operating at these high temperatures) and the potential production of process heat for industrial uses (MacDonald et al., 2003; 2004). In the United States, recent work on Generation-IV reactors has focused on the Very High Temperature Reactor (VHTR), investigated in this thesis and described in this chapter. This chapter also provides background information on earlier gas cooled reactors, outlines some of the challenges to thermal-hydraulics modeling of this reactor, and reviews the work done to overcome some of these challenges.

2.1. History of gas cooled reactors

Commercial use of gas cooled reactors (GCRs) dates back nearly as far as the initial development of light water reactors (LWRs), more than five decades ago. Work on gas cooled reactors began in the 1950s in the United Kingdom. A series of 40 (26 Magnox and 14 "advanced GCRs") were constructed to provide electrical power over the following two decades. The original Magnox facility at Calder Hall in the UK, originally designed for the production of weapons-grade plutonium, generated a substantial amount of electrical power. Each of the four reactor units generated 50-60 MW_e (Beck et al., 2010).

Magnox reactors were carbon dioxide cooled, graphite moderated, and used natural uranium fuel elements clad in magnox alloy (hence the name of the reactor) (Murphy,

2004). The UK's second generation gas cooled reactors came online in the 1970s. These reactors were also graphite moderated and carbon dioxide cooled, but operated at high temperatures. Thus they could not use the magnox alloy as a clad, and instead opted for stainless steel. This required using UO_2 fuel, with ~ 2.7 to 3.4 percent enrichment (Murphy, 2004).

Graphite has been the moderator of choice in gas cooled reactors for a number of reasons. It has favorable thermal properties (a high heat capacity and relatively high thermal conductivity) when compared with other solid moderators. It also stores a large fraction of the decay heat after reactor shutdown, and is relatively inexpensive and non-toxic when compared with other solid moderators like Beryllium and Beryllium oxide. Graphite has a very high ignition temperature, which enhances reactor safety and permits operation at very high reactor exit temperatures (800-1250 K), allowing plants to achieve a thermal efficiency upwards of 40%, compared to the 30-35% achieved in most LWR plants. Operation at high temperatures also alleviates the Wigner effect for graphite.

The Wigner effect occurs due to the displacement of atoms from the lattice by neutron irradiation (Minshall and Wickham, 2001). Neutron collisions with carbon atoms within the graphite's lattice structure move them into interstitial spaces within the lattice, which is then in an unstable configuration. Atoms in these unstable positions have significant amounts of stored energy that can be released suddenly when attempting to re-align and thus cause a rapid increase in temperature. This effect is mitigated in higher temperature regimes because of the self-annealing that takes place during reactor operation. In the early low temperature (400-600 K) Magnox reactors, the Wigner effect

was a major safety issue resulting in graphite fires in some cases, such as at the Windscale facility (Minshall and Wickham, 2001).

2.1.1 Development of high temperature gas cooled reactors

The development of the early designs of High-Temperature Gas Reactors (HTGRs) were driven by an interest in increasing the reactor exit temperature in addition to capitalizing on the attractive safety features of these reactors. However, material issues arose because of the temperature limitations on the fuel cladding and vessel materials, generally stainless steel, and earlier generation gas cooled reactors had operating temperatures on the order of: clad temperatures of ~800 K, fuel temperatures of ~900 K, and coolant temperatures of 650-750 K (Murphy, 2004). The higher thermal efficiencies at high reactor temperatures motivated the development of HTGRs.

Initial operation of high temperature gas-cooled reactors (HTGRs) occurred in 3 countries: the United Kingdom's 20 MW_{th} Dragon reactor, the United States' 115 MW_{th} Peach Bottom unit 1, and Germany's 46 MW_{th} Arbeitsgemeinschaft Versuchsreaktor *(*AVR) (Beck et al., 2010). All of these reactors were helium cooled. Both the Dragon and Peach Bottom reactors used a prismatic fuel element design with coated fuel particles dispersed in graphite, while the AVR used fueled pebbles of coated particles dispersed in graphite (Beck et al., 2010).

Helium is the preferred coolant for HTGRs and offers a number of advantages when compared with other gases like CO_2. It is chemically inert, does not experience neutron activation during reactor operation, and has some of the best thermal properties of all gases as well as favorable transport properties. Unfortunately, its low molecular weight increases the size of the turbo-machinery for Brayton cycle energy conversion (Tournier

and El-Genk, 2009). This is not a concern for HTGRs that are coupled to an indirect superheated steam Rankine cycle for energy conversion (Fig. 2.1) (Idaho National Laboratory, 2011; Zhu et al., 2008).

Both the Dragon and Peach Bottom reactors were of prismatic design and operated from the mid-1960s to the mid-1970s. The reactor core is comprised of hexagonal fuel element blocks that could be replaced or moved separately during refueling. The Dragon reactor operated at inlet and exit temperatures of 623 K (350 °C) and 1023 K (750 °C), respectively, and was used primarily for fuel and material testing (Beck et al., 2010). The Peach Bottom reactor operated at inlet and exit temperatures of 600 K (327 °C) and 973 K (700 °C) and was used mostly for the testing of fuel elements. The original fuel element design for these reactors consisted of coated fuel particles in a single layer of pyrolytic carbon. Such fuel particles were prone to early failure due to cracking of the coating (Beck et al., 2010). This led to the development of BISO (two–layer encapsulated) fuel particles, which led to the development of the TRISO fuel particles used in the Ft. St. Vrain reactor (Copinger, 2004) and the current VHTR design (MacDonald et al., 2004).

The German AVR, on the other hand, had been used as a demonstration test facility for the pebble-bed reactor concept. In a pebble-bed reactor, a packed bed of spherical fuel pellets is circulated through the reactor core (i.e. flowing from a reservoir or through a pipe and exiting through the bottom of the reactor) (Fig. 2.2). The gas flows up through the pellet bed, removing the fission heat generated in the fuel pebbles to the power conversion assembly. The AVR operated at inlet and exit temperatures of 548 K (275 °C) and 1223 K (950 °C) and was operational from 1967 to 1988 (Beck et al., 2010).

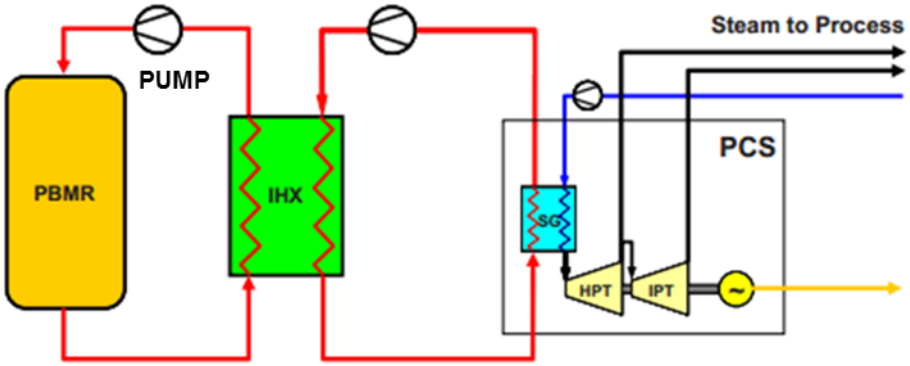

Figure 2.1 – A line diagram of an HTGR with a superheated steam Rankine cycle for energy conversion (Idaho National Laboratory, 2011).

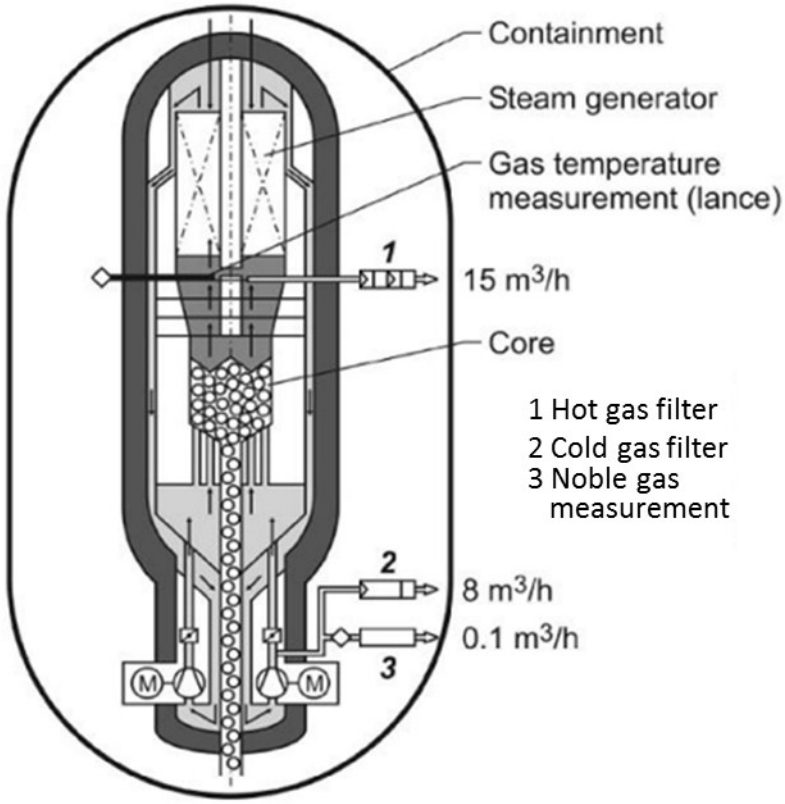

Figure 2.2 – An axial cutaway of the German AVR (Beck et al., 2010).

The Ft. St. Vrain reactor was a HTGR design which operated from 1974 to 1989 at inlet and exit temperatures of 677 K (404 °C) and 1050 K (777 °C), and its plant produced 330 MW_e of power using a secondary Rankine steam cycle (Copinger, 2004). The Ft. St. Vrain reactor had a prismatic core with hexagonal fuel elements loaded with TRISO fuel particles. It may be considered a precursor to the prismatic core, Generation-IV Very High Temperature Reactor (VHTR) (Copinger, 2004).

Recent efforts to deploy HTGRs occurred in Japan and China (Shiozawa et al., 2004; Zhang et al., 2006). Japan's High Temperature Test Reactor (HTTR) began operation in 1998 and is still operating today. This helium cooled reactor nominally operates at inlet and exit temperatures of 668 K and 1123 K (395 and 850 °C), and has been tested at exit temperatures as high as 1223 K (950 °C) (Shiozawa et al., 2004; Fujimoto et al., 2004). Such higher temperature operation testing makes the HTTR a valuable asset when considering the materials issues that future HTGRs face at those higher temperatures (Shiozawa et al., 2004). China, on the other hand, has developed, built and operated the High Temperature Reactor-10MW_{th} (HTR-10) since 2003. The HTTR is particularly interesting, not only because of its current high temperature operation, but also because of work done to couple it to a sulfur-iodine (SI) cycle to

The HTR-10 is a pebble-bed reactor design with an exit temperature of 973 K (700 °C). It is currently the baseline for the Chinese commercial HTR-PM (High Temperature gas-cooled Reactor-Pebble bed Module) project. The HTR-PM, 458 MW_{th} small modular reactors would provide economically scalable nuclear power in China (Zhang et al., 2006). As this is the only current effort in the commercial sector involving HTGRs, the experiences will be relevant and valuable for other nations considering using these small

and medium modular reactors for their energy future. These reactor are particularly attractive to underdeveloped countries or remote communities, with no or limited electrical grids, or limited access to fossil fuels on a continuous basses.

The HTTR is particularly interesting not only because of its current high temperature operation, but also because of work done to couple it to a sulfur-iodine (SI) cycle to produce hydrogen (Sakaba et al., 2007). In the HTTR-SI plant, the HTTR's primary helium coolant loop is coupled to a secondary helium loop via an intermediate heat exchanger to supply high temperature heat to the chemical reactors used in the sulfur-iodine cycle discussed later (Fig. 2.4). Preliminary results indicate that an optimized SI system coupled to the HTTR could produce ~100 m^3/h of hydrogen at a plant efficiency of ~44% (Sakaba et al., 2007).

Other earlier generations of gas cooled reactors have been operated by many nations, including France, Italy, Spain, and Russia. A timeline of development of gas cooled reactors can be seen in Fig. 2.3 (Beck et al., 2010). In general, HTGRs are characterized by their helium coolant, graphite moderation, and high operation temperatures (upwards of 900 K). They use either an indirect steam Rankine cycle or a helium direct closed Brayton cycle (CBC) for electricity generation. The high operation temperatures not only increase the thermal efficiency of the power plant, but also provide a potentially valuable source of process heat. Process heat is an important consideration for future co-generation for these reactors, as summarized in the next section. This process heat could be used for the production of hydrogen using thermo-chemical processes and also for other industrial uses, such oil recovery, seawater desalination, chemical production and manufacturing of heavy equipment.

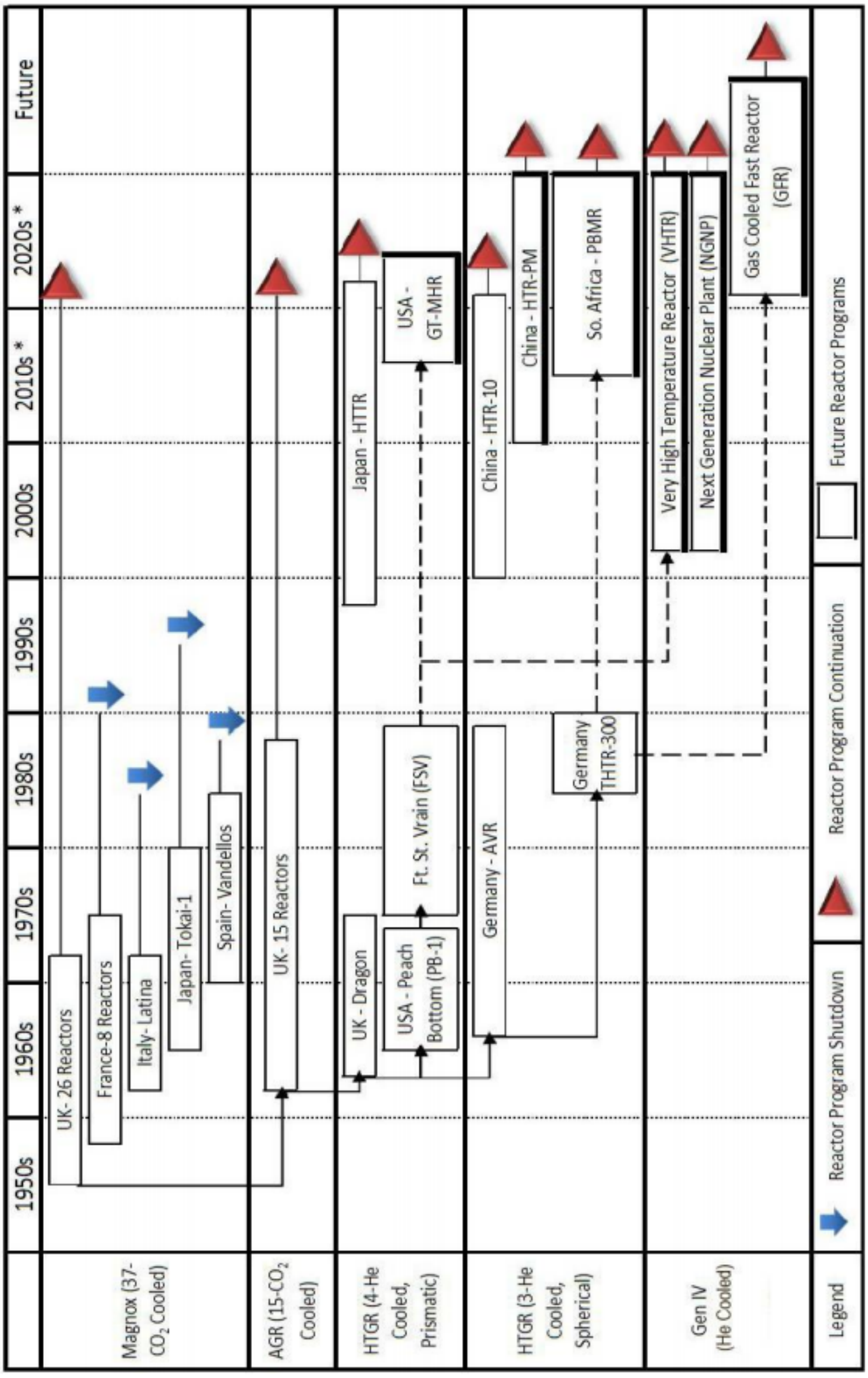

Figure 2.3 - History of the development of GCRs, HTGRs and VHTRs (Beck et al., 2010).

2.2 Process heat applications of HTGRs

President George W. Bush, in his 2003 State of the Union address, expressed an interest in investing in hydrogen energy (MacDonald et al., 2004). Hydrogen is not only useful as a next generation transportation fuel, but is also widely used today to produce chemicals and assist in refining crude petroleum (MacDonald et al., 2004). The United States' primary current source of hydrogen comes from steam reforming of methane, which releases significant amounts of CO_2 and other greenhouse gases.

More efficient and cleaner means of hydrogen production require high temperature heat sources. The Very High Temperature gas cooled Reactors (VHTRs) could not only produce electricity at high plant thermal efficiency, but also provide process heat for a host of industrial uses. These may include cogeneration (the use of the process heat to burn or generate other types of fuel like biomass) or hydrogen production using thermo-chemical processes (Elder and Allen, 2009). The thermo-chemical splitting of water (via the sulfur-iodine cycle, Fig. 2.4 or the hybrid sulfur cycle, Fig. 2.5) and high temperature electrolysis both require a high temperature heat source which the VHTR is uniquely suited to provide (Elder and Allen, 2009). VHTRs operate at 200 – 300 K higher exit temperatures than HTGRs (up to 1200 K), but none have yet been built.

Fig. 2.4 highlights the sulfur iodine cycle for the production of hydrogen; it has three stages (Elder and Allen, 2009). The first, located in the center of the diagram, requires a continual input of water to react with sulfur dioxide and iodine. The other two stages are temperature and catalyst dependent, with the top, higher temperature stage providing the necessary base compounds to refresh stage one. The bottom stage produces hydrogen.

Fig. 2.5 displays the hybrid sulfur cycle for the production of hydrogen. This cycle combines the electrolysis of water to extract hydrogen (top right of Fig 2.5) with the decomposition of sulfuric acid to renew the base components for the electrolysis. As Figs. 2.4 and 2.5 display, significant amounts of high temperature heat, in excess of 1073 K (800 °C) are required for both cycles (Elder and Allen, 2009).

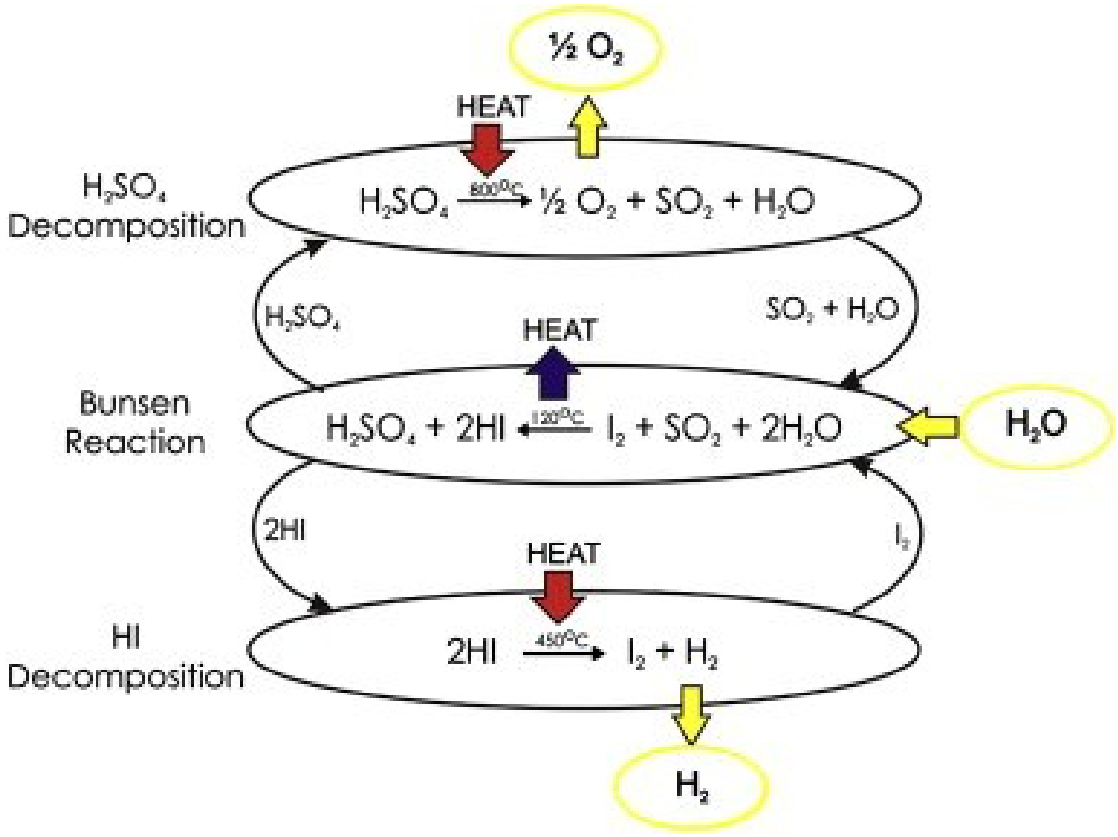

Figure 2.4 – An illustration of the sulfur iodine cycle for the thermo-chemical generation of hydrogen (Elder and Allen, 2009).

This potential for producing hydrogen fuel is one of the reasons that HTGRs and VHTRs have recently been considered by several countries, including the United States, for future design development and technology demonstration. VHTRs could be deployed as early as 2030-2050. However, China is currently deploying small modular HTGRs (HTR-PM), based on the demonstrated technology of their HTR-10, using superheated

steam Rankine cycles for electricity generation (Zhang et al., 2006). The US efforts to develop a Gen-IV VHTR are briefly summarized next.

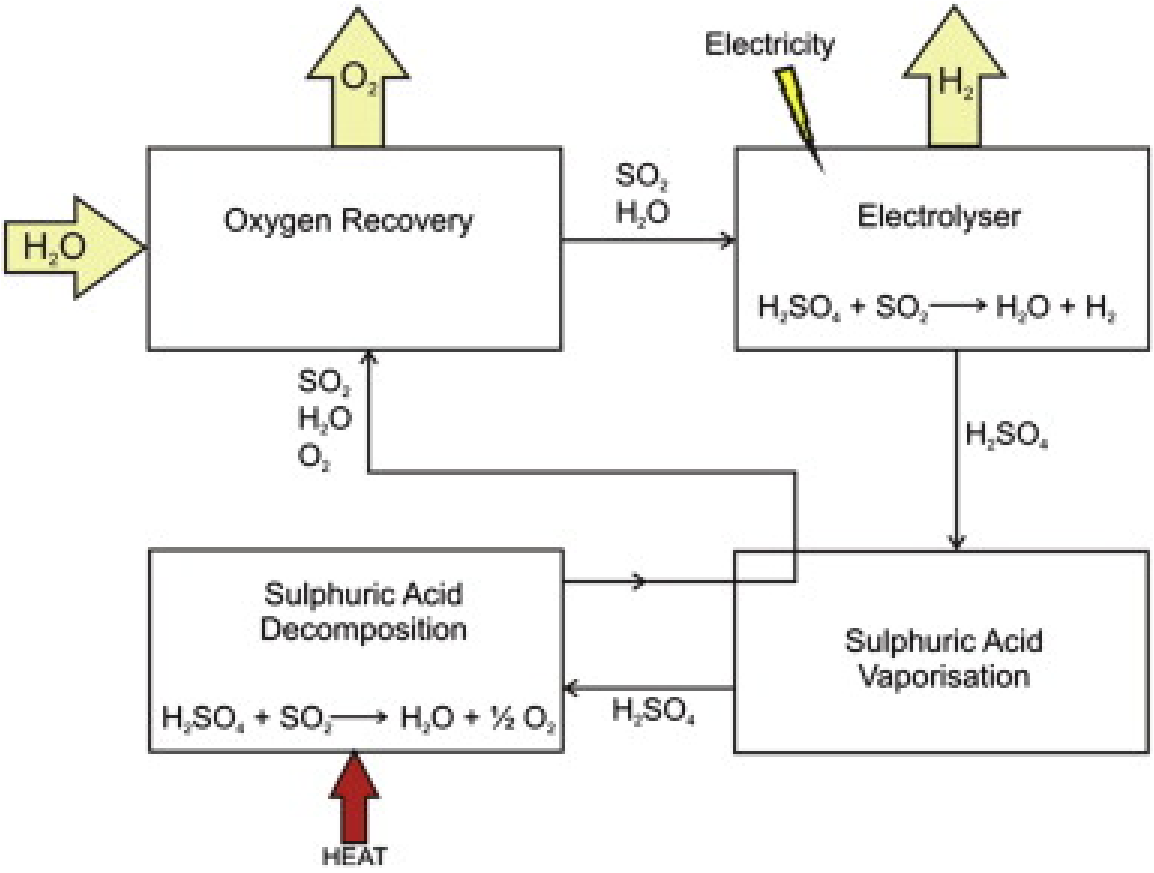

Figure 2.5 – A block diagram of primary processes involved in the hybrid sulfur cycle for the production of hydrogen (Elder and Allen, 2009).

2.3 The next generation nuclear plant project

The original intent of the Next Generation Nuclear Power Plant (NGNP) project was to: *"demonstrate a full scale prototype reactor [by 2020]; demonstrate high-temperature Brayton Cycle electrical production at full scale; demonstrate [the viability of] nuclear assisted production of hydrogen; demonstrate by test the exceptional safety capabilities of advanced gas cooled reactors; obtain an NRC license to construct and operate the*

NGNP; and support the development, testing and prototyping of hydrogen infrastructures" (MacDonald et al., 2004).

The development of the Next Generation Nuclear Power Plant (NGNP) was the primary focus of the United States' plan for developing and demonstrating the viability of commercial HTGRs and VHTRs in the US. Exploratory work on scoping designs that used TRISO particles began in 2004 and continued through 2006 (Idaho National Laboratory, 2011b). Originally, two reference designs were selected; they were the prismatic core VHTR and the PBMR, enumerated on in the next section. The original NGNP is a prototype VHTR demonstration plant, a project that has been put on hold in 2011 and reconfigured into a research and development project focusing on qualifying materials for a reactor design and laying the groundwork for future licensing (Idaho National Laboratory, 2011b). Consequently, very little actual design work is planned, although it must eventually be performed in order to license the reactor. The NGNP industrial alliance within the private sector is still active, and may at some point (with government assistance) attempt to build a demonstration plant (Idaho National Laboratory, 2011b).

2.3.1 The pebble bed modular reactor

The pebble bed modular reactor (PBMR) design considered for the NGNP, as seen in Fig. 2.6, functions with a large annular reservoir filled with spherical fuel pebbles that circulate through the reactor core, entering through the top and leaving through the bottom (Matzner, 2004). These pebbles have a packing fraction of 0.61, and consist of a graphite matrix containing TRISO fuel particles with a packing fraction of 0.09-0.10 (MacDonald et al., 2003; IAEA, 2001). The UO_2 within the TRISO particles are

generally enriched to 7-10%, lower than the 10-19.7% considered in the VHTR design (Idaho National Laboratory, 2011a). The PBMR reactor employs helium for cooling the packed bed of fuel pebbles in the core. The NGNP reactor had an outer core diameter of 3.5 m and inner diameter of 1.75 m, and had projected inlet and outlet temperatures of 780 K (503 °C) and 1181 K (908 °C) respectively (MacDonald et al., 2004).

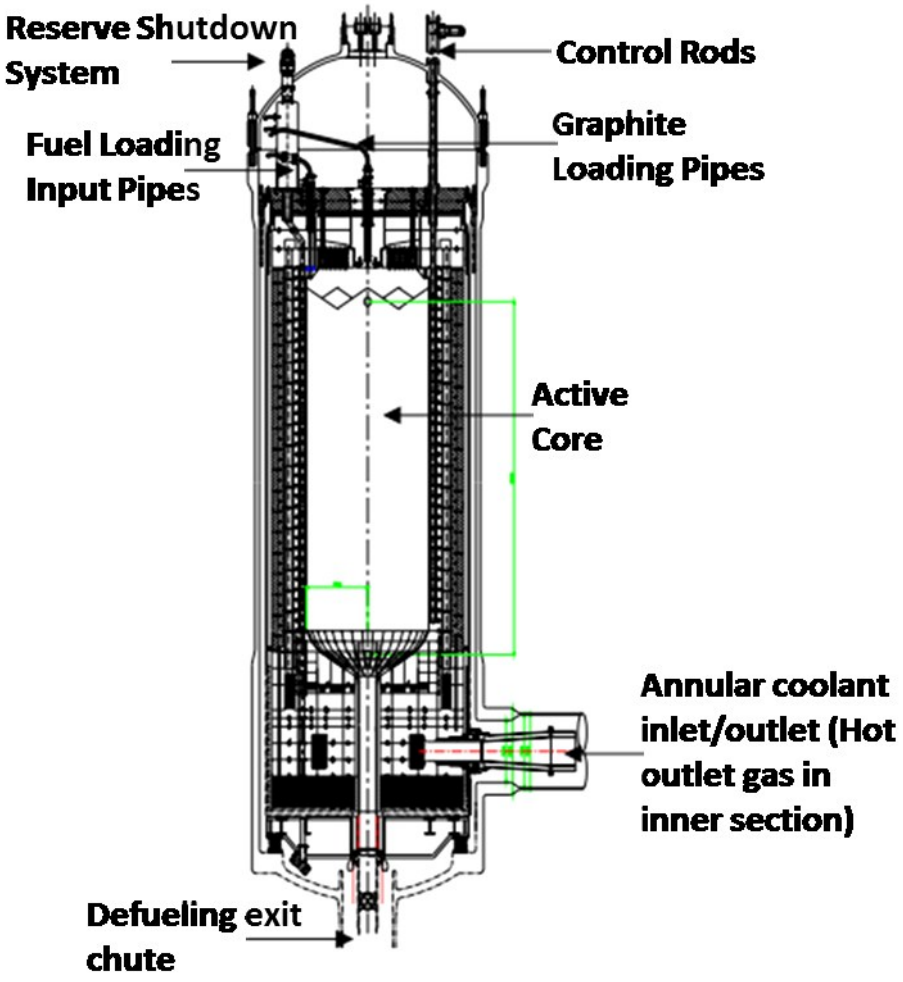

Figure 2.6 – An axial cutaway view of the PBMR (Matzner, 2004).

The displacement of the fuel pebbles in the PBMR is tightly controlled, and as such the fuel could achieve a very high burn up, ~90-100 GWD/MT (Idaho National Laboratory, 2011a). The use of pebbles increases the heat transfer area, thus allowing for

higher power than that of a prismatic core VHTR (MacDonald et al., 2004). The PBMR operates at a relatively low thermal power production (~300 MW_{th} as opposed to 600 MW_{th} for VHTRs). The rather large and irregular pressure drop over the bed of the fuel particles in the PBMR, seen in Fig. 2.6, may cause hot spots in the core (Becker and Laurien, 2003). Circulating the helium coolant through the core consumes ~8% of the plant's available electricity generation in the compressors, in comparison to only ~2% in the prismatic core VHTR (Idaho National Laboratory, 2011a).

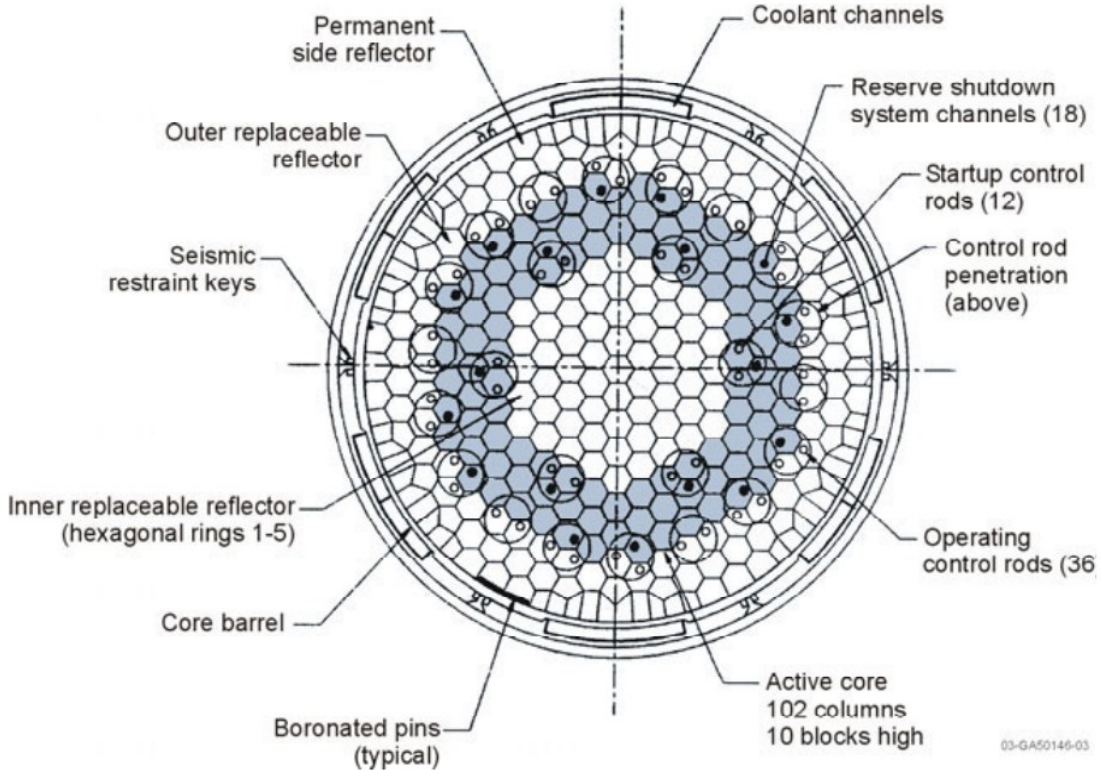

Figure 2.7 – A radial cross-section of a prismatic VHTR or HTGR core (MacDonald et al., 2004).

2.3.2 Very high temperature gas-cooled reactor

The Very High Temperature gas-cooled Reactor (VHTR) considered for the NGNP project is a prismatic core, graphite moderated design. The reactor consists of vertically stacked hexagonal fuel elements in three concentric rings (Schultz et al., 2004). A radial

cross section of the core can be seen in Fig. 2.7; the darker shaded blocks make up the active core, while the lighter blocks surrounding the annular active core make up the graphite reflector.

The primary features of the VHTR are: (a) its relatively low power density (approx. 6-8 MW/m^3 as compared with 60-100 MW/m^3 in LWRs (Beck et al., 2010); (b) the very high operating temperatures up to 1273 K (exit), especially applicable when considering co-generation of hydrogen and process heat; (c) its use of a coated fuel particle designed to fully contain fission products; (d) its inherent level of safety stemming from the aforementioned relatively low power density; (e) the use of graphite for large parts of the reactor core, enhancing safety by serving as an excellent heat transfer and storage medium; and (f) the prismatic graphite core blocks, which are designed to be easily replaced or moved during refueling. The VHTR design, chosen for a demonstration prototype to be built for the NGNP project (MacDonald et al., 2004; Schultz et al., 2004), is further detailed next.

2.4 VHTR design details

The specific reactor design considered for the NGNP demonstration unit and investigated in this thesis is a high temperature variant of the General Atomics GT-MHR, (General Atomics, 1996). It has an exit temperature of either 1123 K or 1263 K (850 °C or 990 °C) and an operating exit pressure of 7.07 MPa (McDonald et al., 2004). This thesis considers the prismatic VHTR design with an outlet temperature of 1263 K. General Atomics' GT-MHR plant was intended to consist of four reactor plant modules, each capable of generating 600 MW_{th} with a plant thermal efficiency close to 45% (MacDonald et al., 2004). The GT-MHR design draws heavily on the experience from

Ft. St. Vrain (General Atomics, 1996). A cutaway view of a full VHTR can be seen in Fig. 2.8. The helium coolant enters the VHTR through the outer ring of the annulus at the lower left of Fig. 2.8, and travels up the space between the outer graphite reflector and the reactor vessel, cooling the vessel wall. In some cases, such as in the Japanese HTTR, the helium cooling the vessel is bled directly from the energy conversion cycle before entering the compressor unit of the CBC energy conversion turbo-machinery; this bleed cooling affects the performance of the VHTR plants (Tournier and El-Genk, 2009).

The helium coolant flows into the upper plenum of the VHTR, where it mixes and then reverses direction, flowing down through the individual channels in the active core fuel elements (Fig. 2.9) before exiting into the lower plenum. It then exits to the energy conversion assembly. Some of the helium coolant in the upper plenum flows through orifices into the control rod channels in order to cool the control elements in these channels (Fig. 2.9) (General Atomics, 1996). This flow typically represents less than 3 percent of the total helium flow into the VHTR. Reactor control is achieved using two separate independent means: (a) large control rods that are inserted at preset locations in specified fuel elements in the core, seen in Fig 2.9, and (b) reserve shutdown pellets.

The control rods are made of enriched B_4C neutron absorber dispersed in a graphite matrix and formed into cylindrical compacts. These compacts are placed into canisters to fill control rod holes (General Atomics, 1996). These canisters are connected by a cable and can be inserted into the active core at varying depths during reactor operation as needed. The reserve shutdown pellets are 1.4 cm diameter and can be inserted through holes designated in Fig. 2.9. The pellets consist of enriched B_4C granules dispersed in a

graphite matrix (General Atomics, 1996). The pellets, kept in storage above the reactor are released into the reactor in the case of an emergency shutdown.

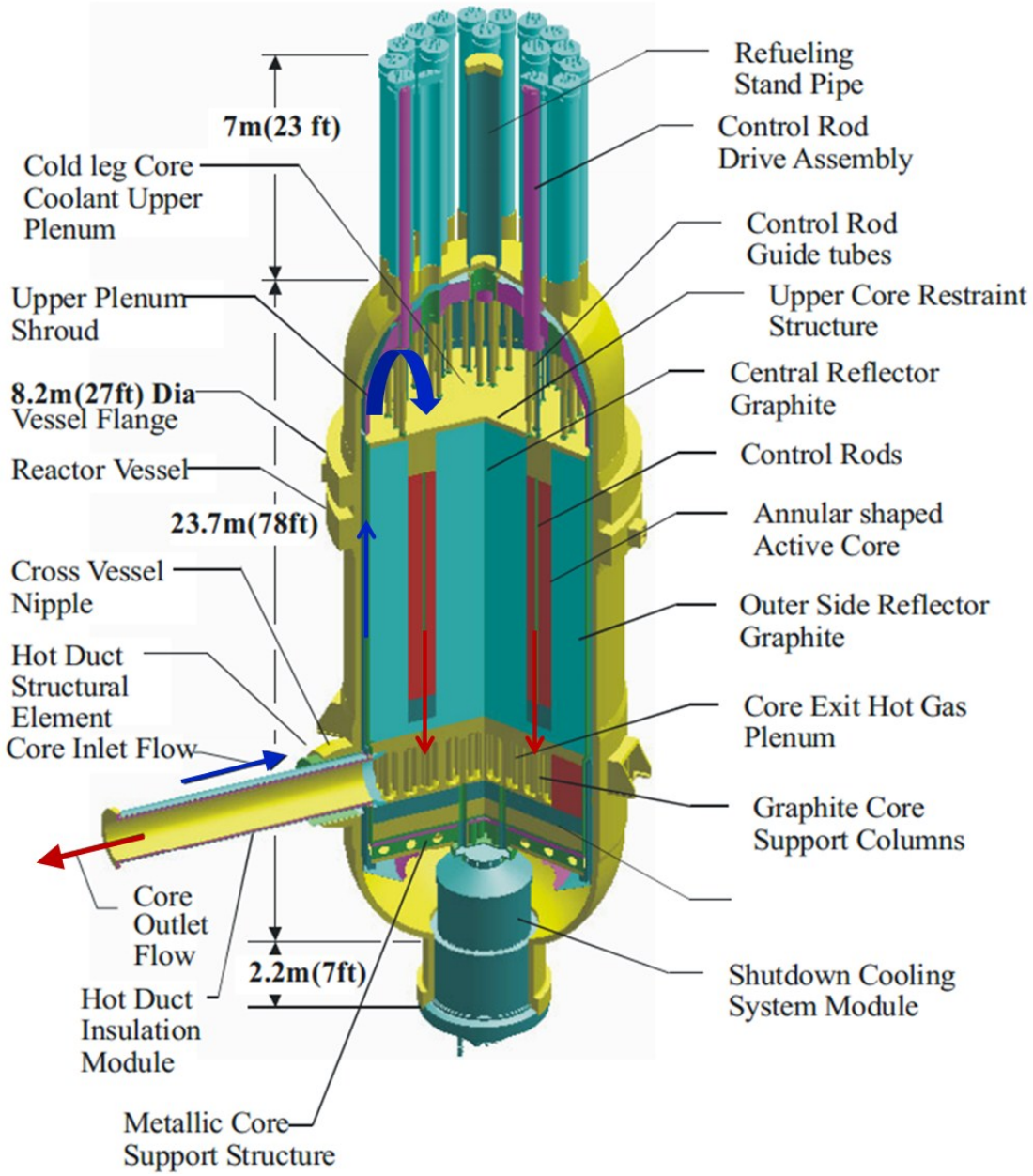

Figure 2.8 - A cutaway view of a VHTR (MacDonald et al. 2004).

Fig. 2.9 shows a radial cross sectional layout of a quarter of the VHTR core. The 1/6 core section is highlighted with the dashed lines. The annular active core of the prismatic VHTR is comprised of 102 prismatic, hexagonal fuel elements (Fig. 2.9) in 2 to 3 rings,

and stacked 10 blocks high totaling 7.93 m. The active core has an effective inner diameter of 2.96 m and outer diameter of 4.83 m (General Atomics, 1996). The reactor vessel itself has an inner diameter of 7.23 m. The active core fuel elements are shown in dark grey in Fig. 2.9. Fuel elements are 0.36 m flat-to-flat and 0.793 m tall. Most fuel elements have 210 holes loaded with fuel compacts (Schultz et al., 2004) (Fig. 2.10a), 6 holes loaded with burnable poison rods and 108 helium coolant channels, 6 of which are of a smaller diameter and placed near the center of fuel element.

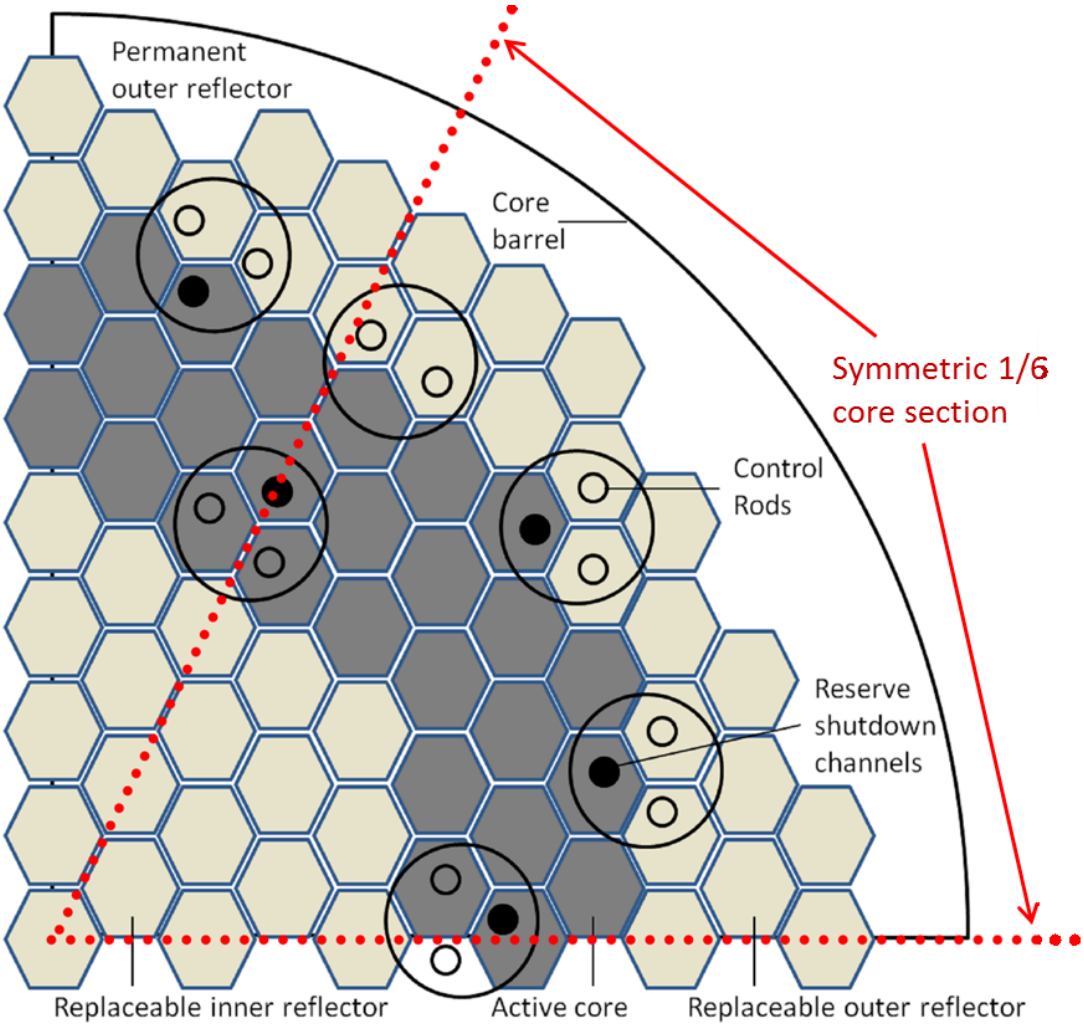

Figure 2.9 – A radial cross-sectional view of a VHTR 1/6 core with prismatic fuel elements (grey shade) and graphite reflector (light shade) blocks.

(a) Standard fuel element

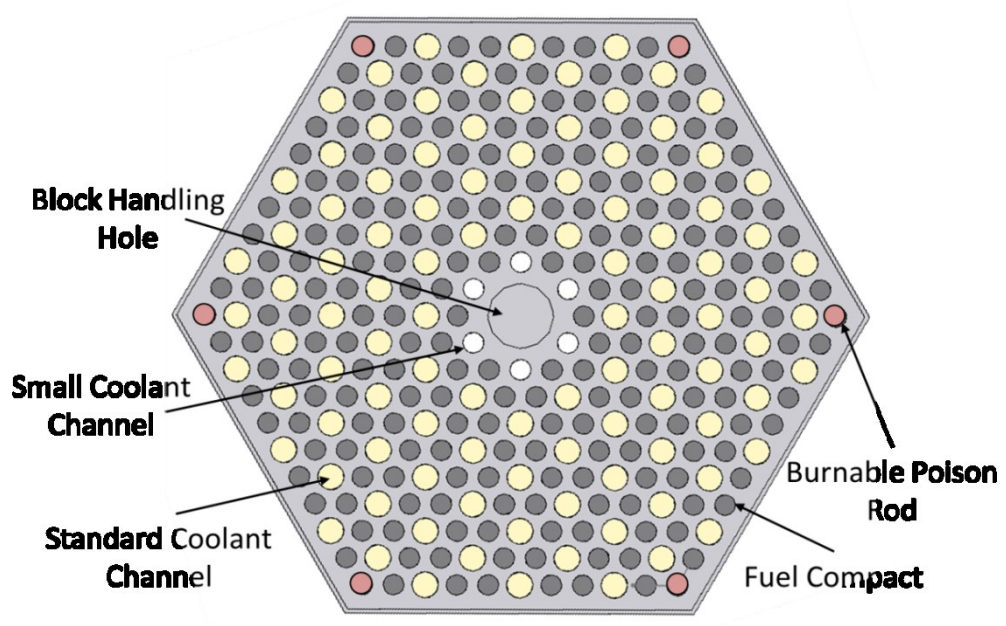

(b) Fuel element with a control rod channel

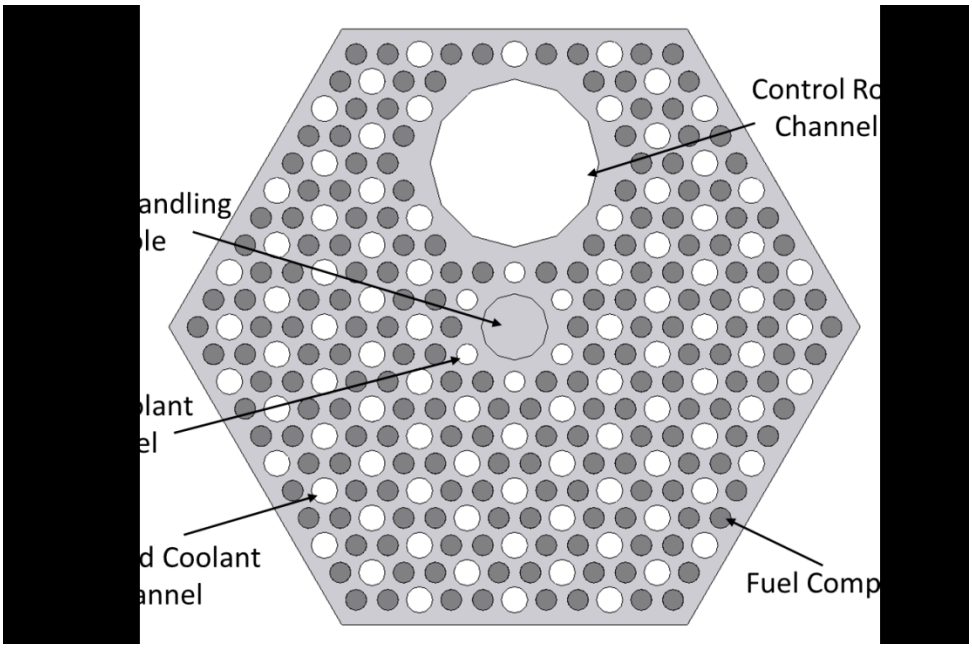

Figure 2.10 – Radial cross-sectional view of VHTR core fuel elements.

Fig. 2.10 displays the layout of the fuel elements used in the active core of the VHTR. Fig. 2.10a shows an example of a standard fuel element; these standard elements compose most of the active core, as seen in Fig. 2.9. Fig. 2.10b, on the other hand, shows

an example of a fuel element with a control rod hole. A few of the core fuel elements have a large control rod or reserve shutdown channel that replaces some of the coolant channels and fuel compacts (Fig. 2.10b). The active core fuel elements are surrounded by graphite reflector blocks in the inner five and the outer 2-3 rings of the reactor core (lighter grey highlights in Fig. 2.5). In addition, there are axial graphite reflector blocks stacked on the top (1.2 m) and bottom (0.8 m) of the active core (Fig. 2.8). The burnable poison rods mentioned earlier are located at the 6 corners of the hexagonal fuel elements. The amount of enriched boron in each poison rod varies with location in the reactor core and the reload status of the fuel elements (i.e., the burnable poison rod content changes with each fuel loading and element arrangement in the VHTR core). Each of these burnable poison rods, as well as the fuel compacts and coolant channels, run parallel axially through the fuel elements.

On average, there are six fuel compacts surrounding each of the larger diameter helium coolant channels in the fuel elements, and each channel removes the fission heat generated in two fuel compacts. The coolant channels within the fuel elements in the active core region extend into the top and bottom axial reflectors. The majority of them are 1.5875 cm in diameter, while some channels near the center of each block (Fig. 2.10a and b) have a smaller diameter of 1.275 cm. The fuel compacts' design is discussed next.

2.4.1 TRISO fuel particles in prismatic fuel elements

The coated fuel particles have been used as far back as the Dragon reactor in the United Kingdom (Beck et al., 2010). Continued development of the coated fuel particles added additional coatings, and tested different coating materials and layering schemes, which are partially incorporated into the particles used in the German Thorium High

Temperature Reactor (THTR) (Beck et al., 2010). Coated Tristructural-isotropic (TRISO) microspheres (Fig. 2.11) are also used in the Japanese HTTR and Chinese HTR-10. The VHTR's spherical TRISO fuel particles consist of uranium oxy-carbide (or in some cases, UO_2) kernels enriched to 19.8 wt% and encapsulated by interlaced PyC and SiC coatings. The SiC coating retain fission products and restrain fuel kernel swelling during nominal reactor operation (Kiryushin et al., 1997; MacDonald et al., 2003; Lee et. al, 2006; LaBar et al., 2004; Schultz et. al., 2004; Johnson, 2008; Yan et al., 2003).

The layout of the encapsulation of the fuel kernel in the TRISO particle can be seen in Fig. 2.11. The fuel kernel is surrounded by a very porous carbon layer that accommodates fuel swelling and the released fission gases from the kernel during reactor operation. This layer is then surrounded by a layer of pyrolytic carbon (PyC), which serves to accommodate thermal stresses and the differential thermal expansion between the inner porous graphite layer and the outer SiC coating. The SiC layer provides the mechanical and structural strength for retaining the fission products, while not impeding heat flow out of the fuel kernel. This layer is then surrounded by another PyC layer, which may serve as a secondary containment barrier for the fission products, to provide a compatible bond for the TRISO particles with the graphite matrix of the fuel compacts (Figs. 2.12a, b) (General Atomics, 1996).

The fuel compacts of the VHTR fuel elements are comprised of TRISO particles dispersed in nuclear graphite with a packing fraction of 0.289 (General Atomics, 1996). These fuel compacts, 1.245 cm in diameter and 4.95 cm tall (Fig. 2.12b), are loaded into vertical channels in a triangular lattice within the prismatic fuel elements (Fig. 2.12c).

The TRISO particles in the fuel compacts are the primary source of the heat generation by fission within the VHTR core fuel elements.

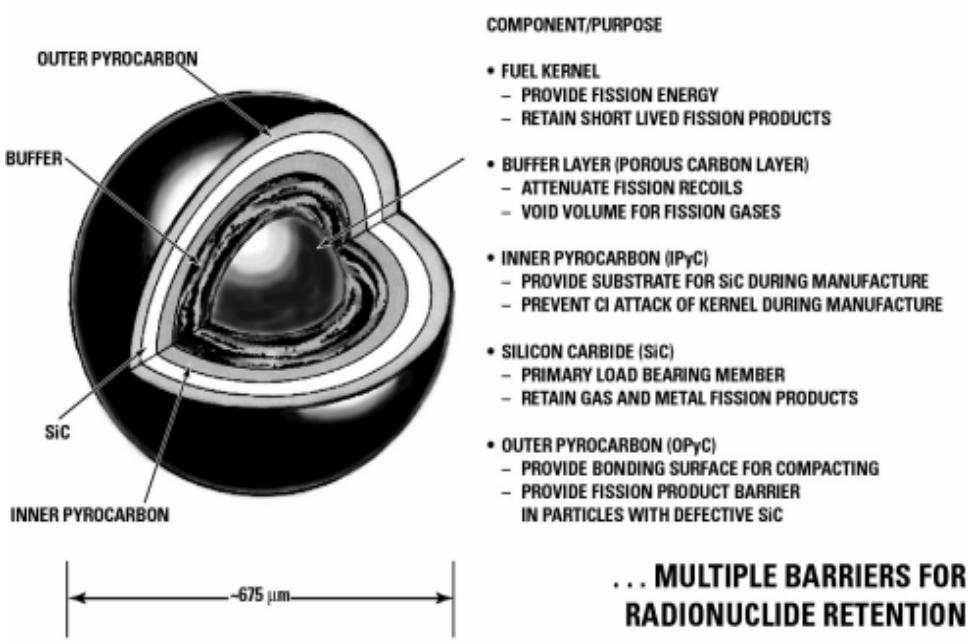

Figure 2.11 – A TRISO fuel particle with multiple coatings (General Atomics, 1996).

Figure 2.12 – TRISO fuel particles, fuel compacts, and prismatic fuel element (MacDonald, 2003).

The fission power generated in the fuel elements is removed from the fuel elements by the helium coolant flowing through the surrounding coolant channels. On average, each coolant channel removes the fission power generated in two fuel compacts. Not all the helium coolant entering the VHTR flows through the coolant channels; some flows through the interstitial gaps between the fuel elements in the VHTR annular core region (~ 5 – 11%, depending on the width of the gaps) and a small fraction (~3%) flows through the control rod channels for cooling.

2.4.2 Interstitial bypass helium coolant flow in the VHTR core

The helium bypass flow in the interstitial spaces between fuel elements further complicates the flow distribution and the thermal-hydraulics analysis of the VHTR core. These spaces or small gaps between the VHTR core prismatic fuel elements develop due to the manufacturing tolerances of the elements, and thermal expansion and irradiation induced swelling during reactor operation. These spaces are seen obliquely in Fig. 2.9 as the white gaps between the hexagonal fuel elements (both within the active core and in the radial reflector). Their width varies in the different sections of the core, depending on the fabrication tolerances, and the operation time and history of the elements within the reactor core. Although the exact dimension of these passages is not well characterized, they could be up to 5-10 mm in width.

Helium coolant bypass flow is that which flows through the interstitial spaces between the fuel elements. In addition, a helium coolant "bleed" flow enters from the upper plenum through orifices into the control rod channels, discussed earlier (General Atomics, 1996), flows through the control rod channels in the core fuel elements and exits into the lower plenum. The control rod channel's diameter is much larger (10.16

cm) than that of the regular helium coolant channels (1.5875 cm). Although the helium inlet temperature into the control rod channels is comparable to that entering the coolant channels, its exit temperature is significantly lower. The total amount of helium flow through the control rod channels varies with the reactor design (some designs have an insignificant amount as the control element does not require cooling), but is typically limited to ~ 3% of the total helium flow into the reactor (General Atomics, 1996). The helium bypass flow as well as the "bleed" flow through the control rod channels must be addressed in thermal-hydraulics analyses of the VHTR, addressed in section 2.5.

2.4.3 VHTR power conversion assembly

The power generated in the VHTR is converted to electricity through a direct coupling to the power conversion assembly. In plants with indirect coupling of the VHTR to the power conversion assembly, heat from the reactor primary helium loop is transferred through a heat exchanger to the turbo-machinery working fluid. A direct Closed Brayton Cycle (CBC) uses a single-shaft turbo-machinery for energy conversion (Fig. 2.13a) (El-Genk and Tournier, 2009, 2010; Tournier and El-Genk, 2009). The bleed cooling of the VHTR vessel in Fig 2.13a increases the plant thermal efficiency significantly versus the case of direct CBC cooling without a bleed cooling of the reactor vessel as in the GT-MHR (Fig 2.13b) (El-Genk and Tournier, 2009). Bleeding helium at the inlet of the low pressure compressor (LPC) to cool the reactor vessel allows the inlet temperatures (that now do not need to be fixed) to rise commensurate with increasing the reactor exit temperature for enhanced plant operation (Fig. 2.13a). Thus, only a small amount of helium coolant is needed to cool the reactor vessel to a sufficiently low temperature, rather than maintaining the vessel temperature constant at the coolant's inlet

temperature regardless of any increase in the reactor's exit temperature. VHTR plants with vessel bleed cooling are more efficient with increasing reactor exit temperature.

(a) VHTR direct helium CBC with bleed cooing of reactor vessel

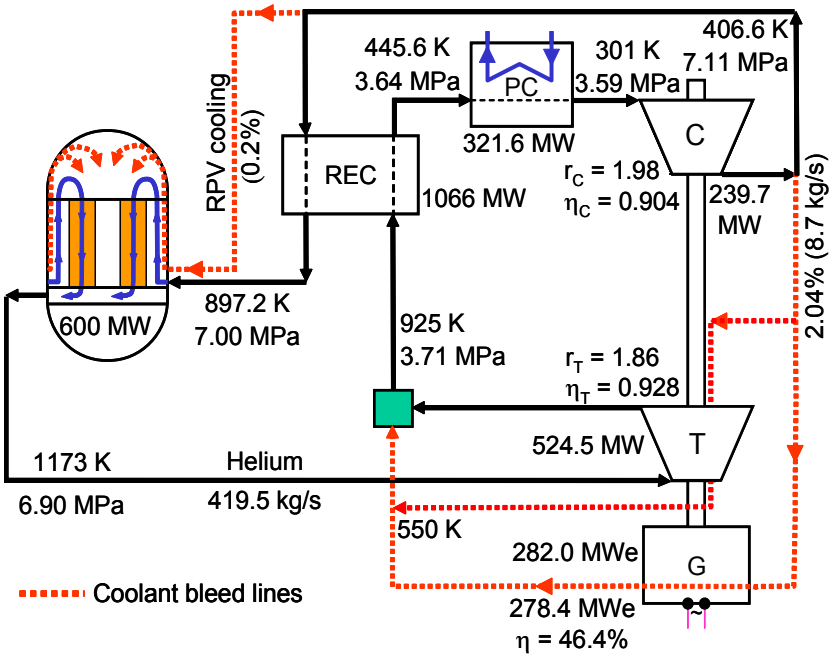

(b) VHTR direct helium CBC, without bleed cooing of reactor vessel

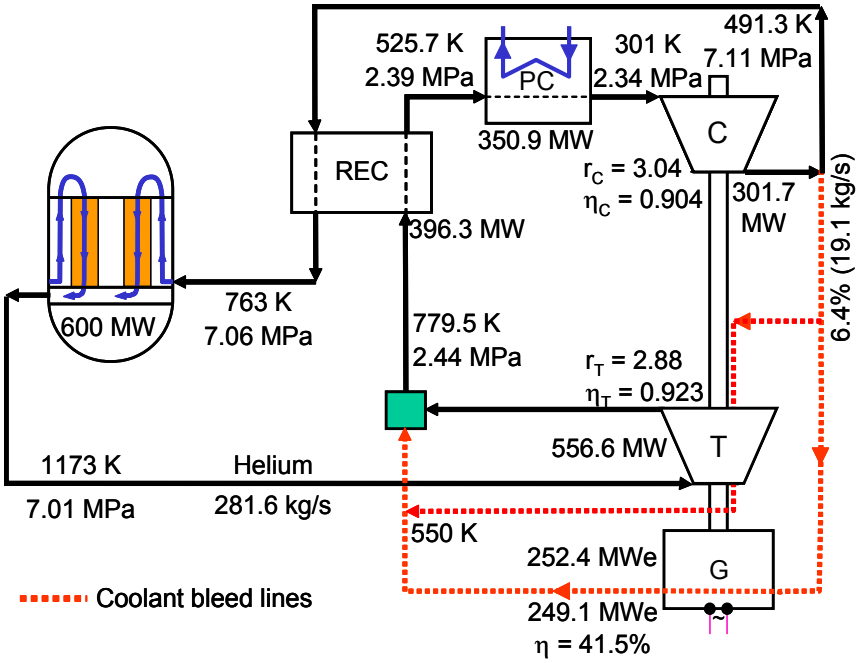

Figure 2.13 - CBC with / without bleed cooling of reactor vessel (El-Genk and Tournier, 2009).

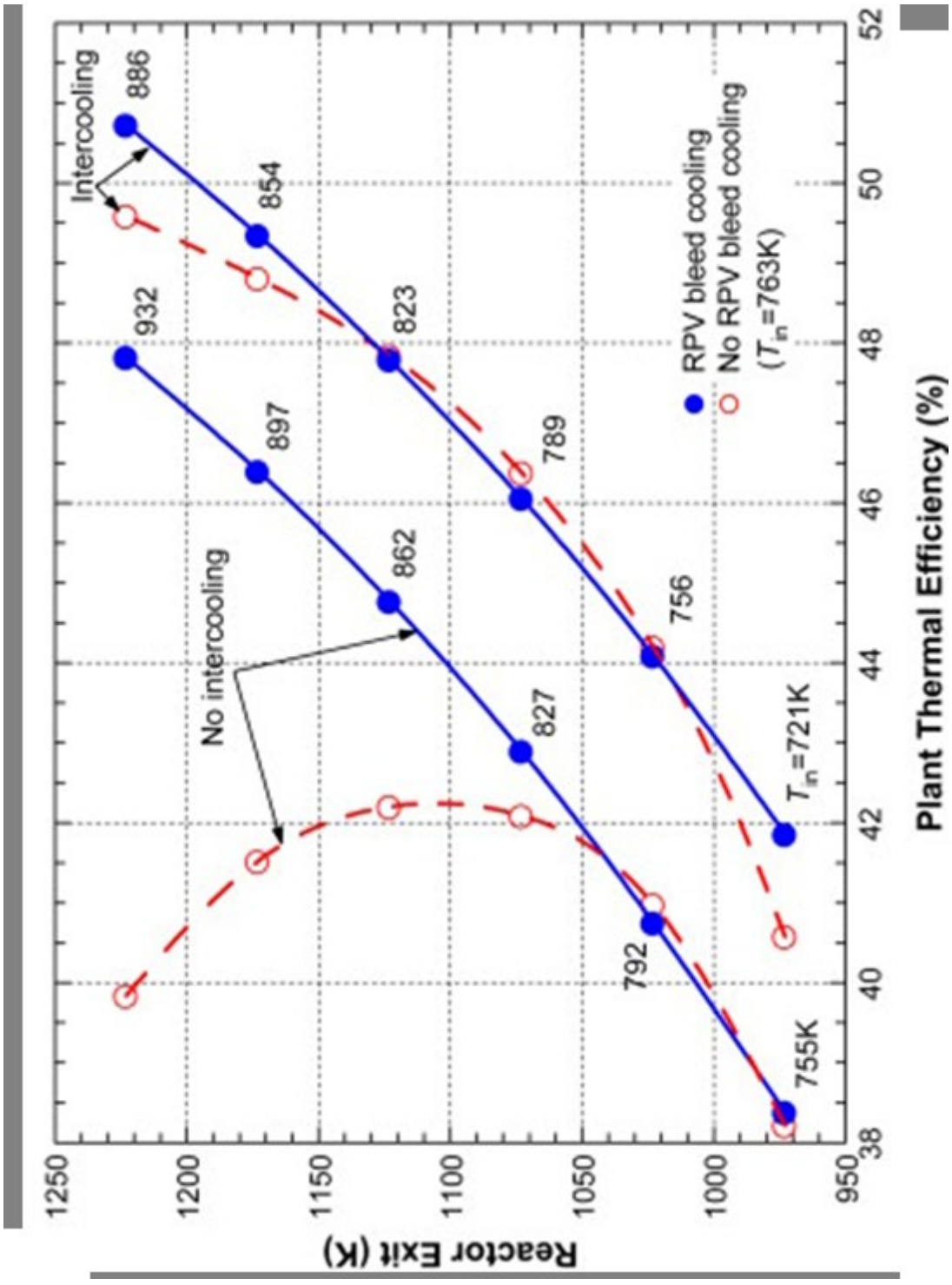

Figure 2.14 - Effects on the plant thermal efficiency of the reactor exit temperature, bleed cooling of the VHTR vessel and intercooling between the LPC and HPC of helium direct CBC (El-Genk and Tournier, 2009).

2.5 Challenges to thermal-hydraulics analyses of the VHTR

Ideally, one would perform a full core thermal-hydraulics analysis in order to optimize the performance and design of a prismatic HTGR or VHTR. However, due to the complexity and large size of the core, such an analysis would require extensive computation capabilities (on the order of a supercomputer cluster) and a relatively long time (weeks to months) to complete. Such requirements can in large part be attributed to the 3-D CFD simulation of the helium gas flow, both in the coolant channels and bypass spaces. The VHTR core with the graphite reflector is about 10 meters tall and 8 m in diameter, and special detail must be paid to the fuel compacts and coolant channels. In addition, modeling features with very small dimensions on a very large scale complicates the numerical meshing for the computations, as each of these small features requires a large number of computational elements to properly model. This reproduction, which involves thousands of fuel compacts and coolant channels, greatly complicates analysis.

The helium interstitial bypass flow further complicates matters – not only can bypass features have even smaller sizes than those of the coolant channels (~5 mm), but also the nature of the flow through these bypass features is not well understood or as easily characterized as that through the regular coolant channels. Modeling the helium bypass flow requires large number of numerical mesh elements to adequately simulate the 3-D helium flow. As the total number of numerical mesh elements increases into the millions, the computational time and resources required for modeling the VHTR core fuel elements with helium bypass flow skyrockets (Sato et al., 2010). The next section reviews previous work reported on the thermal-hydraulics modeling of VHTR core and fuel elements.

2.6 Review of prior thermal-hydraulics modeling of VHTR

Numerous works have been reported on thermal-hydraulics analyses of the VHTR core during nominal operation. Nominal operation conditions include an inlet temperature of either 764 K or 914 K (491 °C or 641 °C), with a corresponding outlet temperature of 1123 K or 1263 K (850 °C or 990 °C), a total helium coolant mass flow rate of ~ 330 kg/s and a system or helium exit pressure of ~ 7.07 MPa. These parameters can vary somewhat in the individual research based on the specified conditions of the VHTR (two different temperature regimes exist, MacDonald et al., 2004). In early modeling efforts, such as the GT-MHR reports and the INEEL point design study (Kiryushin et al., 1997; MacDonald et al., 2003), various codes have been used to perform the thermal-hydraulics analyses of the reactor. POKE, a relatively simple (when compared to CFD) thermal analysis code, was used in order to execute rapid, parametric analysis on the effects of changing the inlet and outlet temperatures as well as total reactor power and active core height (MacDonald et al., 2003). Using the parameters from POKE, a reactor design was then input into RELAP5-3-D/ATHENA (a multi-physics 3-D volume code), in order to provide some of the same insights as a full 3-D CFD code, while being somewhat less detailed. These codes both provide valuable design insight, but do not fully capture all the details that a full CFD analysis can (e.g. specific hot spots, turbulence effects in bypass regions, etc.).

Full 3-D CFD thermal-hydraulics analyses of VHTRs provide a reasonable degree of fidelity, but take significantly longer times to perform. One of the first large scale full 3-D analysis of a VHTR was reported by Pointer and Thomas at ANL (Pointer and Thomas, 2010). They used an in-house code called SHARP, which incorporates

DeCART and STAR-CD, in addition to using STAR-CCM+ (the code used in this thesis, CD-adapco, 2012) in order to perform the VHTR thermal-hydraulics analysis. Pointer and Thomas (2010) began by benchmarking and evaluating their code on a representative "unit cell" geometry consisting of a coolant channel surrounded by a hexagonal section of a graphite fuel element and six, one-third fuel compact segments. This single channel "unit cell" was primarily employed to investigate the effect of the mesh intensity on the thermal-hydraulics results. Pointer and Thomas (2010) also investigated the effect of varying the turbulence model on the analysis results and determined that the k-ε model was the most appropriate for performing the VHTR thermal-hydraulics analysis. Additional information on the choice of turbulence models, including numerical testing done in this thesis, can be found in Appendix B.

Once validated with the single channel module, the code was used to simulate a full height 1/6 section of the VHTR (Pointer and Thomas, 2010). They modeled the VHTR in full 3-D CFD, including the helium "bleed" flow through the control channels, confirming the viability of using CFD in modeling the VHTR core but highlighting the need for simplified methods. This simulation analysis required 305 CPU hours on a 25.9 teraflop supercomputer cluster to complete (Pointer and Thomas, 2010).

Pointer and Thomas (2010) ran their simulations of a VHTR using constant axial and radial power profiles and with helium flow through control rod channels and unspecified interstitial gaps. An example of the results from their simulations can be seen in Fig. 2.15. Even with the significant computational resources used to perform the analysis, their work confirmed that Reynolds Averaged CFD models are a viable choice for modeling the thermal-hydraulics behavior of a prismatic core VHTR.

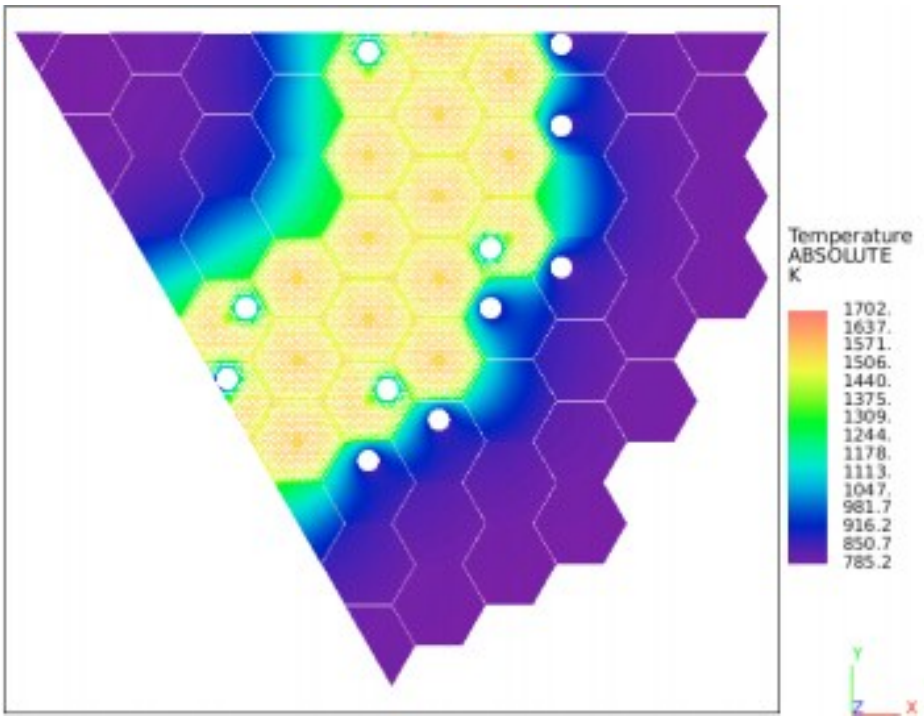

Figure 2.15 – Calculated radial temperature field using a full 3-D thermal-hydraulics simulation of a full height, VHTR 1/6 core (Pointer and Thomas, 2010).

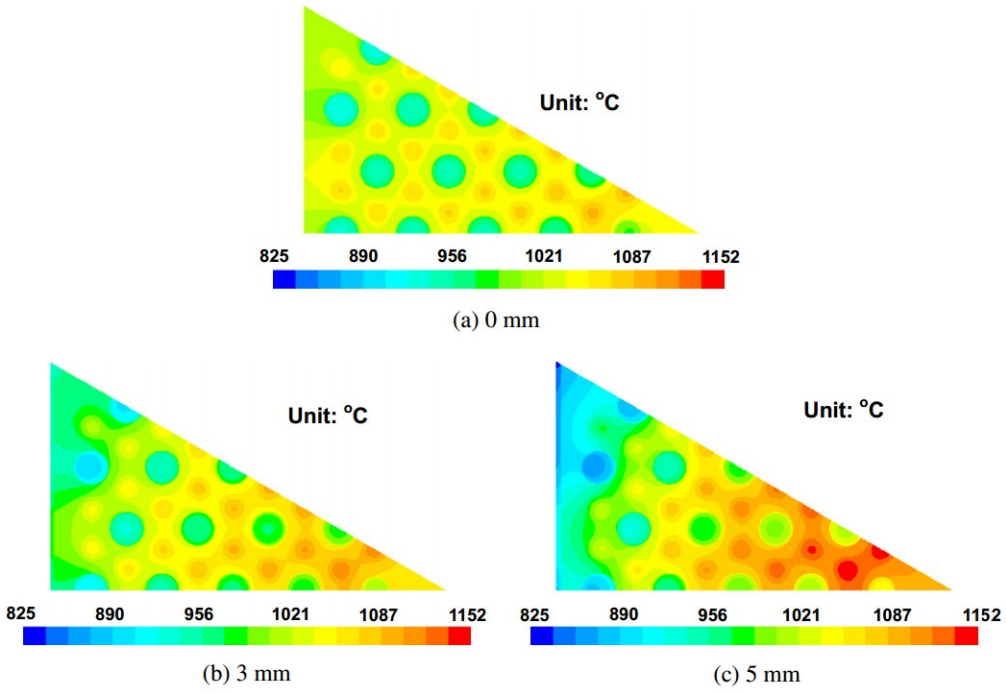

Figure 2.16 - Results of increasing the width of the interstitial bypass flow gap (0 mm (no gap), 3 mm and 5 mm) on the calculated temperature field in a 1/12 fuel element (Sato et al., 2010).

Pointer and Thomas (2010) highlighted the need for a better understanding of the operational core conditions in addition to some means of simplifying the large scale simulations, such as an optimized or simplified meshing scheme, without compromising the accuracy of the calculations (Pointer and Thomas, 2010).

In an attempt to simplify the methods used in thermal-hydraulics modeling of a VHTR, Tak et al. (2008, 2010) took an inventive approach to reducing the computational requirements, while still maintaining the fidelity of the calculations (Tak et al. 2008, 2010). They streamlined the numerical mesh using a number of different unit cells to configure a fuel element block in their own version of a system code.

Each cell was a small self-contained unit encompassing a fuel element, a coolant channel, or burnable poison rod. Instead of explicitly modeling the 3-D helium flow in the coolant channels, they used a 1-D flow (using convection) in the coolant channels in conjunction with conduction in the graphite block and fuel compacts. The turbulent convection heat transfer coefficient was calculated using the Dittus-Boelter correlation (Dittus and Boelter, 1930) developed for heated pipes and is applicable for fully developed flow conditions when the temperature difference between the heated wall and coolant bulk is $\leq 10\ ^{o}F$. As such, this correlation should not be used in entrance region of the VHTR coolant channels where helium flow is not fully developed.

Such a simplification of modeling thermal-hydraulics a VHTR flow channel also allowed Tak et al. (2008, 2010) to avoid the complexity of 3-D CFD simulation of the coolant in the channel. They employed a chopped cosine axial power profile of their own derivation and assumed a helium bypass flow in an interstitial gap that was 1-mm by reducing the total helium flow in the core by 1.1 percent, but did not explicitly simulate

the actual helium bypass flow. They ran their thermal-hydraulics simulation on a "typical" personal computer, defined as a 3 GHz Intel Core 2 with 3 GB of RAM. On this machine, the simplified 1-D calculations were completed in a matter of minutes while a full 3-D CFD on a similar test section took "several hours" of computation time to conclude (Tak et al. 2008 and 2010). They demonstrated a significant reduction in the required computational time using their simplified method, while maintaining reasonable accuracy in the results. Their findings demonstrated that a simplified method could be capable of producing comparable results to a full 3-D CFD analysis in a fraction of the time required to execute the latter. This approach laid the foundation for the current work presented in this thesis and partially documented elsewhere (Travis and El-Genk, 2012).

Helium bypass has been identified as an important phenomenon that could affect the thermal behavior and potential development of hot regions in the fuel elements of a VHTR core, and thus should be studied and accounted for in future thermal-hydraulics analyses. The most extensive study of the helium bypass flow and its effect on the thermal-hydraulics performance of a prismatic VHTR is that of Sato et al. (2010). They analyzed a 1/12 section of a 7.93 m tall prismatic fuel element within a VHTR core under different bypass flow conditions (Fig. 2.16). While Pointer and Thomas (2010) accounted for helium bypass insofar as to reduce the helium flow in the coolant channels, Sato et al. (2010) performed a full 3-D CFD analysis of helium bypass flow in the interstitial gaps of different widths and at different reactor power levels. They found that helium bypass flow significantly impacts the temperature distribution in the fuel elements, cooling the edges and increasing the temperature gradient across the element from the edge to the center. This gradient is clearly identified in Figs. 2.16a – 2.16c,

which display the results reported by Sato et al. (2010). These figures show that increasing the dimensions of the bypass gap between the fuel elements in a VHTR core from 0 (no gaps) to 3 and 5 mm has a profound effect on the temperatures within the fuel elements as well as cooling the edges. The 5-mm wide bypass gap (Fig. 2.16c) increases the temperatures near the center of the fuel element by as much as 50 K, compared to the case with no helium bypass gap (Fig. 2.16a). Results also show that helium bypass potentially increases the intensity and likelihood of causing hot spots because it "robs" from the helium flow that would otherwise go into the coolant channels in the core. The increased temperature of the helium gas exiting the coolant channels could contribute to the formation of hot spots in the lower support plate of the VHTR lower plenum. In addition, Sato et al. (2010) indicated that using the k-omega turbulence model to simulate the helium flow in the interstitial gaps did not adequately capture the physics near the walls, while the results using the k-epsilon turbulence model agreed with empirical correlations relatively well (Sato et al., 2010). These findings enforced the choice of the k-epsilon turbulence model in the current thermal-hydraulics analysis of VHTR fuel elements with helium bypass flow (see Appendix B).

Helium bypass between VHTR core fuel elements has also been modeled by Shultz et al. (2012) in a scaled experiment at Idaho national Laboratory (INL). Although expensive, these sorts of experiments go a long way towards helping understand the behavior of the bypass flow. A scaled multi-block air test facility was built at the Korea Atomic Energy Research Institute based on the PMR 200 developed in Korea, and another, different multi-block flow test geometry was developed at INL's MIR facility based on the GT-MHR prismatic VHTR. The model based on the GT-MHR (Shultz et al.,

2012) was much more limited, consisting solely of the corner region between 3 prismatic fuel element blocks. Experiments were run on both geometries in addition to performing CFD analyses to determine the nature of the bypass flow. All of the experimental work was done using unheated sections (including the work done at INL on the geometry based on the GT-MHR), and attempted to enumerate pressure losses and flow rate in various bypass gaps (Schultz et al., 2012). The work done the groups (Schultz et al., 2012) determined that the helium bypass flow could be either laminar or turbulent, depending on the gap size, and that bypass gap flow preferentially traveled near the vertex points (where three fuel element blocks meet) in the bypass gaps. The experimental tests performed were then used to validate and improve upon the CFD modeling tools used, with these measures still ongoing (Schultz et al., 2012). The performed experimental tests allowed INL and KAERI to begin preliminary investigation of means for reducing the bypass helium flow in a typical VHTR core; they determined that three of the most promising means involved sealing the gaps at the fuel elements near the bottom of the core, staggering the fuel element arrangement within the core, and manufacturing grooves along the graphite reflector blocks to further reduce flow to them. As these measures develop, they may merit further investigation in future work depending on the test results.

2.7 Research needs

The prismatic core VHTR is based on a long history of design work on gas cooled reactors (Idaho National Laboratory, 2011a). The prismatic VHTR is the preferred choice of the NGNP project in the United States. The chosen design was based on the GT-MHR

design of General Atomics. This design is used as the baseline for the analyses, performed at the UNM-ISNPS and documented in the following chapters..

Some attempts have been reported in the literature to perform thermal-hydraulics analysis of the VHTR core and fuel elements, using varying simplifying assumptions and modeling approaches (See section 2.6). The large size of a VHTR core and the complexity of the helium flow in the core coolant channels, as well as accounting for the helium bypass flow in interstitial gaps between fuel elements and the helium bleed flow in the control rod channels makes modeling the core a very challenging task. In addition to the extensive need for advanced and fast supercomputing capabilities, a typical case could take a long time (weeks to months) to complete. Therefore, there is a need to develop and demonstrate effective computational tools and methodologies for performing future thermal-hydraulics and safety analyses of VHTRs. In addition to reducing the numerical meshing requirements and computational time, it is desirable to maintain acceptable accuracy of the results. Such computational tools and methodologies would be useful to the design optimization, operation and safety analyses of VHTRs. These needs are the focus of the performed research at UNM-ISNPS and documented in this Thesis. The numerical meshing techniques and options implemented in the course of demonstrating the effectiveness of the developed methodologies and performing thermal-hydraulics analysis of the VHTR fuel elements and core are detailed in the ensuing chapter.

Chapter 3 - Numerical codes, meshing, and methodology

Further needs exist to develop and validate effective computational methodologies for thermal-hydraulics analysis of VHTRs and to investigate the effects of the helium bypass flow in the interstitial gaps and control rod channels on the temperature distribution in the core. In addition to ensuring the accuracy of the results, such methodologies should effectively reduce the numerical meshing requirements and computational time to complete the analyses. A simplified analysis methodology for thermal-hydraulics analysis of a VHTR core and fuel elements is developed and validated in Chapter 4. This chapter presents the numerical meshing tools and options implemented in Chapters 4 and 5 for the analysis of the single channel module, VHTR fuel elements and VHTR 1/6 core. In addition to the computer codes and numerical meshing schemes used in those analyses, this chapter introduces the employed computational hardware.

During the course of the development of the VHTRs and HTGRs, many computer codes have been employed to model the thermal-hydraulics behavior of their reactor cores. An early work at INL used a simple code, POKE, in conjunction with a full 3-D finite volume code, RELAP5-3-D/ATHENA (Idaho National Laboratory, 2012). POKE is suitable for performing simplified thermal-hydraulics analysis of pre-specified regions of the core; in the case of the VHTR, each stack of fuel elements was modeled as a single region. This simplified treatment made it possible to carry out quick parametric analyses on flow characteristics, which could then be used in the input for a more detailed code like RELAP5-3-D (Idaho National Laboratory, 2012). RELAP5-3-D/ATHENA is the result of iteration on the original RELAP code used for analyzing nuclear reactor behavior in the 1950s (Idaho National Laboratory, 2012). RELAP5-3-D/ATHENA

specifically is an evolution of the RELAP5 code developed in the 1980s, and is a finite volume thermal hydrodynamics code with an integrated neutron kinetics package; it is used as the primary code for reactor analysis at Idaho National Laboratory. Recent work at INL focused on the verification and validation of RELAP5-3-D/ATHENA with the FLOTRAN package of ANSYS, which is a commercially available finite element code package. Results showed that the two codes produce comparable results (Carbajo et al., 2008). ANSYS is one of many codes used by industry and research organizations for smaller scale simulations.

Another code package that is gaining widespread usage within the nuclear industry for thermal-hydraulics simulations is STAR-CCM+ (CD-adapco, 2012). Pointer and Thomas (2010) at Argonne National Laboratory (ANL) have used STAR-CCM+ as part of a portfolio of codes to perform thermal-hydraulics simulation of a VHTR. Researchers at Idaho National Laboratory used STAR-CCM+ to validate its effectiveness for simulating experimental work done on flow modeling in the VHTR lower plenum (Johnson, 2009). Given the traction within the industry that STAR-CCM+ is gaining, combined with the increasing acceptance within academia, it was selected by UNM-ISNPS to perform the thermal-hydraulics analyses of the VHTR, documented in this Thesis. A summary of the primary features of the STAR-CCM+ code as well as a recount of the experience gained in the course of using this code are given next.

3.1 Numerical meshing and computer codes used in present research

STAR-CCM+, a commercial Computational Fluid Dynamics (CFD) code (CD-adapco, 2012), is a finite volume code that includes a suite of modeling options ranging from 1-D to 3-D. It offers options for simulating single phase, multi-phase, multi-

component fluid flow and convection heat transfer, in addition to heat conduction in solids. The physics models in this code are capable of handling both steady state and transient (both implicit and explicit) problems. In addition, STAR-CCM+ incorporates 3-D CAD capabilities for creating complex geometries. It also is capable of importing more complex 3-D models from other CAD programs such as Solidworks. For numerical analysis, STAR-CCM+ employs its own proprietary meshing schemes for discretizing the user's model into finite volumes for analysis. The materials properties can be selected from among those provided in the code or introduced by the user.

The different numerical meshing schemes in STAR-CCM+ code include polyhedral, tetrahedral, and trimmed square prisms, which are shown in Figs. 2.1(a), (b) and (c), respectively. The numerical mesh elements in Fig. 2.1 use the same base and target cell sizes and display the effect of the mesh type on the relative size and shape of the mesh elements or cells. In STAR-CCM+, the user's primary control is specifying the size of the numerical mesh element or cell. The user can specify the minimum cell size – that is, the lowest average distance across the cell – and the target cell size, best interpreted as the average effective diameter of the average cell in the mesh. In general, the size of the mesh elements will be on the order of the minimum cell size near interfaces and boundaries and grow to the target size away from the interfaces and boundaries. The order or the multiplier for the numerical mesh cells progressively to grow from the minimum to the target size is also specified by the user. A growth multiplier of 1 represents average growth, while higher growth multiplier will result in the cells growing to the target cell size almost immediately. A growth multiplier of less than 1 will result in each numerical mesh cell being much closer to the size of the proceeding cell near the

boundary, resulting in a longer distance to grow to the target cell size. By default, boundaries are meshed at the smallest cell size, but this is not recommended. Instead, the user may opt to use the optional prism layer meshing model in order to employ smaller cells that are better fit to simulating the heat transfer at a boundary or an interface.

The research detailed in the next three chapters employed the prism layer meshing model at the boundaries and interfaces between regions. This model is compatible with the various basic meshing elements shown in Fig 2.1. Recently, the prism layer meshing model has been made compatible with the tetrahedral mesher, an option that was not available in earlier versions of STAR-CCM+. This meshing model automatically conforms to the contours of the surface shape in order to produce a user-set number of prism layers. These prism layers can be seen easily in Fig. 2.1, where each of the examples employs the prism layer meshing model near the top boundary. In the prism layers, the numerical mesh cells get progressively (geometrically) smaller as they approach the boundary. The user can specify the number of layers, the total thickness of all the layers (up to an upper bound controlled by the code), and the growth multiplier from one layer to the next.

The present thermal-hydraulics analyses of the VHTR employed the polyhedral meshing model unique to STAR-CCM+, in conjunction with the prism layer mesher to properly treat the perpendicular heat transfer at common boundaries or surfaces. Although the prism layer mesher significantly increases the number of numerical mesh cells or elements in a simulation, it not only increases the accuracy of the results, but also helps concentrate numerical cells in the areas of interest, such as in the boundary layers and at common interfaces. The polyhedral meshing model is chosen for performing the

present thermal-hydraulics analyses based on extensive testing with the other two primary meshing models in the code.

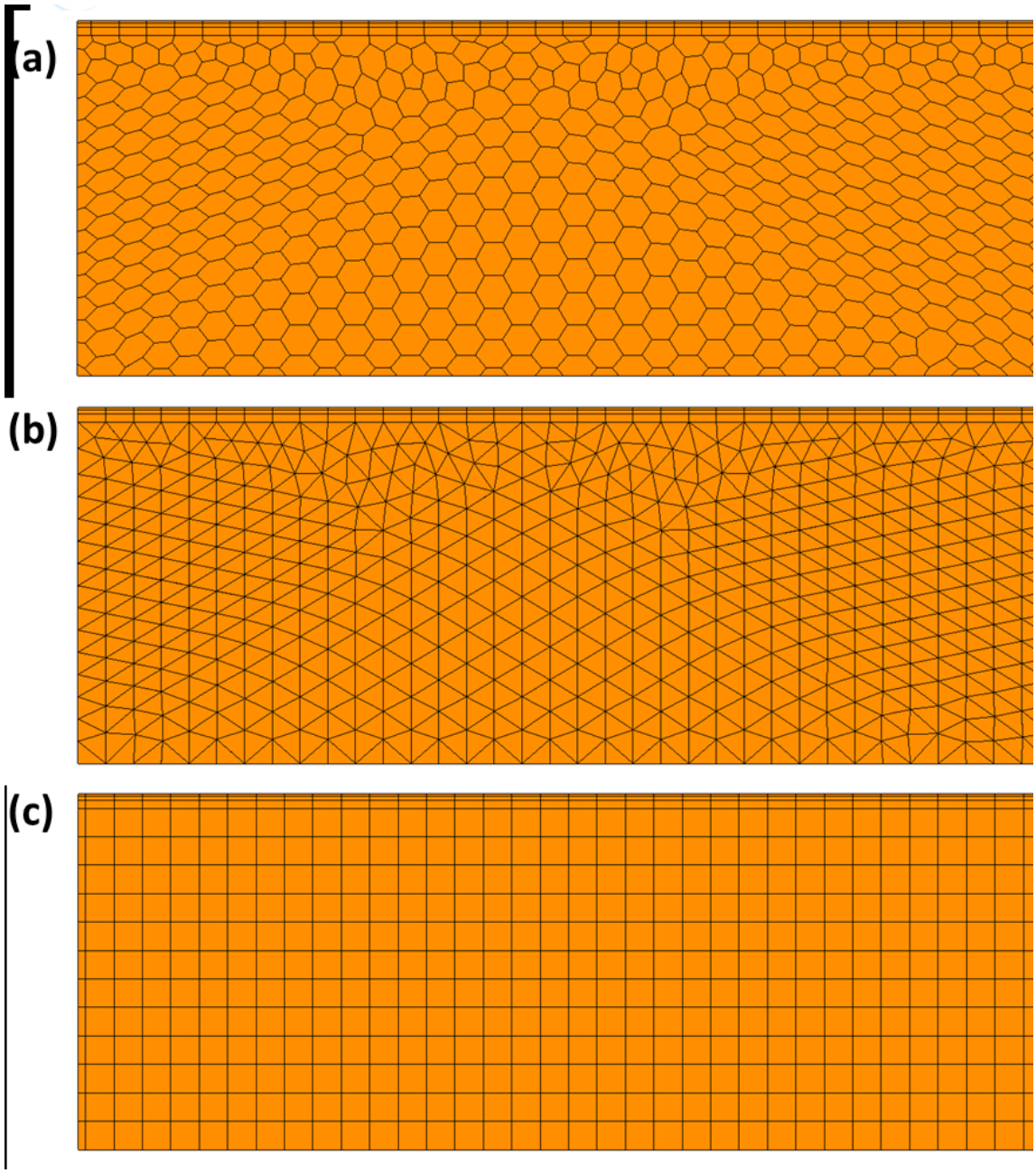

Figure 3.1 – Examples of (a) polyhedral, (b) tetrahedral, and (c) trimmer numerical meshing schemes in STAR-CCM+ (CD-adapco, 2012).

In general, the trimmer meshing model requires a larger number of cells to produce the same results as the polyhedral mesher. The tetrahedral mesher generally provides an inferior version of the polyhedral meshing model for the same number of cells. Even though the meshing models within STAR-CCM+ are highly sophisticated, some identified drawbacks encountered in the course of this research are enumerated on below.

Although the user can directly control the meshing scheme within the geometry of interest, this requires a significant time to carry out because each individual region within the geometry must be broken down into suitable subsections. Such a procedure is not practical for large and/or complicated geometries, like that of a VHTR 1/6 core, in which individual fuel rods and fuel elements need to be hand-detailed. Normally this is not an issue due to the extensive capabilities of the mesher, but the code has a limitation on the axial stretching of cells past a certain aspect ratio, unless more specific controls like the user-defined mesh are established. In the case of a single channel module (Chapter 4) or even the single fuel element block (Chapter 5) analyzed in this work, such controls are unnecessary because the default meshing tools achieve sufficient radial refinement in conjunction with some stretching in the axial direction. In the case of the full height 1/6 core analysis, however, a radially refined but axially coarse mesh is needed. In this case, the extruder meshing model is employed. The extruder model, which is an optional add-on that is usable with any mesh type discussed, takes a given surface and extrudes it into axial segments of the user's specified length in the normal direction. This model, although not originally intended for this type of use, but rather to extrude geometries like channel entrance regions, performs well. The STAR-CCM+ code also includes mesh refinement tools that automatically identify and remove or repair poor quality cells.

These tools are implemented in the current work, and executed as a part of the meshing utility without input. Specifics on each of the meshed geometries (sizes, number of prism layers, etc.) and their implementation can be found in the following chapters.

The STAR-CCM+ code incorporates various physics models for fluid flow, including those of primary concern for this work, turbulent flow simulation. Direct solution of turbulent models is not an option except in simple cases due to the unrealistically large amount of computational power required to directly solve the Navier-Stokes equations, so a model that makes adjustments to simplify the equations is required. STAR-CCM+ includes a reasonable number of options to model turbulent flows. For the problems considered in the current work, appropriate choices available in the code are the Reynolds-Averaged Navier-Stokes (RANS) approaches with a variety of different implementations, which include the following models: (a) K-epsilon; (b) K-omega; (c) Spalart-Allmaras; and (d) Reynolds Stress Turbulence. Of those models, the realizable two-layer k-ε model is employed in the present research, based on the testing results presented in Appendix B and the findings of Pointer and Thomas (2010) and Sato et al. (2010). More information on turbulence modeling in the thermal-hydraulics analyses in this research can be found in Appendix B.

All thermal-hydraulics analyses conducted in this work are for steady-state operating conditions. The analyses reported in Chapters 4 and 5 of this document are conducted using STAR-CCM+ versions 5.02, 5.04, 6.04, 7.02, and 7.04. The code version was changed to the most current release once the stability and suitability of the newest version was determined.

This research also used Solidworks 2006 SP version 4.1 in order to produce the design of the parts of the VHTR core modeled in STAR-CCM+. Solidworks is a standard CAD package (Solidworks, 2006) that is capable of generating full 3-D models to the user's specifications. These models can be exported to various CFD packages, including STAR-CCM+. Exporting models in this work is done using the STEP 214 file protocol (CD-adapco, 2012). These codes are implemented on the employed computer hardware at UNM-ISNPS, discussed next.

3.2 Computer hardware

The commercial software codes discussed above are implemented on a number of different physical machines at UNM-ISNPS. Thermal-hydraulics analyses are conducted on a pair of server nodes acting independently. Both nodes use the 64-bit Windows Server 2007 operating system, and have two, 2.27 GHz quad-core Intel Xeon processors each. One of the nodes used for less intense simulation (most of the work in Chapter 4) has 24 GB of registered RAM. The other node, used primarily for the work in Chapter 5, has 48 GB of registered RAM.

These machines are roughly equivalent to modern desktop workstation hardware with the exception of the installed RAM, which is significantly more than an average workstation. Due to the nature of the STAR-CCM+ code as a finite volume solver, the intensity of the numerical meshing directly impacts the memory requirements for the simulations. The most intense numerical mesh grids, like those used in the VHTR 1/6 core analyses, heavily taxed not only the installed RAM but also the virtual memory (with up to 114 GB of total memory usage), significantly slowing down the calculations. Such a slowdown can be mitigated by running entirely on the faster physical flash-based

RAM. Even with the capabilities of the aforementioned hardware, thermal-hydraulics analyses of the VHTR core and fuel elements remained a challenging task. The next chapter discusses the basis for developing an effective methodology for conducting such analyses using a less intense numerical mesh grid and hence requiring a shorter time to complete the calculation.

Chapter 4 - A Simplified thermal-hydraulics analysis methodology

As discussed earlier, a means of simplifying the process of modeling the VHTR would be helpful in furthering efforts to evaluate the design of the reactor. A simplified modeling approach that involves using 3-D conduction in the graphite and fuel compact regions and 1-D convective helium gas flow in the coolant channel to replace the 3-D simulation of the gas is presented in this chapter. The 3-D computational fluid dynamics simulation of the helium coolant flow in the coolant channels of a VHTR adds greatly to the number of numerical mesh elements and the time needed to complete a thermal-hydraulics analysis of the reactor core. The simplified methodology with a 1-D flow using a convective heat transfer correlation serves as a surrogate replacement of a full 3-D CFD simulation in the coolant channels.

4.1 Procedures for developing a convection heat transfer correlation

The numerical calculations needed to develop a turbulent convection heat transfer correlation for the helium flow in the VHTR coolant channels are carried out using a 3-D numerical analysis of a single coolant channel fuel module (Fig. 4.1). The thermal-hydraulics analysis of this module is performed using the STAR-CCM+ commercial software. Once converged, the results of the analysis are used to develop a Nusselt number correlation in terms of the helium coolant flow Reynolds number and Prandtl number. The helium properties in these dimensionless numbers are evaluated at the local coolant bulk temperatures. The determined quantities in the full 3-D thermal-hydraulics analysis of the single channel fuel module are: the local heat flux, q'', the wall and helium bulk temperatures, T_w and T_b, respectively, and the helium coolant flow rate, $\dot{m}$. These quantities, in conjunction with knowledge of the temperature dependent material

properties (presented in Appendix A) are used to calculate the local values of the convective heat transfer coefficient, *h*, and the values of the following dimensionless quantities as:

$$h = \frac{q''}{(T_w - T_b)} \tag{4.1}$$

$$\mathrm{Re} = \frac{4\,\dot{m}}{\pi\, D\, \mu_b} \tag{4.2}$$

$$Nu = \frac{hD}{k_b} \tag{4.3}$$

4.2 Review of other turbulent convection correlations

Tak et al. (2008, 2010) investigated a method closely related to the methodology developed in this chapter (using a 1-D correlation as part of a system code). They used the fully developed Nusselt correlation of Dittus-Boelter (1930) to determine the local heat transfer coefficient of the helium flow inside a coolant channel of a prismatic fuel element block. The Dittus-Boelter correlation, given as:

$$Nu_{FD} = 0.023\, \mathrm{Re}_b^{0.8}\, \mathrm{Pr}_b^{.4}, \tag{4.4}$$

is applicable for $0.7 \leq \mathrm{Pr_b} \leq 160$, $\mathrm{Re_b} \geq 10{,}000$, $z/D \geq 10$ and for a small temperature rise in the boundary layer, with the fluid properties evaluated at the bulk flow temperature. Dittus-Boelter's correlation is widely used for pipe flow and has proven to be relatively accurate, given that the conditions are satisfied by the problem being modeled. The correlation however, does not account for the effect of flow mixing at the entrance of the coolant channel. In the case of the VHTR, this is not valid near the entrance of the active

core. Even so, the results of Tak et al. demonstrated a substantial reduction in the computation time compared to using a 3-D CFD simulation for the entire simulation (Tak, 2008).

The Seider-Tate correlation (1936) is also intended for fully developed turbulent convection in circular tubes, but with large differences between the wall and the bulk fluid temperatures. It does not account for the effect of the entrance mixing and is applicable for the same range of parameters as the Dittus-Boelter correlation (1930). The Seider-Tate correlation is given as:

$$Nu_{FD} = 0.023\,\mathrm{Re}_b^{0.8}\,\mathrm{Pr}_b^{1/3}\left(\mu_b/\mu_w\right)^{0.14} \qquad (4.5)$$

Other forms of this correlation have been reported with a larger coefficient of as much as 0.027 (McEligot et al., 1965). This correlation is valid for $1.0 \times 10^4 \leq \mathrm{Re} \leq 5.0 \times 10^5$, $0.67 \leq \mathrm{Pr} \leq 100$ and $0.0044 \leq (\mu_b/\mu_w) < 9.75$. At lower film temperatures, the last term on the right hand side is almost unity and this correlation becomes that of Dittus-Boelter with a different Prandtl exponent. The Seider-Tate correlation, unfortunately, does not account for any entrance effects, and is therefore only functional for fully developed flow.

Better correlations exist that do account for the effect of entrance mixing on the local convective heat transfer coefficient of gas: the correlations of Taylor (1967) and McEligot et al. (1965) are based on experimental heat transfer data for turbulent gas and liquid flows in uniformly heated tubes. They account for the effects of both entrance mixing and the relative changes in the fluid viscosity at the wall, μ_w, and in the bulk flow, μ_b. Thus, these correlations are more applicable to conducting the 1-D analysis of the

helium flow in the coolant channels of a HTGR or VHTR. However, their predictions of the values of local heat transfer coefficients in the entrance length of the coolant channels in the heated core section for fully developed turbulent convection and of the length of the entrance region could differ by as much as 20%; more on this will be expounded on in section 4.3. Furthermore, these correlations have not been validated for a non-uniform axial thermal power profile, similar to that in the active core of a HTGR or VHTR.

A representative correlation for turbulent convection of helium in the coolant channels of a HTGR or VHTR core, including the entrance mixing length, is developed in this chapter and validated using experimental data and a full 3-D CFD analysis of the single coolant channel module. This correlation also accounts for the effects of the non-uniform axial fission power profile in a HTGR or VHTR core and the changes in the properties of graphite, fuel compacts and helium gas with temperature along the coolant channel.

4.3 CFD modeling and development of a convective heat transfer correlation

To develop a representative correlation in order to determine the local turbulent convection heat transfer coefficient for helium gas flow in the VHTR coolant channels, this thesis uses a single flow channel module (Fig. 4.1). The data used to develop this correlation are obtained by coupling the 3-D conduction in the graphite and fuel compacts with a full 3-D simulation of the helium coolant in a central flow channel of the hexagonal unit channel module (Fig. 4.1). Fig. 4.1 highlights the unit channel module, which is 8.0 m tall, similar to the active core of a VHTR, and has a central helium flow channel surrounded by a hexagonal section of graphite and 6, 120 degree sections of the fuel compacts; the coolant channel also penetrates the 1.2 m and 0.8 m thick graphite

reflector on top and bottom. Heating in these regions is neglected as it is significantly lower than the heating in the active core.

This single flow channel module can be applied to rectify an entire fuel element in n HTGR or VHTR core, except those near the central handling hole (Fig. 2.4), or the control element holes in other elements. Of the many divisions possible, the one used in the present analysis (Fig. 4.1) is the smallest and self-contained; when repeated it provides a fair representation of the fuel elements. A triangular sector that is 1/12 the size of the single channel module in Fig. 4.1 and 4.2 is also capable of replicating the fuel elements (Fig. 2.4) via symmetry, but does not contain an entire coolant channel. The single channel module is applicable to both symmetrical and non-symmetrical geometrical or power loading conditions. The 3-D numerical thermal-hydraulics analysis of the single channel fuel model is performed using the STAR-CCM+ commercial software package, discussed in Chapter 3.

In addition to the fully developed entrance region, this analysis must account for increased flow mixing at the entrance of the heated section of the flow channel, primarily due to the abrupt switch from the negligibly heated top graphite reflector (less than 1 K temperature rise in the coolant channel) to the heated active core. The performed thermal-hydraulics analysis accounts for changes in material properties with temperature. Material properties that change include those of the graphite, helium gas and the constituent materials of the fuel compacts, and are listed in Appendix A (Table A.1). The thermal-hydraulics analysis also accounts for the effect of the axial fission power profile in a VHTR core, namely by using both a constant and chopped-cosine axial profiles with the same total power generated.

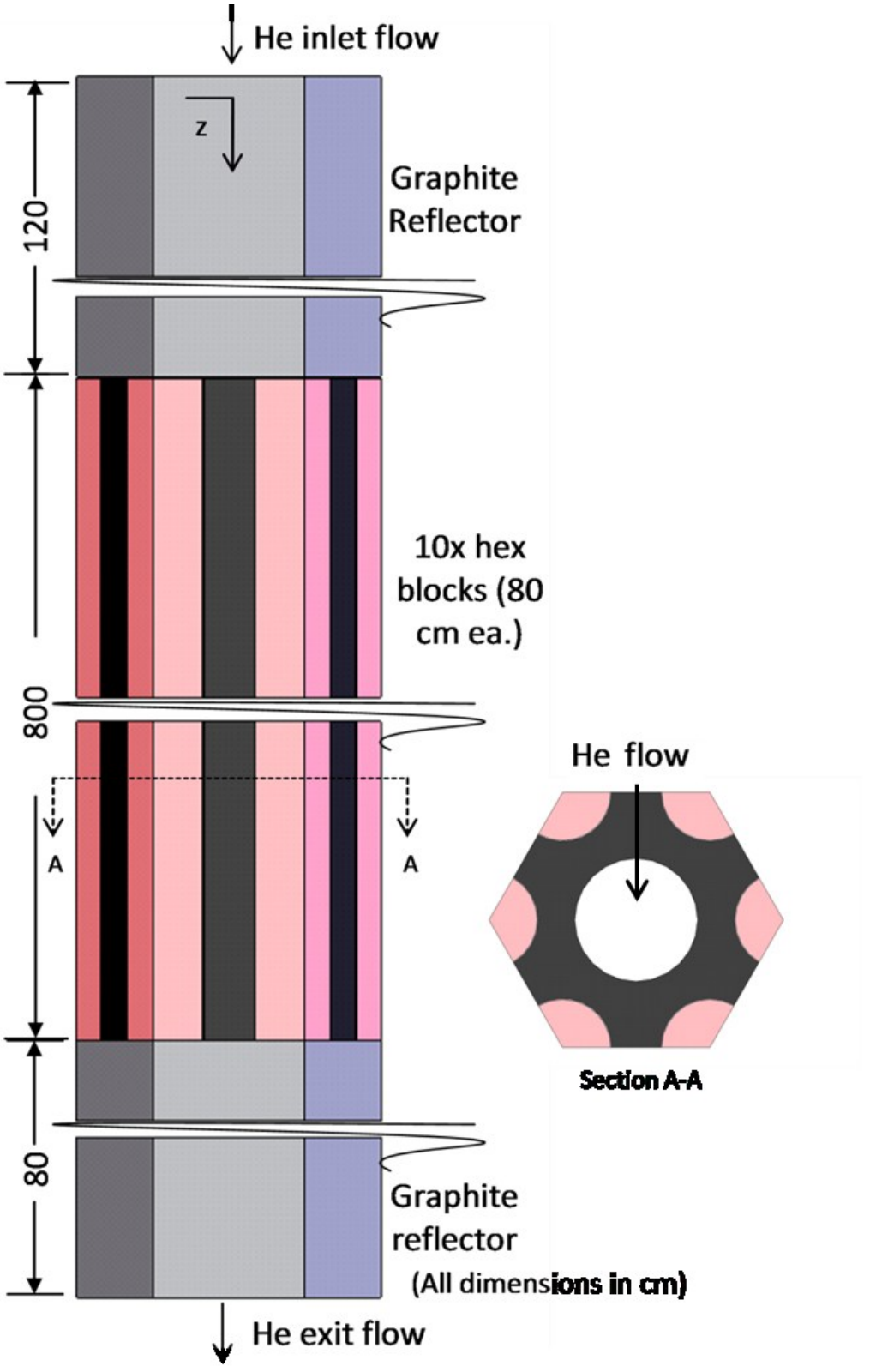

Figure 4.1 - Axial isometric view and a radial cross-section of the single channel fuel module.

The heat in the middle section of the single channel module (Fig. 4.1) is provided by the thermal power generated in the 120 degree segments of the 6 stacks of fuel compacts at the corners of the module. Figure 4.2 shows these segments in a cross-sectional view of the single channel module. Although in the actual reactor, the stack of fuel compacts does not extend the full length of the core (each stack of compacts is ~78.15 cm long and each fuel element is 79.3 cm long), the performed thermal-hydraulics analysis models the stacks of fuel compacts as one contiguous 8.0 m long fuel compact, in order to simplify the numerical meshing by reducing the size/number of interfaces. The heat generation rate in the compacts is kept constant by reducing the volumetric heat generation rate commensurate with the increase in size of the fuel compacts. The employed boundary conditions in Fig. 4.2 are as follows: the outer surfaces of the graphite and fuel compacts are assumed adiabatic, while the interfaces between graphite and fuel and graphite and coolant are assumed negligible resistance contact interfaces. The top and bottom surfaces of the graphite reflector regions in Fig. 4.1 are also assumed adiabatic.

The 1.2 m long section of the coolant channel in the top graphite reflector ($L/D > 75$) is more than adequate for the helium flow to become hydrodynamically fully developed before entering the heated core region. However, the axial conduction from the core to the top graphite reflector block and the large heating rate in the heated core causes the helium flow entering the core to no longer be thermally or hydrodynamically fully developed. The flow mixing in the entrance length of the helium coolant channels in the core increases the local heat transfer coefficient. Such an effect decreases gradually with increased distance from the entrance to the coolant channels in active core and eventually diminishes as the helium gas flow becomes fully developed.

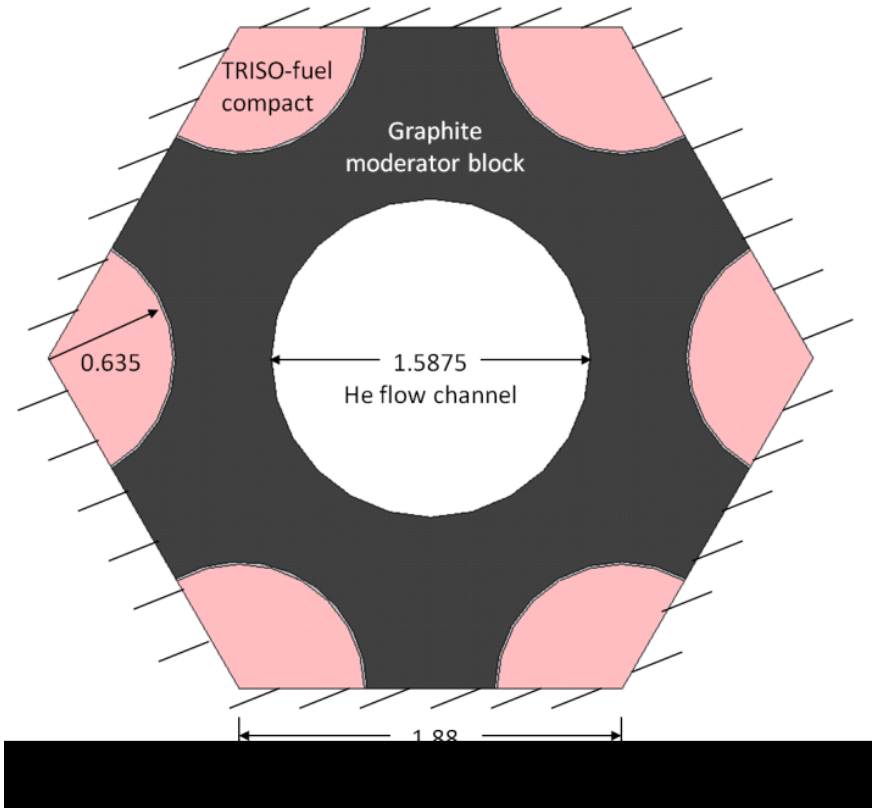

Figure 4.2 - Radial cross-section cutaway view of the single channel module.

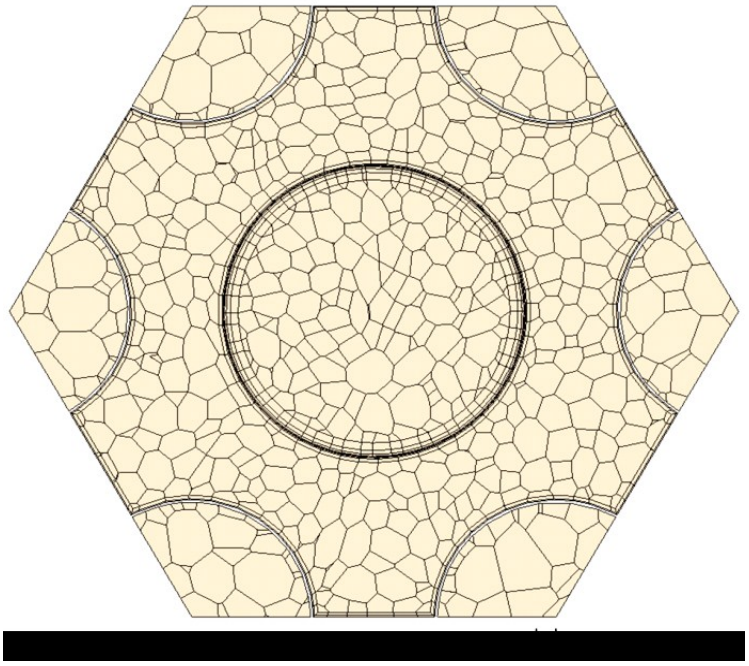

Figure 4.3 - Mesh employed in the thermal-hydraulics analysis of the channel module.

The local values of Nusselt number in the helium coolant channel are collated and formulated into a dimensionless correlation for the local Nusselt number (Nu) as a function of the local bulk Reynolds number (Re_b), local bulk Prandtl number (Pr_b) of the helium coolant flow. Helium properties used in the correlation are evaluated at the calculated local helium bulk temperature. The developed turbulent convection correlation is compared to those of Taylor (1967) and McEligot et al. (1965) and to the results of the full 3-D thermal-hydraulics numerical analysis of the single channel fuel module (Fig. 4.1). This correlation is to be used as a surrogate of a full 3-D CFD simulation of the helium gas flow in the coolant channels of a prismatic core HTGR or VHTR.

The simplified thermal-hydraulics analysis methodology that employs the developed Nusselt number correlation couples the 3-D heat conduction in the graphite and fuel compacts to a 1-D helium gas flow in the coolant channels of a VHTR. The accuracy as well as the effectiveness of this methodology for reducing the meshing requirement and computation time of the thermal-hydraulics analysis of a single channel fuel module are investigated in this chapter. Since the developed correlation is based on 3-D numerical results for a wide range of helium gas flow rates, it is used for the thermal-hydraulics analysis of a full height VHTR 1/6 core in Chapter 5.

4.4 Numerical meshing

The single channel module used the polyhedral meshing model native to STAR-CCM+ (a finite volume code) by way of an imported CAD model of the module from Solidworks. Due to the small dimensions of the single channel module in the radial direction (compact radius of 0.635 cm and flow channel radius of 0.79375 cm) compared to the very long axial dimensions (1.2 m top axial reflector + 8.0 m active core + 0.8 m

bottom axial reflector = 10 m), the meshing model ensures that the numerical mesh cells do not become distorted in the axial direction, and are not too large. Fig. 4.3 displays the numerical mesh implemented in the performed thermal-hydraulics analysis of the single channel module with a full 3-D simulation of the helium flow in the channel.

A fine numerical mesh grid is implemented in the 3-D analysis (Fig. 4.3). It contained a total of 6.67 million cell elements, 4.12 million of which reside in the graphite block and fuel compacts for simulating the 3-D heat conduction, and 2.07 million of which are used in the CFD simulation of the helium flow in the central channel. An additional 480,000 numerical mesh elements are located in the reflectors. A less refined numerical mesh grid is also used with little effect on the solution convergence and the accuracy of the results. The unrefined grid employed a total of 4.67 million cell elements, 2.62 million of which in the graphite and fuel compacts and 1.60 million of which are in the helium flow channel. The results showed a difference of < 0.1% in the calculated values of the wall, T_w and helium bulk, T_b temperatures and in the heat flux at the wall of the flow channel, compared to those calculated with the finer mesh grid of 6.67 million mesh elements. When a coarser numerical mesh grid of 2.55 million cell elements (1.08 million in the graphite block and fuel compacts and 1.06 million in the flow channel) is used, the numerical solution did not converge. In the present 3-D thermal-hydraulics analysis, it appears that a mesh grid of at least 2.6 million elements in the graphite and the fuel compacts of the module (Fig. 4.1) and 1.6 million mesh elements in the helium flow channel are required to achieve complete convergence.

As Fig. 4.3 shows, the implemented numerical mesh grid employs prism layers along interfaces in order to better simulate heat transfer at the interfaces and increase the

accuracy and resolution of the calculations. These prism layers form concentric circles around and inside the channel to better track the heat flow perpendicular to the interfaces while also retaining a set of radially uniform layers in the boundary layer at the channel wall. The refinement in these layers assists in accurately modeling the heat flow in the boundary layer.

A number of different numerical meshing schemes are used in the prism layers (in conjunction with the mesh sensitivity analysis discussed earlier) before settling on the one seen in Fig. 4.3. The employed meshing scheme uses five prism layers near the channel wall with a total thickness of 0.8 mm with a total thickness ranging from 0.1 mm to 1 mm. Mesh grids with as many as six and as few as four prism layers are also used. Four prism layers often proved insufficient for adequately simulating the boundary layer along the wall, unless the mesh size within the rest of the flow channel is decreased, compared to when using five or six prim layers. Increasing the number of prism layers beyond 6 has little effect on the calculated results, but increases the total number of numerical mesh elements in the calculations. A total prism layer thickness of 0.8 mm is chosen to increase the total size of the prism layers to best capture heat transfer through the boundary layer in the region near the wall. Increasing the number of prism layers and their thickness beyond the set limits in the code could cause difficulty in numerical meshing. STAR-CCM+ limits the total thickness of prism layers near the wall, which if exceeded, the code could create “false” prism layers or mesh elements having “negative volumes”, resulting in a corrupt meshing to start the numerical simulation. The user’s selected setting in the prism layers affects the numerical meshing as well as the fidelity of the results. The proper setting depends on the nature of the problem, thus the user may

wish to experiment with the different schemes to assess the fidelity on the calculations and the effect on the size of the numerical mesh grid and the time to complete the calculations.

The meshing elements in the prims layers near the wall or interfaces are the smallest anywhere in the implemented numerical grid, with a size of 0.08 mm at the interfaces, growing to an average cell size of 1.2 mm across near the center of the channel. The size of the numerical mesh elements in the axial direction is larger, up to 6 mm. In the numerical grid, the aspect ratio of the mesh elements is an important consideration that needs to be investigated by the user, depending on the nature of the problem. For the numerical grid used in the single channel module analysis, most mesh elements in the center of the coolant channel have an aspect ratio of ~ 2, a few elements in the center of the channel have an aspect ratio as high as 3 and most elements in the prism layers near have an aspect ratio of 5 or higher. Although these aspect ratios could be smaller in the prism layers, which would significantly increase the size of the numerical mesh grid and the computation time, the values used in the present analysis are a good compromise between accuracy in the results and computation time.

Meshing in the fuel compacts and graphite region is somewhat more relaxed (Fig. 4.3). In the fuel compacts, the smallest mesh size used is 1.5 mm across; the mesh elements average 6 mm in length. The size of the numerical mesh elements in the graphite are even larger, with a maximum size of 10 mm away from the interfaces with the fuel compacts and the coolant channel, where the prism layer meshing model is employed. The mesh used in Fig. 4.3 is the primary mesh used in the following section for the results.

The numerical simulation is deemed converged when a set of criteria is satisfied: (a) the normalized residual of the overall energy balance reaches or drops below 10^{-4}; (b) the residuals of the momentum balances in the three primary coordinates in the flow channel (x, y, and z) and of the two turbulence transport variables ($T_{ke,}$ the turbulent kinetic energy and $T_{dr,}$ the turbulent dissipation rate) reach or drop below 10^{-5}; (c) the average rates of the change in the values of the above residuals approach zero (i.e., the residuals flat line); and (d) the changes in successive iterations of the values of select variables (the helium gas bulk temperature near the inlet of the heated section of the flow channel, the gas bulk temperature near the exit of the channel and the wall surface temperatures at 4 locations along the heated section of the channel) are $\leq$ 0.01 K.

Table 4.1 - Operational parameters for single channel module

Parameter:	**Value**
Helium temperature entering the coolant channel (K)	914
Helium inlet pressure (MPa)	7.07
Nominal helium mass flow rates:	
- Reactor core total (kg/s)	330
- Single channel fuel module (Fig. 4.2) (kg/s)	0.0306
Total thermal power input to the single channel module (kW_{th}) (Fig. 4.2)	55.4

4.5 Results and discussion

Operational parameters used in the thermal-hydraulics analysis of the single channel module are listed in Table 4.1. Numerical simulations used a 3-D CFD model in the coolant channel with mass flow rates ranging from 40 to 100 percent of the nominal flow rate with no bypass in the VHTR core. These flow rates correspond to a maximum local

Mach number of approximately 0.05 for Helium at these conditions, and thus the flow can safely be assumed incompressible. The thermal power profile for the fuel compacts in Table 4.1 corresponds to a total VHTR thermal power of 600 MW_{th}, and assumes that the channel being modeled receives an amount of power equal to that of an average channel in the VHTR.

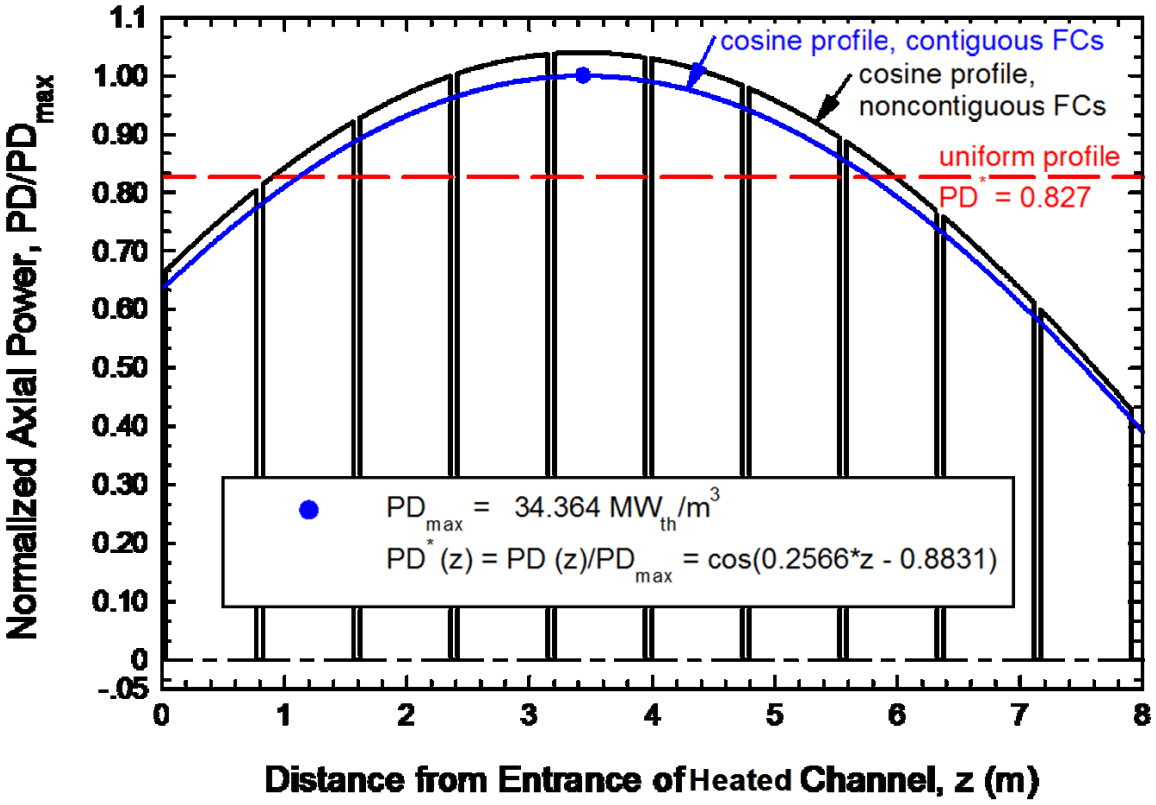

Figure 4.4 - Axial power profiles in the thermal-hydraulics analysis of the single channel fuel module.

Fig. 4.4 shows the chopped-cosine axial and constant power profiles used in the thermal-hydraulics analysis of the single channel module and separately references the actual power profile with gaps in the fuel compacts in the VHTR core. The maximum power density in the chopped-cosine axial profile is 34.364 MW_{th}/m^3, at 3.44 m from the entrance of the active core. The constant and chopped-cosine power profiles will be used

in the thermal-hydraulics analysis of the unit channel module to evaluate their effect on the calculated temperatures and the values of Nu along the coolant channel.

Figure 4.5 compares the calculated local axial wall and helium bulk temperatures in the heated section (8 m) of the flow channel in the module in Fig. 4.1. For both axial power profiles (Fig. 4.4), the total heat removed by the helium flow in the central channel is identical and thus so is the exit helium bulk temperature, T_b, in Fig. 4.5; in addition the local wall and helium bulk temperatures are very similar in the first 1/3 of the heated section of the flow channel. They are higher for the chopped-cosine axial power profile in the remainder of the channel, except near the exit where the temperatures are slightly lower than for the uniform axial power profile. On the other hand, the differences between the local wall and helium bulk temperatures (T_w - T_b) along the heated section of the flow channel are almost identical for both axial power profiles. Thus, the effects on the local values of the turbulent convection heat transfer coefficient and Nu are also small (Figs. 4.6 and 4.7). The results of the 3-D thermal-hydraulics analysis of the single channel fuel module show that the entrance length in the heated section of the channel is z/D = 25. Beyond this length, the convective turbulent heat transfer coefficient the heated channel becomes fully developed, and thus independent of the axial location. For z/D > 25, the obtained values of the local wall and helium bulk temperatures and of the local wall heat flux, using both the uniform and chopped-cosine axial power profiles, are used to determine the local values of the heat transfer coefficient and Nusselt numbers, Nu_{FD}, for fully developed turbulent convection. The values of Nu_{FD} are correlated in terms of local Reynolds, Re_b, and Prandtl, Pr_b (Fig. 4.6).

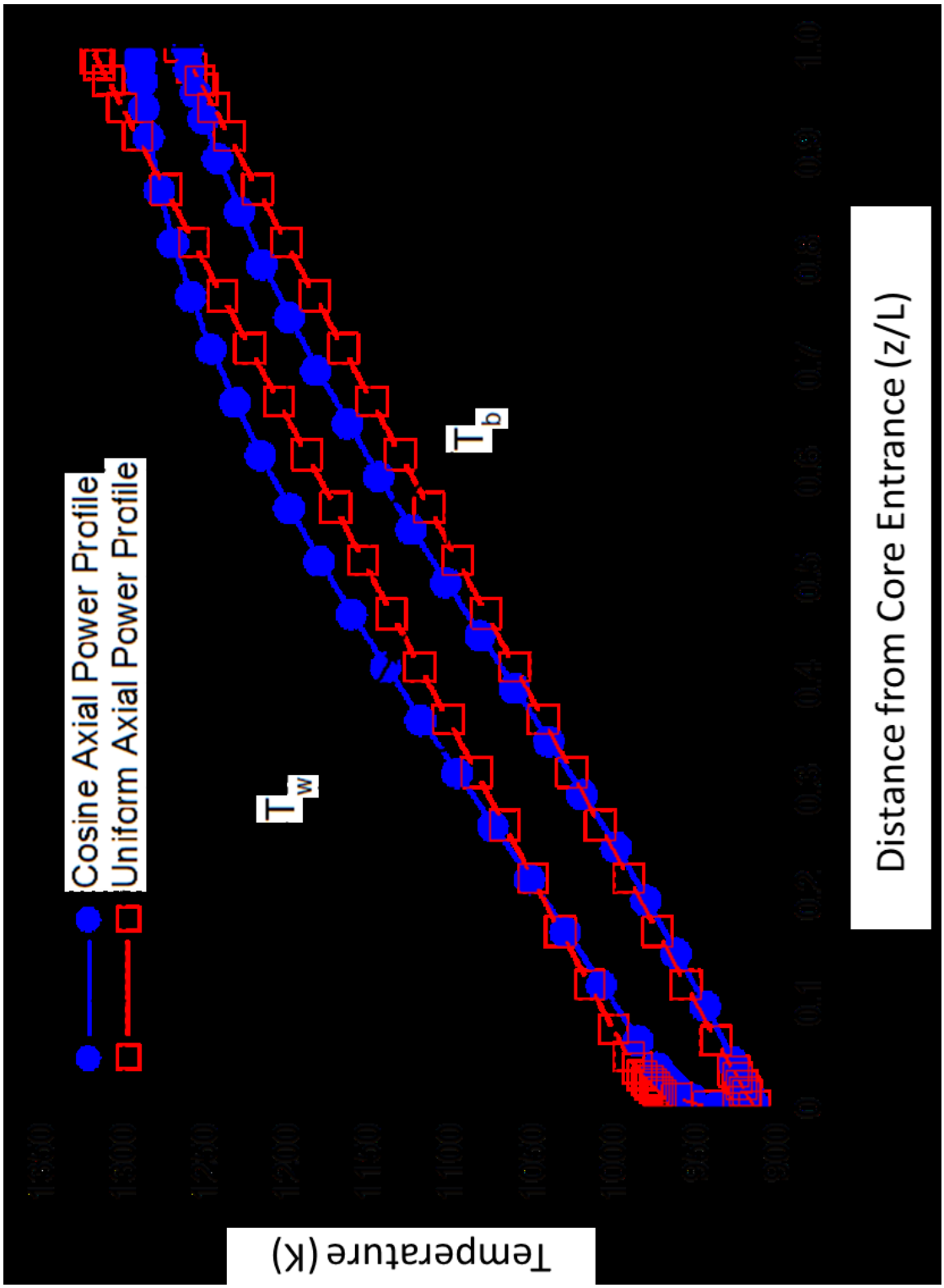

Figure 4.5 - Comparison of temperature profiles as a function of power profile for the single channel module analysis.

4.5.1 Developing the turbulent Nusselt number correlation

This subsection presents and discusses the developed correlation for turbulent convection in the coolant channels of VHTR core. Fig 4.6 shows the calculated values of local Nusselt Number for fully developed turbulent convection, Nu_{FD}, in the heated channel where z/D >25. The values of Nu_{FD} are insensitive to the axial power profile used in the 3-D thermal-hydraulics analysis of the single channel module. The developed correlation of Nu_{FD}, for z/D >25 is given as:

$$Nu_{FD} = 0.11\,\mathrm{Re}_b^{0.646}\,\mathrm{Pr}_b^{0.4} \tag{4.6}$$

This correlation is within $\pm$ 3% of the values calculated from the present analysis for bulk Reynolds numbers ranging from 22,000 to 58,000 and $0.64 \leq \mathrm{Pr} \leq 0.68$.

For the values of Nu used to develop the correlation in Eq. 4.6, the temperature difference between the film and bulk temperatures are between 40 and 60 K, for which the Dittus-Boelter correlation (Eq. 4.4) is not valid. Instead the Seider-Tate correlation (Eq. 4.5) is used for comparison in the fully developed region only, as it does not account for the entrance mixing. The present thermal-hydraulics results for fully developed turbulent convection (Eq. 4.5) are in disagreement with the correlation of Seider-Tate (Eq. 4.5) by up to 13%, of Taylor (1967) (Eq. 4.7a) by up to 11% and of McEligot, et al. (1965) (Eq. 4.8a) up to 20% (Fig. 4.6). Differences of 10 to 20 percent, however, are in line with the differences between the correlations and the data reported by McEligot and Taylor (Taylor, 1967; McEligot et al., 1965). Such differences are particularly important since they are largest at the values of Re_b (~40,000 to 56,000) in the VHTR coolant channels during nominal operation.

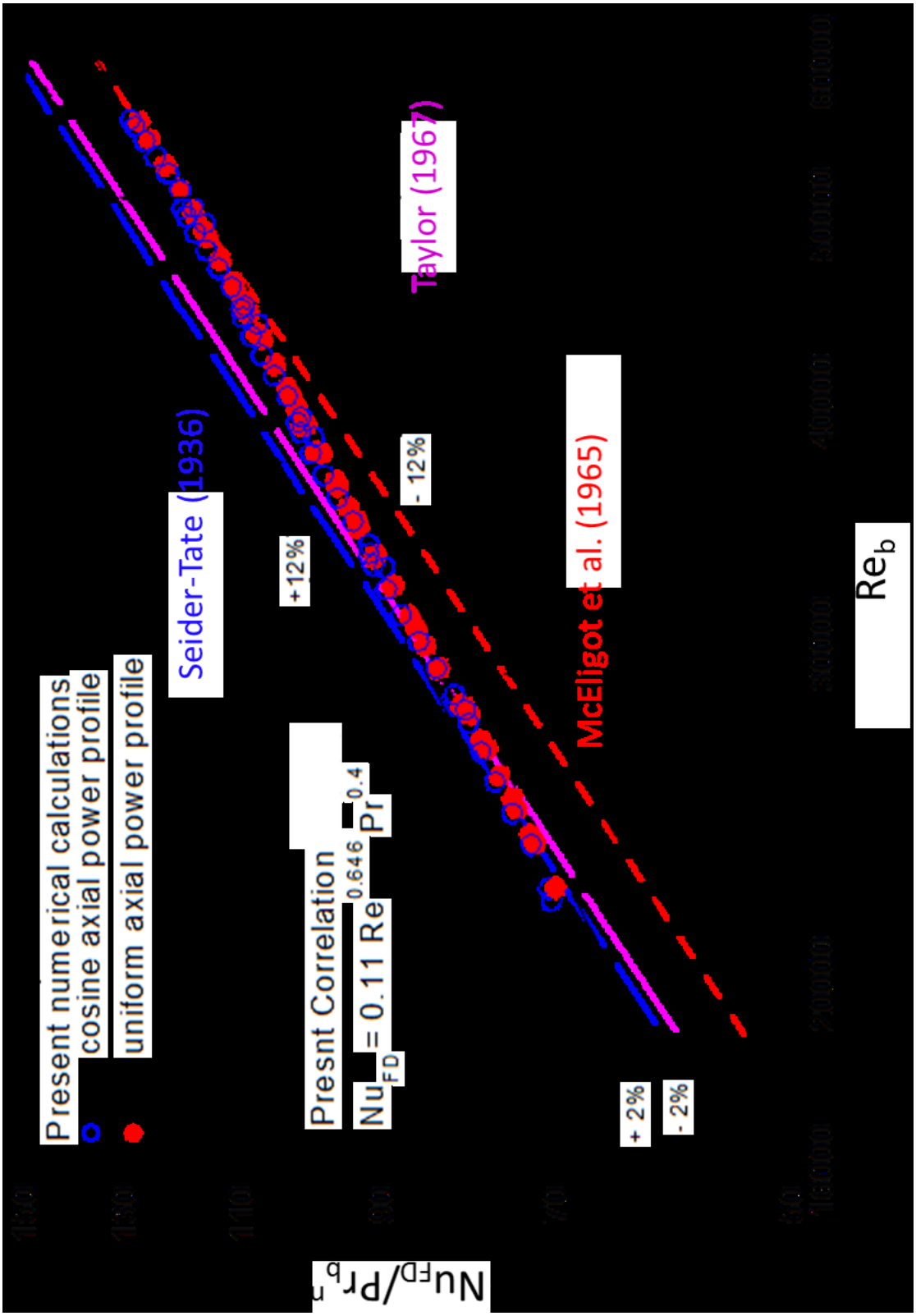

Figure 4.6 – Comparison of the fully developed turbulent convection data for reported correlations with the correlation developed in this work (Eq. 4.6).

The increased mixing at the entrance of the heated section of the flow channel (8.0 m) increases the local heat transfer coefficient and the Nusselt number. When the helium flow enters the channels in the active core, it is hydrodynamically developed, but thermally developing due to the sudden influx of heat. Such mixing and the resulting increase in the local Nusselt number decrease gradually with increased axial distance from the entrance of the heated channel section. The effect of the entrance mixing diminishes as the helium flow becomes hydrodynamically and thermally fully developed. The local values of the turbulent convection heat transfer coefficient and Nu approach those for fully developed turbulent convection when z/D $\geq$ 25 (Fig. 4.7).

Taylor's correlation in its entirety does a reasonable job of capturing the entrance effect measured in the channel. Taylor's correlation (1967) for fully developed turbulent convection in uniformly heated circular tubes is given as:

$$Nu_{FD} = 0.023\,\mathrm{Re}_b^{0.8}\,\mathrm{Pr}_b^{0.4}\,(T_w/T_b)^{-0.57} \tag{4.7a}$$

$$Nu = Nu_{FD}\left[T_w/T_b\right]^{-[0.57-1.59/(z/D)]} \tag{4.7b}$$

This correlation developed for hydrogen gas flow at high temperatures is valid for 7.3 x10^3 $\leq$ Re $\leq$ 1.3 x 10^7, 0.71 $\leq$ Pr $\leq$ 10.0 and 1.1 $\leq$ (T_w/T_b) < 27.6. The last term on the right hand side of Eq. 4.4a, similar to that in Eq. 4.5, accounts for the changes in the fluid viscosity in the boundary layer by placing greater emphasis on the ratio of the local wall and bulk temperatures. As the flow progresses down the channel and becomes fully developed, the corrective entrance term, the second on the right side of Eq. (4.7b) approaches unity and the correlation becomes identical to that of Dittus-Boelter. Taylor's correlation has never been validated for helium gas at VHTR operation conditions.

The correlation of McEligot et al. (1965) for fully developed turbulent convection in uniformly heated circular tubes is given as:

$$Nu_{FD} = 0.021\,\mathrm{Re}_b^{0.8}\ \mathrm{Pr}_b^{0.4}\ (T_w/T_b)^{-0.50} \tag{4.8a}$$

$$Nu = Nu_{FD}\ \left[1 + (z/D)^{-0.70}\right]. \tag{4.8b}$$

Similar to equation (4.5), the last term on the right hand side of Eq. (4.8a) accounts for the changes in the fluid viscosity at the heated wall, with an emphasis on the ratio of the local wall and fluid bulk temperatures. The second term on the right hand side of Eq. (4.8b) accounts for the effect of flow mixing on the local heat transfer coefficient in the entrance length of the coolant channel. For helium gas flow, Equation (4.8b) is valid for $1.64 \times 10^4 \leq \mathrm{Re} \leq 6.05 \times 10^5$, $0.65 \leq \mathrm{Pr} \leq 0.68$ and $1.0 \leq (T_w/T_b) < 2.12$.

Fig. 4.6 and 4.7 compare the developed correlation with the correlations of McEligot and Taylor. The developed correlation in its entirety is given as:

$$Nu = Nu_{FD}\ \left[1 + 0.57\, e^{-0.20 z/D}\right]. \tag{4.9}$$

The second term on the right-hand side accounts for the entrance effect and approaches zero as the flow progresses down the channel. The correlation in Eq. (4.9) is compared with Taylor's correlation in Fig. 4.7. The two correlations compare favorably, although variance in the numerical calculations near the entrance of the channel cause some slight scatter in the determined local values of the heat transfer coefficient and Nusselt number.

Figure 4.7 shows that the developed correlation (Eqs. 4.6 and 4.9) is in excellent agreement with the 3-D numerical results to within $\pm$ 2%, for both the uniform and chopped-cosine axial power profiles. Although Taylor's correlation (Eq. 4.7) captures the

trend of the present numerical calculations at the entrance of the heated section of the helium flow channel, its predictions are as much as 20% lower than the present numerical results. Equation (4.7b) also predicts that the entrance mixing effect diminishes within a shorter distance into the flow channel (~ $z/D \geq 10$), compared to $z/D \geq 25$ for the present 3-D numerical thermal-hydraulics results and correlation (Fig. 4.7).

The correlation of McEligot et al. (1965) (Eq. 4.8) highly over predicts the values of the local Nusselt number in and the length of the entrance mixing section (Fig 4.7). This correlation indicates that the effect of entrance flow mixing diminishes after a distance ~ $z/D = 150$. This value in much higher than those indicated by the present 3-D numerical results and correlation (Eq. 4.9) (of $z/D = 25$) and by Taylor's correlation (1967) (Eq. 4.7) of only $z/D = 10$. In general, the results of the present 3-D numerical analysis and the present correlation (Eqs. 4.6 and 4.9) are consistent and in good agreement with Taylor's correlation. When compared to Taylor's (1967), the correlation by McEligot et al. (1965) (Eq. 4.8) under predicts the values of the heat transfer coefficient for fully developed turbulent convection, Nu_{FD}, and over predicts the local heat transfer coefficient in the entrance section by more than 20% (Figs. 4.6 and 4.7). Furthermore, the extent of the entrance mixing section (~ $z/D = 150$) in the helium flow channel is 15 times that given by Taylor's correlation (1967) and 6 times that for the present correlation (Eq. 4.9).

The effect of the non-contiguous fuel compacts also bears investigation. A single continuous fuel element is chosen to reduce meshing requirements, but in order to be certain the effect from such a simplification is small, the impact of the axial power distribution (Fig. 4.4) associated with the actual fuel elements is considered.

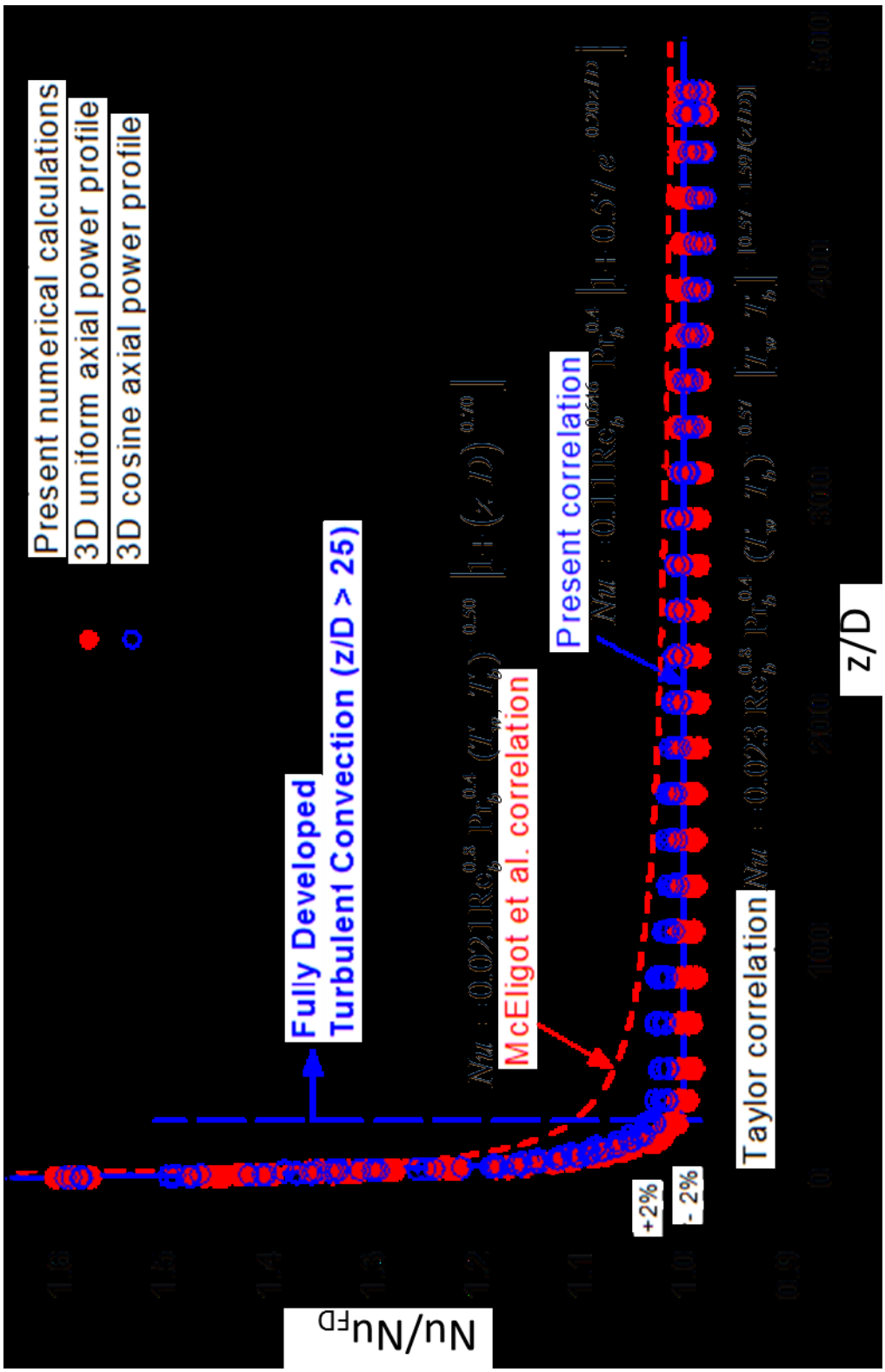

Figure 4.7 – Comparison of the fully developed correlation in this work, including the entrance region, and the correlations of Taylor (1967) and McEligot et al. (1965).

The temperature data from the thermal-hydraulics analysis of the single channel module are determined with the gapped power profile and presented in Fig. 4.8. Although the gaps in the stack of fuel compact have a fairly profound effect on the local wall temperature where they occur, their effect on the local helium bulk temperature is negligible (small, localized decreases in the slope near the gaps). In addition, because the differences in the wall temperature line up fairly well with the sharp power decreases where no fuel compacts are present, the effect on the local heat transfer coefficient (calculated from q'' and (T_w-T_b)) is mitigated. The gaps in the fuel compacts tend to cause a reduced local Nusselt number for the small width of the gap, while the local Nusselt number within the fueled region is slightly higher than that of the simulation with contiguous fuel compacts. The net effect of the non-contiguous compacts is thus negligible, and the calculation results agree fairly well with the developed correlation.

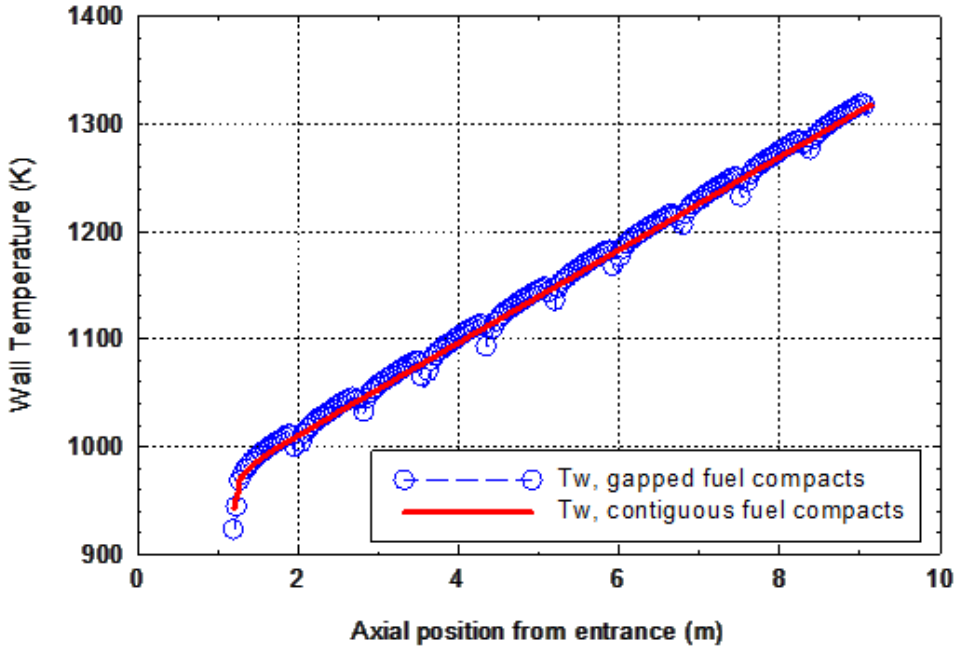

Figure 4.8 - Effect of gaps in fuel compacts on the calculated axial temperature profiles.

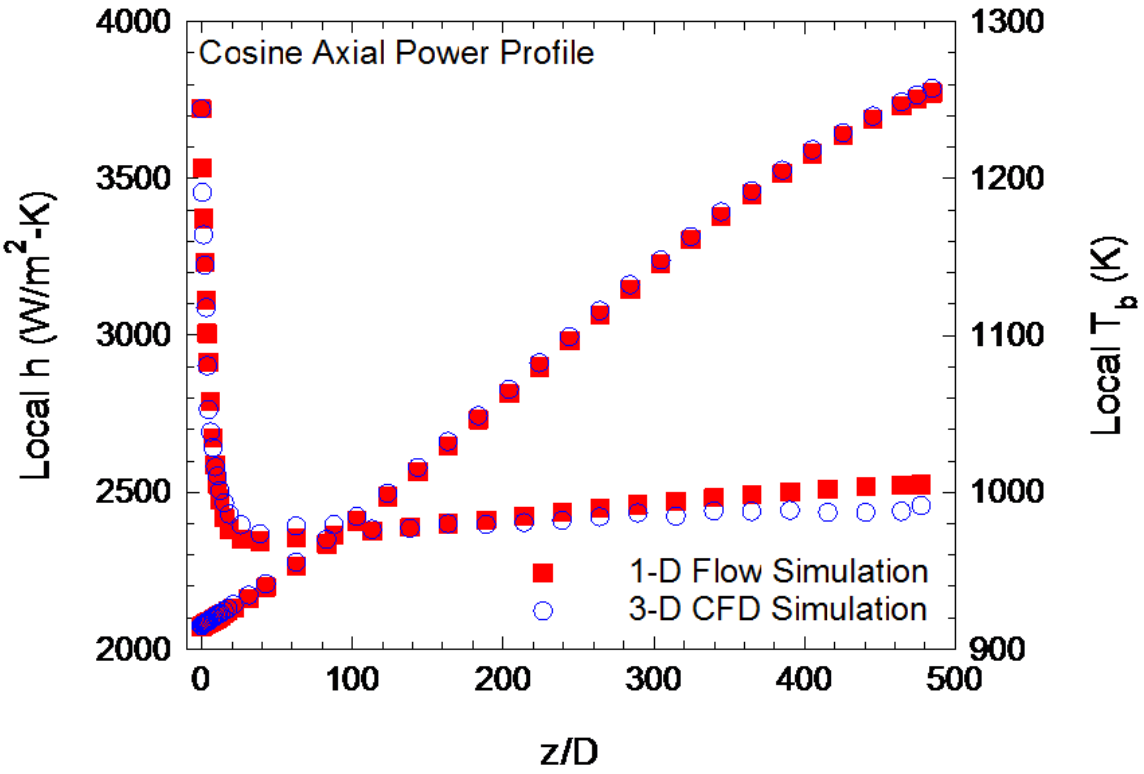

Figure 4.9 - Comparison of calculated values of the bulk temperature and the local heat transfer coefficient using a full 3-D simulation and the developed simplified methodology.

4.5.2 Validation of 1-D flow simulation

The results of the simplified analysis approach for modeling steady state thermal-hydraulics in a single helium coolant channel module of a HTGR or VHTR core are validated by comparing them to those of the performed numerical analysis involving a coupled full 3-D conduction in the graphite and fuel compact and CFD simulation of the helium flow in the channel. These comparisons are shown in Figs. 4.9 - 4.11. Figure 4.9 compares the local values of the convection heat transfer coefficient and of the helium flow bulk temperature. The results in this figure confirm the accuracy of the simplified simulation approach, based on the use of 3-D conduction in graphite and fuel compacts

and 1-D helium flow in the coolant channel, for calculating the local heat transfer coefficient along the single channel module.

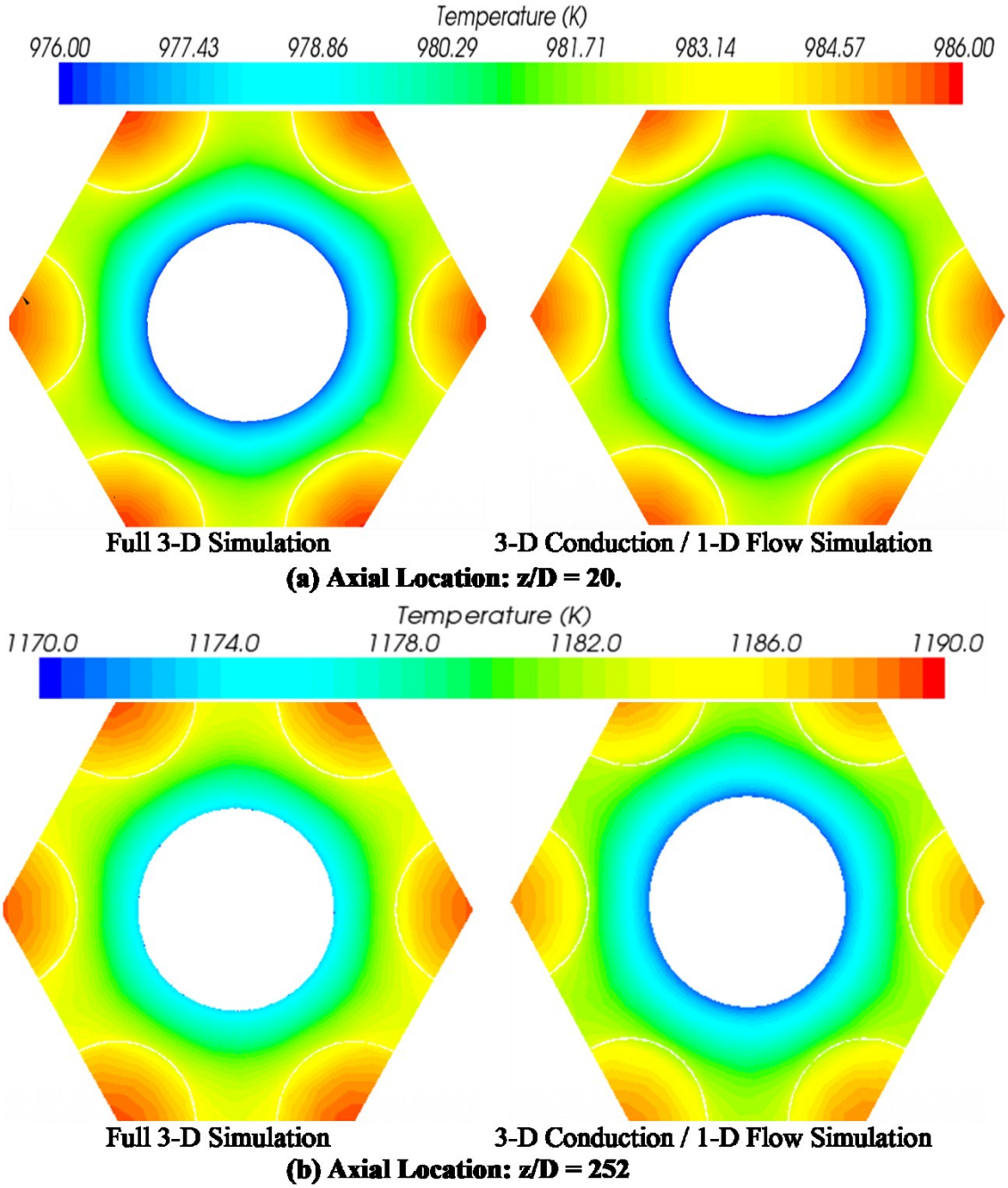

Figure 4.10 - Comparison of radial temperature fields for 1-D and 3-D methodologies in single channel module.

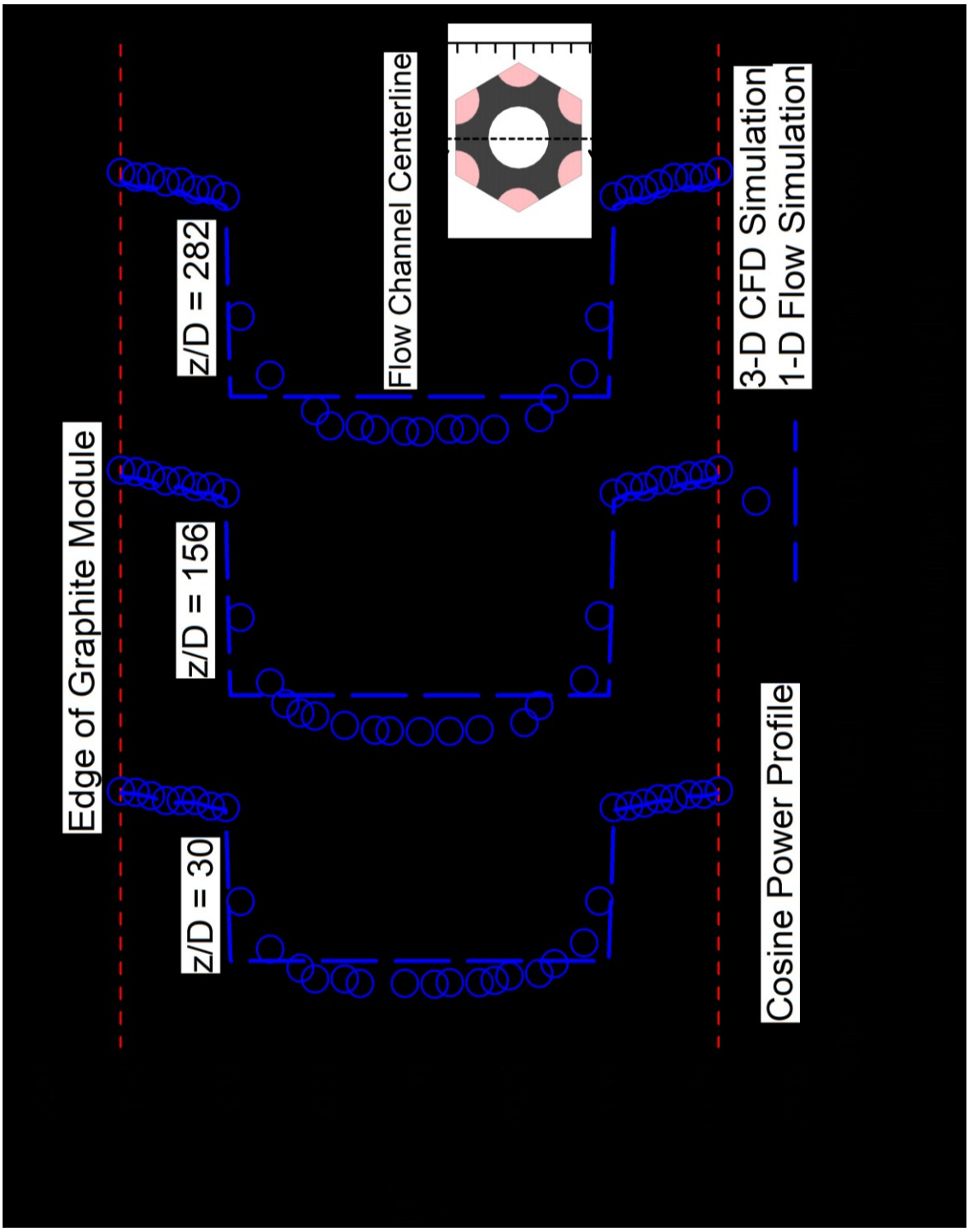

Figure 4.11 - Comparison of the calculated radial temperature profiles in the coolant channel using the simplified methodology and full 3-D analysis of the single channel fuel module.

The values of the local turbulent heat transfer coefficient calculated by the two numerical simulation methods are in good agreement (Fig. 4.9), except near the exit of the heated section of the central flow channel. At that location, the difference between the calculated values of the local heat transfer coefficient by the two simulation methods is < 10%. The results in Fig. 4.9 also show that the local values of the helium bulk temperature along the heated section of the central flow channel are in good agreement with those calculated using the full 3-D thermal-hydraulics analysis; the difference is quite small, amounting to < 3 K.

Both the 1-D and 3-D helium flow simulations predict similar values of the temperature drop in the boundary layer (T_w -T_b), along the heated section of the channel. This is demonstrated in Fig. 4.10, which compares the calculated radial temperature distributions by the two simulation methods, at different axial locations along the heated length of the helium flow channel. Figure 4.10 compares images of the calculated temperature contours in the unit channel module at two axial locations of the heated section of the central flow channel; at z/D = 20 within the entrance mixing length (Fig. 4.10a) and z/D = 252 corresponding to the core mid-plane (Fig. 4.10b). These images show good agreements between the calculated temperatures at these cross-sections within the fuel compacts and the graphite as well as of the helium flow in the central channel. The temperature values in Fig. 4.10a are very close while those in Fig. 4.10b are slightly different, by < 3 K. This difference is within the range of uncertainty ($\pm$ 2%) of the present correlation (Eq. 4.9), when compared to the turbulent convection heat transfer results obtained using the full 3-D thermal-hydraulics analysis.

In addition to simplifying the problem setup and reducing the numerical meshing in the flow channel, the 1-D helium flow simulation significantly reduces the computation time. The numerical solution also converges much faster than that of the full 3-D thermal-hydraulics analysis. In the simplified methodology, only the graphite and fuel compacts are extensively meshed. The present numerical thermal-hydraulics analysis are run on a single server node, whose specifications are given in Chapter 3. A full 3-D numerical simulation on this node took ~ 19 - 28 hours of total time. On the other hand, with the same number of processors, the cases involving 3-D conduction in the fuel compact and graphite and the 1-D helium flow simulation in the channel each took about ~ 30 minutes of total time, representing a ~40 fold decrease in CPU time.

The comparisons of the simulation results in Figs. 4.9 - 4.11 validate the applicability of the simplified analysis methodology that uses 3-D conduction both in the fuel compacts and the graphite, and 1-D simulation of the helium flow in the central channel of the module. The results verify the accuracy of this approach for future implementation to the analysis of a HTGR or VHTR full fuel element or the entire core, at significant savings in the total computation time and meshing requirements. The next chapter examines the validity of the simplified methodology, in conjunction with the developed Nusselt number correlation (Eqs. 4.6 and 4.9), to performing thermal-hydraulics analyses of VHTR fuel element and a VHTR 1/6 core.

Chapter 5 - Prismatic fuel element and 1/6th VHTR core thermal-hydraulics analyses

This chapter examines the effectiveness of the simplified simulation methodology developed in the previous chapter for performing thermal-hydraulics analyses of a VHTR fuel element. The results are compared with those obtained using a full 3-D thermal-hydraulics analysis of a fuel element. The simplified methodology is also used in this chapter to investigate the effects of helium bypass flow in interstitial gaps between fuel elements in a VHTR core on the calculated temperatures as well as the numerical meshing requirements and the computation time to complete the calculations. Analyses of a VHTR fuel element are also performed with and without a helium bleed flow in the control rod channels. In these analyses, the volumetric heat generation rate in the corner burnable poison rods varied from 25% to 100% of that of the fuel compacts. The effects of the helium bypass flow on the intensity of hot spots are investigated. Finally, thermal-hydraulics analyses of a one-element tall and a full height VHTR 1/6 core are performed. The former investigated the effect of the helium bypass and bleed flows, while the latter did not consider helium bypass flow.

5.1 Numerical meshing

The full 3-D thermal-hydraulics analysis of the hexagonal fuel element (Fig. 5.1) employed a total of 43.9 million numerical mesh elements or cells: 31.0 million in the flow channels, 5.7 million in the fuel compacts, 5.3 million in the graphite, and 1.9 million in the axial graphite reflector block. Figs 5.2a and 5.2b show cross-sectional views of the numerical mesh grid implemented in the helium flow channels, the solid graphite and the fuel compacts in a quadrant of a VHTR prismatic fuel element. This

quadrant is marked with a dashed-line in Fig. 2.9. The size of the numerical cells or mesh elements in the graphite of the fuel element increases from 2.0 mm near the interfaces with the helium flow channels to as much as 1.2 cm far from these interfaces. In the helium flow channels, the smallest mesh element size is 1.4 mm. The smallest mesh element size in the cylindrical fuel compacts is 1.6 mm and increases to 6.4 mm at the center of the compacts (Fig. 5.2b).

In order to accurately capture the heat flow at the interfaces between the solid graphite and the helium flow in the coolant channels, 5 prism layers of numerical mesh elements are used near these interfaces (Fig. 5.2a). The prism layers at the interfaces between the solid graphite and both the fuel compacts and the helium flow channels are appropriate for simulating the perpendicular heat flow at these interfaces (Figs. 5.2a and 5.2b). This meshing approach is implemented in the thermal-hydraulics analysis using the simplified thermal-hydraulics methodology developed in the previous chapter, as well as in the full 3-D analysis of the hexagonal fuel element (Fig. 5.1). Since the simplified analysis methodology eliminates meshing in the helium flow channels, the number of numerical grid elements used in the hexagonal fuel element is much smaller than that used in the full 3-D analysis, totaling only 12.9 million mesh elements.

A similar meshing scheme is implemented in the thermal-hydraulics analysis of the prismatic fuel element with interstitial bypass helium flow. Figure 5.3 shows the details of the meshing grid used in the bypass flow interstitial gap, a corner burnable poison rod, fuel compacts and a standard flow channel. The width of the interstitial gap around the fuel elements is taken as 3 and 5 mm and the obtained results are compared to those without a bypass flow.

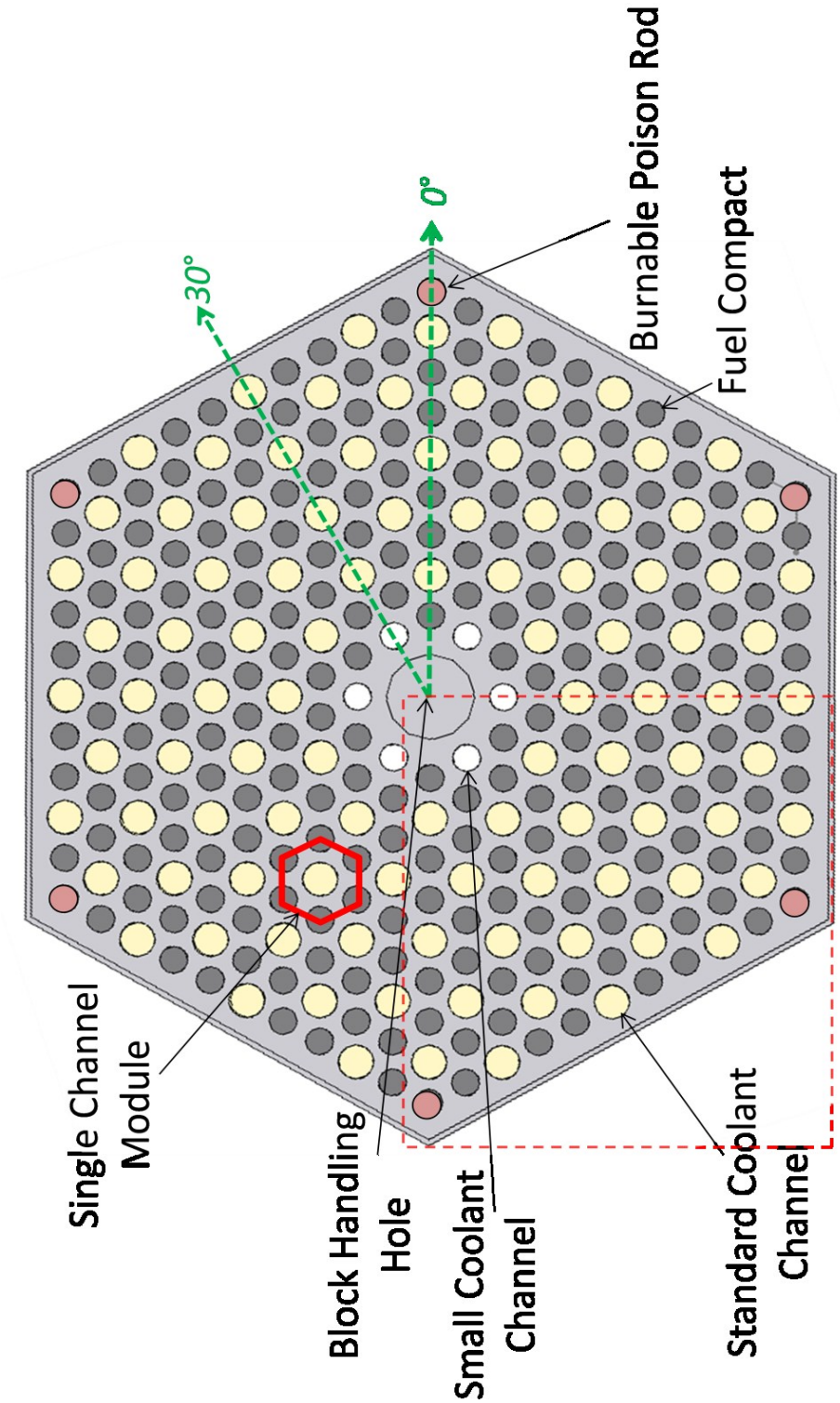

Figure 5.1 - Fuel element block used in single block analysis.

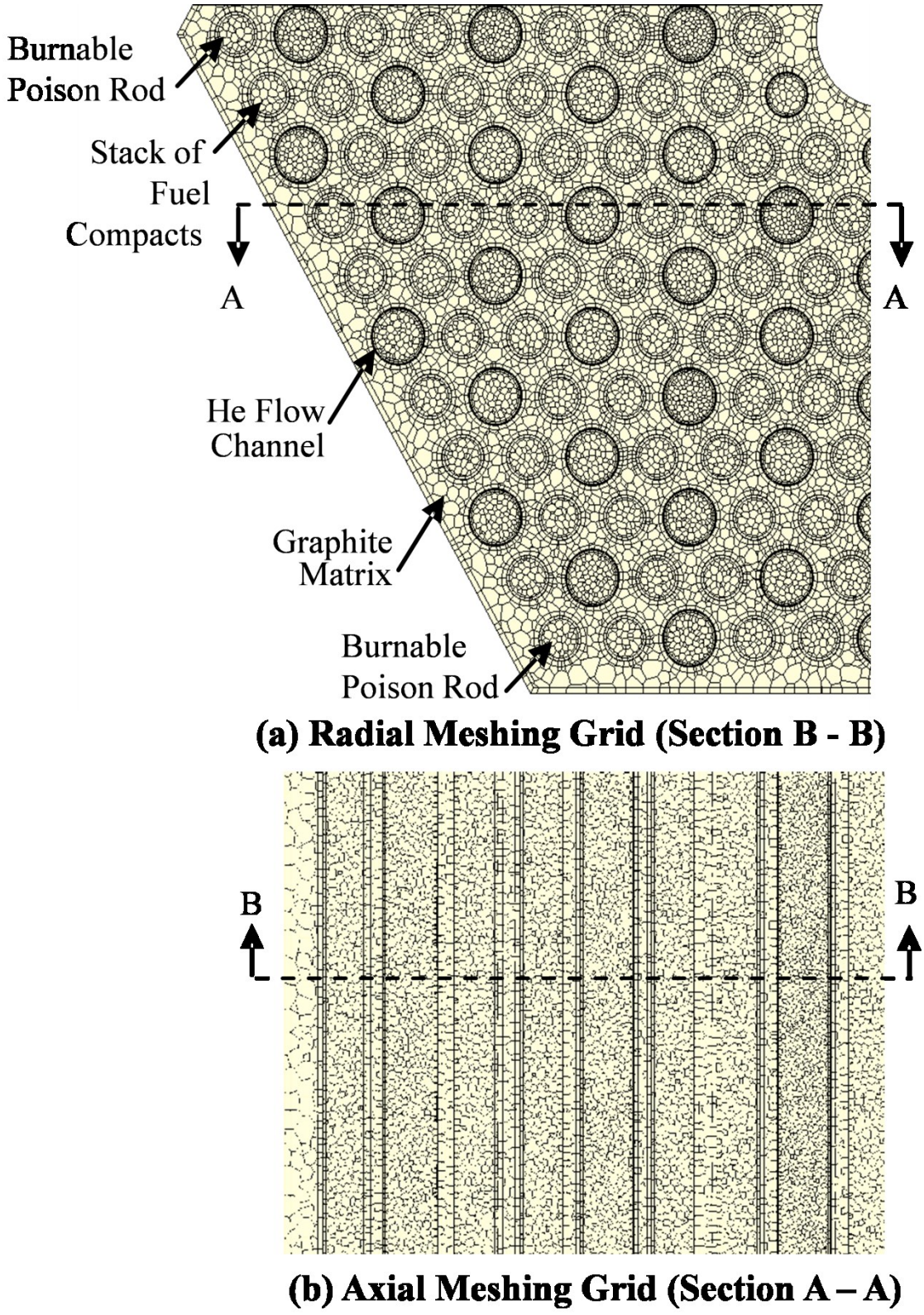

Figure 5.2 - Mesh employed in single fuel element block analysis.

The comparison quantifies the effect of the bypass flow as well as that of the width of the interstitial gap on the helium flow distribution in the coolant channels and the calculated temperature field in the VHTR prismatic fuel element. The helium bypass flow passages and the helium coolant channels share a top plenum region with a constant inlet mass flow rate and constant exit pressure. The prismatic fuel element (Fig. 5.1) is of a "standard" design (i.e. without control rods or reserve shutdown holes but with six burnable poison rods located at the corners). The thermal-hydraulics analysis investigates the effect of changing the volumetric heat generation rate in the poison rods, particularly when it is assumed the same as in the fuel compacts. In reality, the volumetric heat generation rate in the corner poison rods is only a fraction of that in the fuel compacts.

The numerical thermal-hydraulics analysis of the prismatic fuel element with a helium bypass flow employs 4.9 million numerical mesh cells in the fuel compacts and the corner burnable poison rods, 15.8 million cells in the graphite matrix (additional cells are added in the prism layers around the edges of the fuel element, the fuel compacts and the coolant channels), 2.3 million cells in the bypass flow passage, 30.9 million cells in the helium coolant channels, and 1.4 million cells in the connecting top plenum region. The details of the implemented numerical mesh grid can be seen in Fig. 6.

The numerical meshing approach used is particularly important in modeling a full-height, prismatic VHTR 1/6 core. The VHTR full core is ~ 10 m tall and 8 m in outer diameter including the graphite reflector (Fig. 2.9). Although eliminating the numerical meshing in the coolant channels in the simplified analysis methodology significantly decreases the number of the numerical mesh elements, simplifies the numerical grid and markedly decreases the computational time, the simulation task is still extraordinarily

large. Even the 3-D heat conduction in the solid graphite and the fuel compacts with a few million mesh grid elements is computationally taxing.

The present thermal-hydraulics analysis of a full height VHTR 1/6 core uses a fine numerical mesh grid in the radial direction and a relatively coarse mesh grid in the axial direction. This two-dimensional numerical mesh grid is built upward in order to accomplish the meshing task. Although the numerical meshing in the STAR-CCM+ commercial software (CD-adapco, 2012) used to perform the thermal-hydraulics analysis code could be preferentially biased toward a coarser numerical grid in a given coordinate direction, the long computation time due to the larger number of non-uniform numerical grid mesh elements is undesirable. The largest numerical mesh grid used with the conventional polyhedral mesh elements in STAR-CCM+ commercial software code employed a total of ~150 million cells, and captured only three stacks of fuel elements.

Instead, a thin wafer (~2 cm thick) with a radial cross-section identical to that of a the VHTR core is meshed. This wafer is then used in conjunction with the extruder meshing model in the STAR-CCM+ code to generate axial segments of a specified length that varies with the desired refinement of the numerical mesh grid. For the full height VHTR 1/6 core thermal-hydraulics analysis using the simplified method, the length of the axial segments ranges from 2.5 to 8 cm. Although the aspect ratio of these cells is large and in some cases could be as much as 10 – 20, the fact that these cells are for heat conduction in the solid graphite and fuel compacts makes such large aspect ratios acceptable. By contrast, when modeling the helium flow in the coolant channels using 3-D CFD, a small aspect ratio < 3.0 is preferable because of the complexity of the flow turbulence in the channels. These meshing constraints are omitted when using the developed simplified

thermal hydraulics analysis methodology, because no meshing is required in the coolant channels.

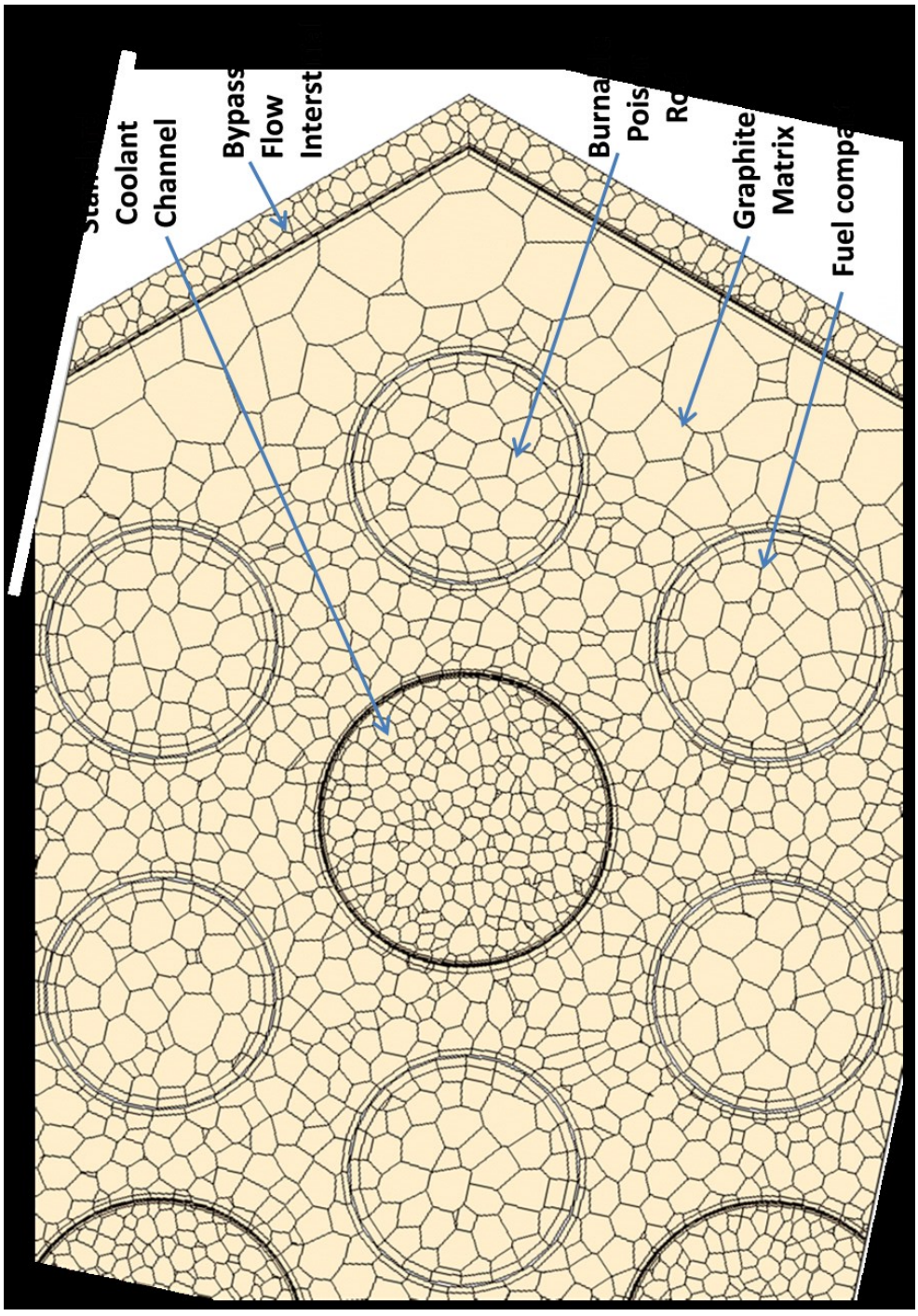

Figure 5.3 - Close up of employed mesh for single fuel element with bypass region.

Figure 5.4 shows a cross-sectional view of the numerical mesh grid used in the core fuel elements and near the interfaces between these elements (darker shade) and the inner graphite reflector elements, or assemblies (lighter shade). The full height 1/6 VHTR core analysis used a relaxed mesh grid in the reflector assemblies (Fig. 5.4). The smallest numerical mesh cells in the reflector near the interfaces with the core fuel elements are 5 mm across, while the larger cells in the reflector elements are 1.5 cm across.

In Fig. 5.4, the numerical mesh grid is refined at the interfaces with the helium coolant channels and the fuel compacts. The smallest mesh size in the solid graphite near the small features is 1.2 mm, increasing to 4.8 mm away from these features. The mesh grid in the graphite bordering the helium coolant channels is comprised of at least one prism layer. The fuel compacts use a similar meshing scheme. Several concentric layers of prism elements are used near the wall of the coolant channels. Thus, when the 3-D heat conduction in the graphite matrix is coupled to the 1-D helium flow in the coolant channels, the inner wall surface temperature and the local heat flux are calculated accurately using the heat transfer coefficient correlation in Eqs. (4.6) and (4.9).

A limitation to the implemented numerical meshing approach in the full height 1/6 core thermal-hydraulics analysis is that the radial sections are of uniform composition. Thus, the non-contiguous stacks of the fuel compacts in the core prismatic elements are modeled as contiguous, 7.93 m long compacts. As such, the volumetric heat generation rate used in the contiguous fuel compacts is lower than that in the actual shorter compacts in the core fuel elements, but the total heat generation rate is the same. Besides simplifying the numerical grid, using contiguous fuel compacts in the thermal-hydraulics analysis insignificantly affects the values of the calculated temperatures.

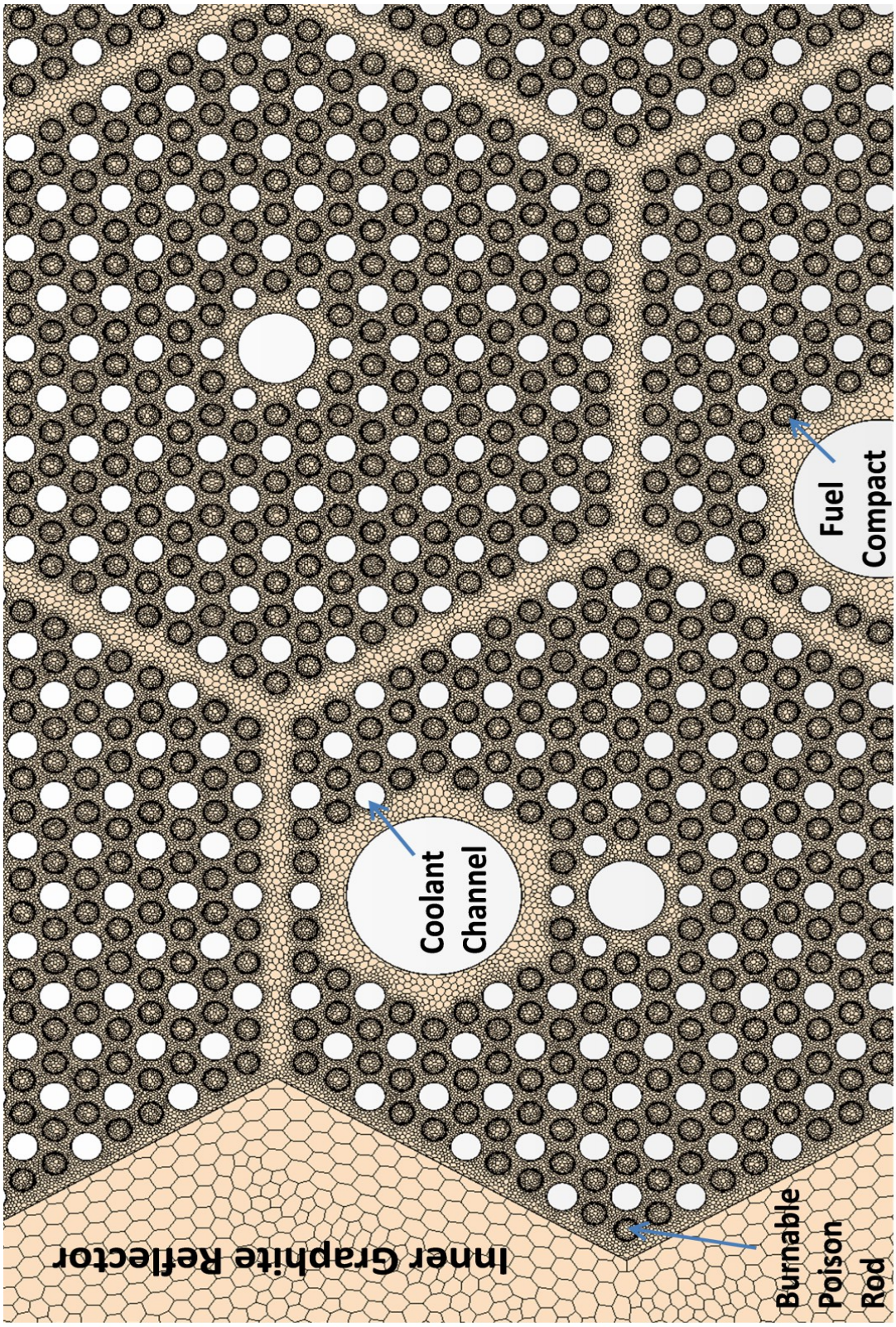

Figure 5.4 - Employed numerical mesh grid for VHTR 1/6 core thermal-hydraulics analysis.

5.2 Thermal-hydraulics analysis

Once the numerical mesh grid is developed and implemented, performing the thermal-hydraulics analyses is relatively straightforward. The input to the analyses includes the axial and radial power profiles in the reactor core region or the fuel element, and the inlet temperature and mass flow rate of the helium in each coolant channel. These and other input parameters used in the thermal-hydraulics analyses are listed in Table 5.1. These parameters are for a typical prismatic VHTR design (MacDonald et al., 2003; LaBar et al., 2004; Schultz et al., 2004). When assuming no helium bypass flow through the interstitial gaps or bleed flow in the channels of the reserve shutdown and control rods in the fuel elements, the total helium flow in Table 5.1 corresponds to an average mass flow rate of 0.0306 kg/s per coolant channel (Figs. 5.1 and 5.4).

The average volumetric heat generation rate used in the fuel compacts corresponds to a reactor nominal power of 600 MW_{th}. The present thermal-hydraulics analysis of a full height 1/6 core employs a uniform radial power profile and either a uniform or a chopped-cosine axial power profile. The full 3-D analyses of the prismatic fuel element and of the full height 1/6 core include a circular plenum above the top axial reflector block. They use the helium coolant parameters in Table 5.1 at the inlet plenum surface (mass flow and temperature) and assume the same total pressure at the exit of all the coolant channels of 7.064 MPa. This pressure corresponds to a total pressure of the helium coolant in upper plenum of the VHTR of 7.07 MPa.

In a prismatic VHTR core fuel element, the majority of the helium coolant channels are 1.5875 cm in diameter and a few near the center of the core fuel elements have a smaller diameter of 1.27 cm (Fig. 5.1). Thus, since the total pressure drop across the

different diameter channels is the same, the coolant mass fluxes in the larger and small diameter channels are different, but proportional to their respective effective cross-section areas. In the present thermal-hydraulics analyses without interstitial bypass flow, the helium flow rate in the small diameter coolant channels is 0.0178 kg/s, which is ~ 58% of that in the large diameter channels (0.0306 kg/s). These flow rates are incorporated in the thermal-hydraulics calculations of the prismatic fuel element, using both the simplified methodology and a full 3-D analysis.

Table 5.1 - Operational parameters for the VHTR 1/6 core thermal-hydraulics analysis

Parameter	Input Value
Coolant total mass flow rate [kg/s]	330
Volumetric heat generation rate [MW/m^3]	28.4
Coolant inlet temperature [K]	914
Coolant exit temperature [K]	1263
Reactor inlet pressure [MPa]	7.07
Reactor total power [MW$_{th}$]	600

The helium bypass flow through the interstitial gaps reduces its total flow rate and distribution in the coolant channels. The helium flow rates in the coolant channels depend on the assumed width of the interstitial gap, taken as 5 mm in the present analysis. These helium flow rates are determined using a full 3-D simulation of the fuel element with no heat generation. The obtained helium flow rate estimates are then used in the thermal-hydraulics analysis of the prismatic fuel element with a helium bypass flow. Although the actual helium flow rates in the coolant channels of the fuel element with fission heating could differ slightly, the results should be applicable to assessing the effect of the helium bypass flow on the temperature distribution within the fuel element. The thermal-hydraulics analysis of the fuel element without a helium bypass flow is

conducted using the simplified methodology and the results are compared with those of the full 3-D analysis. The results of the two methods are comparable, while the savings in the computational time and meshing requirements using the former are significant. The thermal-hydraulics analysis of the prismatic fuel element, with and without helium bypass flow kept the total heat generation in the fuel element constant, but the volumetric heat generation rate in the corner burnable poison rods (Fig. 5.1) is taken equal to 25%, 50% and 100% of that in the fuel compacts. The purpose is to assess the effect of changing the volumetric heat generation rate in the poison rods on the intensity and the extent of the resulting hot spots. In reality, the volumetric heat generation rate in the poison rods (fully enriched B_4C) is estimated using separate neutronics analysis as ~25 - 30% of that in a typical fuel compact.

In the numerical thermal-hydraulics analyses, a solution convergence is considered to be attained when the normalized energy residuals have dropped by at least 3 orders of magnitude and stabilized (stop decreasing). An additional convergence requirement in the full 3-D thermal-hydraulics analysis is that the normalized residuals of the momentum variables in the coolant flow channels in the three principal coordinates are stabilized. In addition, the residuals of the turbulent dissipation and kinetic energy transport variables must fall by more than 4 orders of magnitude before stabilizing. Upon reaching a solution convergence, the error in the overall energy balance is determined by comparing the total energy input to that removed by the helium flow in the coolant channels, based on the total flow rate and inlet and exit enthalpies. The overall energy balance is typically satisfied to within $\pm$ 1%. The next section presents and discusses the obtained thermal-hydraulics analyses results.

5.3 Results and discussion

This section presents the thermal-hydraulics results for a single fuel element (Fig. 5.1) using both the simplified methodology and a full 3-D analysis. The purpose of the performed calculations without a bypass helium flow is to account for the entrance effect in the heated coolant channels as well as validate the effectiveness and fidelity of the simplified methodology in reducing the computation time and memory requirements. Also presented in this section are the thermal-hydraulics analyses results using the simplified methodology for a fuel element with helium bypass flow in a 5 mm wide interstitial gap (Fig. 5.3) and for a full height VHTR 1/6 core. The local values of the heat transfer coefficient of the helium gas flow in the coolant channels, including the entrance mixing section ($z/D \leq 25$), are determined using Eqs. (4.6) and (4.9) based on the calculated inner wall and helium bulk temperatures in the numerical analysis. The results in this section also include the effect of changing the volumetric heat generation rate in the burnable poison rods on the temperatures for prismatic fuel element, without a helium bypass flow.

5.3.1 Fuel element analysis without a bypass flow

The performed thermal-hydraulics analyses of a prismatic fuel element (Fig. 5.1) using both the simplified methodology and a full 3-D numerical analysis are carried out using a node running 64-bit Windows Server 2007 with two, 2.27 GHz quad-core Intel Xeon processors and 48 GB of RAM. The full 3-D thermal-hydraulics analysis took ~ 100 hours of real time to complete, versus only 3 hours using the simplified methodology, representing more than a 33 fold increase in computation time. The results of the two methods are comparable with < 5 K difference in calculated temperatures.

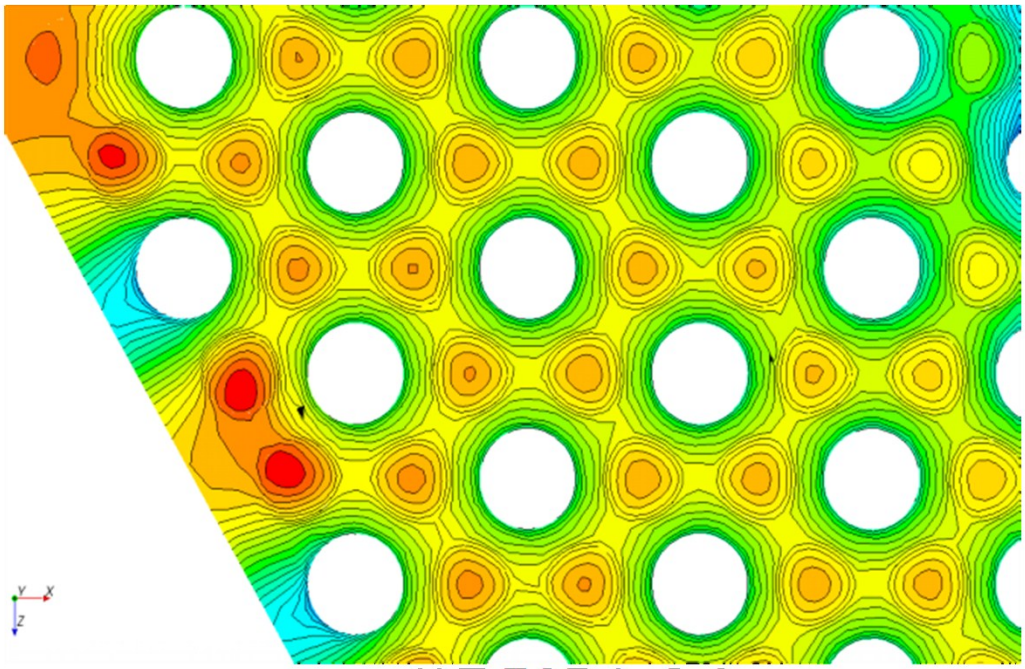

(a) Full 3-D Analysis

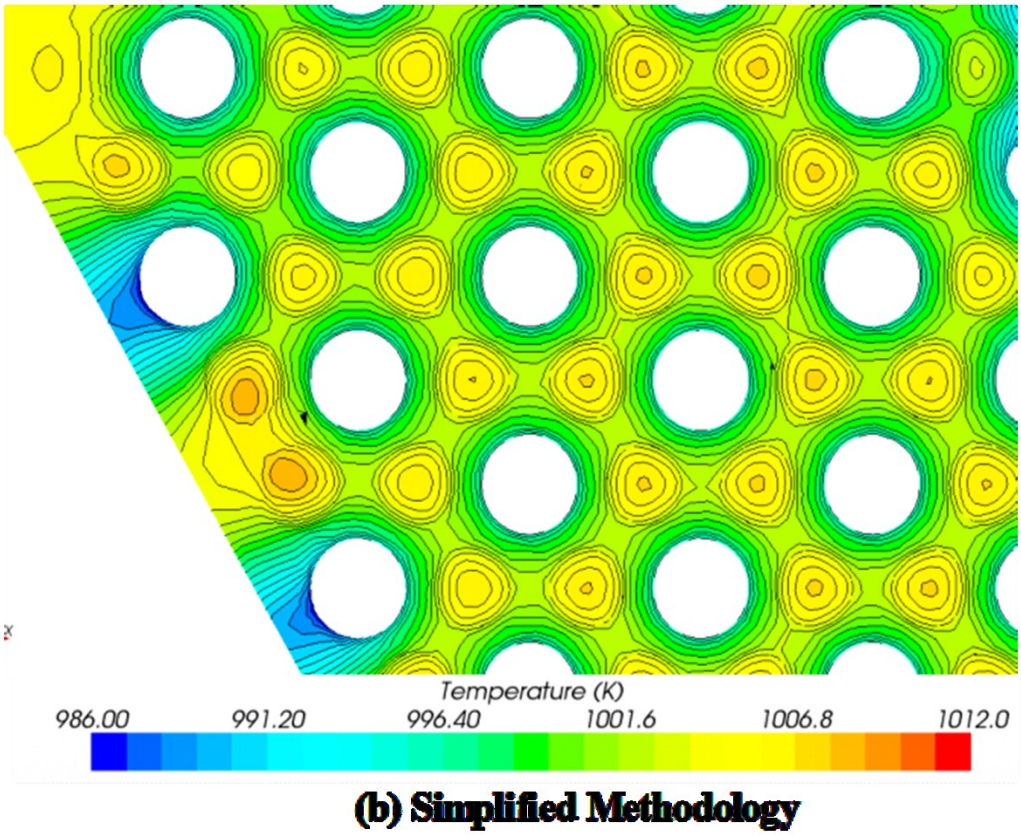

(b) Simplified Methodology

Figure 5.5 - Temperature fields for single fuel element block analysis, 4 cm from bottom.

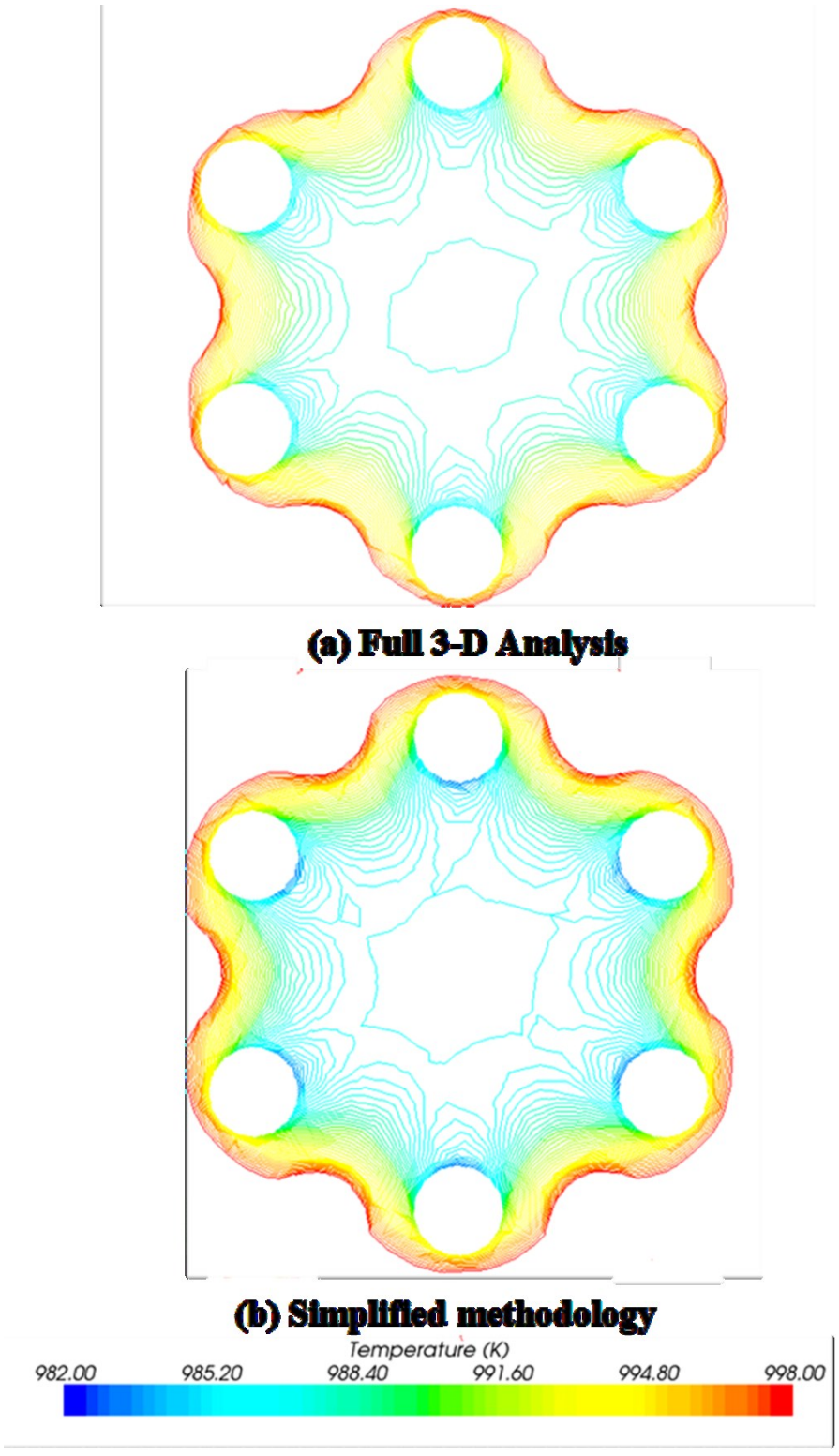

Figure 5.6 - Temperature fields for single fuel element block analysis near center of block, 4 cm from bottom.

The calculated temperature fields in the hexagonal fuel element using the full 3-D thermal-hydraulics analysis (Fig. 5.5a) and the simplified methodology (Fig. 5.5b) are similar and the values are within a few degrees. A more pronounced difference of up to 4 K is seen in Figs. 5.6a and 5.6b near the center of the fuel element, where there is a fuel handling hole surrounded by 6 small diameter helium coolant channels. These channels experience lower helium gas flow rates than the standard larger diameter channels in the fuel element. The simplified analysis methodology assumes that the small diameter coolant channels have 57% of the mass flow of the standard channels, thus receiving ~ 5% more flow than in the full 3-D analysis. The calculated temperatures at the center of the fuel element using the simplified methodology are ~ 2 – 4 K lower than those calculated in the full 3-D thermal-hydraulics analysis (Figs. 5.6a and 5.6b).

The fuel element's thermal-hydraulics analysis results presented in these figures confirm the effectiveness and accuracy of the simplified methodology. There is little difference in the calculated temperatures, compared to those obtained using the full 3-D thermal-hydraulics analysis. Given that the simplified methodology runs ~ 33 times faster for the single element analysis case, it is used next to perform the thermal-hydraulics analyses discussed in the following sections.

5.3.2. Effects of helium bypass flow and heat generation in burnable poison rods

It has been recognized that the helium bypass flow in the interstitial gaps between the prismatic fuel elements in a VHTR core is inevitable and should be accounted for in the thermal-hydraulics analysis. The interstitial gaps are initially present because of the manufacturing tolerances of the prismatic fuel elements, but their width changes during reactor operation due to thermal expansion and graphite swelling by neutron irradiation.

Thus, the width of the interstitial gaps varies with the reactor's nominal operation conditions and history and could be 5 mm or even larger. For the same total helium coolant flow rate in the VHTR, the helium bypass flow cools the edges of the prismatic fuel elements in the core, but effectively decreases the helium flow in the coolant channels. This increases the graphite and fuel compact temperatures in the interior of the fuel elements. Thus, the helium flow rates and distribution would depend on the assumed width of the bypass flow gap.

With no interstitial gaps, the helium flow rate in the standard diameter coolant channels in the fuel elements is fairly uniform, ranging from 30.1 to 30.7 g/s. This flow rate decreases to 28.3 – 29.3 g/s in a fuel element with an assumed 3-mm wide bypass flow gap, and to 26.8 – 27.4 g/s in a fuel element with a 5-mm wide bypass flow gap. The total flow area of a 3-mm wide bypass flow gap represents 5.6% of the total flow area in the fuel element and the helium bypass flow represents 5.5% of the total flow rate. With a 5-mm wide interstitial gap, the helium bypass flow area and rate represent 13% and 11.1% of the total in the fuel element, respectively. These results are obtained from the full 3-D CFD numerical analysis of the prismatic fuel element performed without heat generation.

The total helium flow equals the sum of those in the 5-mm wide bypass gap and the coolant channels. The calculated values are used in the performed thermal-hydraulics analysis of the fuel element with helium bypass flow. For simplicity, the helium mass flux in the coolant channels (small and standard) in the fuel element is taken as constant. The total helium flow rate for a prismatic fuel element of 3.24 kg/s is split into 0.36 kg/s in the 5-mm wide bypass gap and 2.88 kg/s in the coolant channels. The total heat

generation rate in the fuel compacts of the element, which is assumed to represent the average fuel element in the VHTR, is 616 kW_{th}, corresponding to a nominal reactor power of 600 MW_{th}.

The next section presents the results of the thermal-hydraulics analysis of a prismatic VHTR fuel element, with and without helium bypass flow and with different volumetric heating rates in the corner burnable poison rods (Fig. 5.1). The analysis performed using the simplified methodology involves full 3-D heat conduction in the graphite and the fuel compacts, a 3-D helium flow in the interstitial bypass flow gaps, and a 1-D helium flow in the coolant channels. The helium coolant flows downward through the interstitial gaps and coolant channels and exits through the bottom of the fuel element. The total length of the fuel element is the same as those of the coolant channels and bypass flow gaps (79.3 cm). Due to the symmetry in the bypass flow gap, and in order to reduce the number of the numerical mesh elements and computation time, only half the gap width (2.5 mm) is used with an adiabatic boundary at the vertical plane of symmetry. The results of the analysis for the conditions in Table 5.1 are presented in Figs. 5.7a – 5.7d. Owing to the small height of the fuel element (0.793 m), compared to that of the core (7.93 m), the axial thermal power in the fuel compacts assumed uniform ~ 28.4 MW/m^3 (Table 5.1).

The images of the traversed temperature fields in Figs. 5.7a – 5.7d are taken at an axial location 55 cm from the inlet (or top) of the prismatic fuel element. The results in Fig. 5.7a show that the helium bypass flow has a profound effect on cooling the edges of the fuel element, including the corner burnable poison rods, but increases the temperatures in the rest of the fuel element. This is because the helium bypass flow (11% of the total) decreases its flow rate in the coolant channels of the fuel element. In the

absence of a bypass flow, all the helium coolant flows through the channels in the fuel element, further lowering its temperatures.

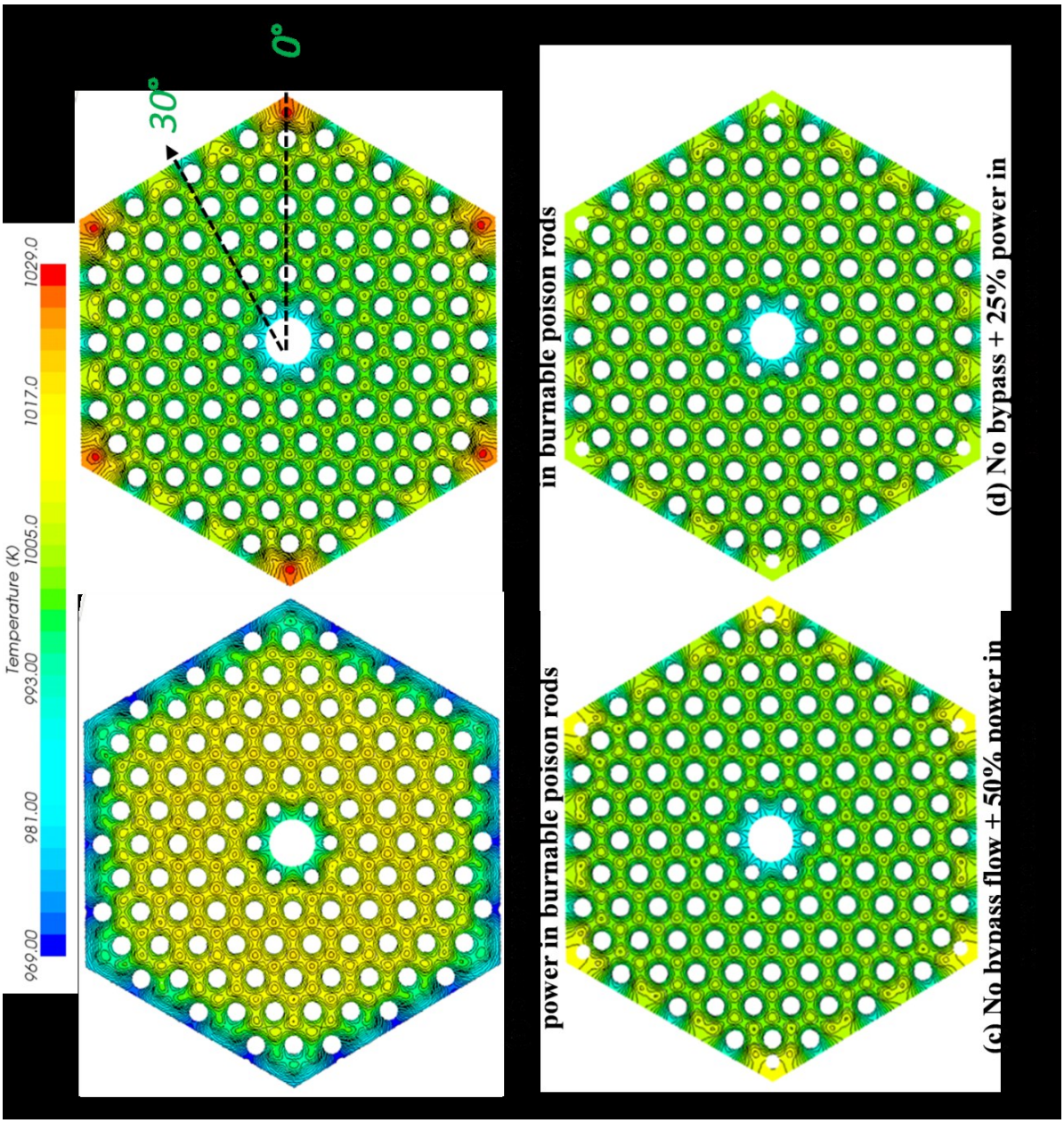

Figure 5.7 - Calculated temperature fields, 55 cm from the top of the prismatic fuel element, with and without bypass flow and different heating rates of the corner poison rods.

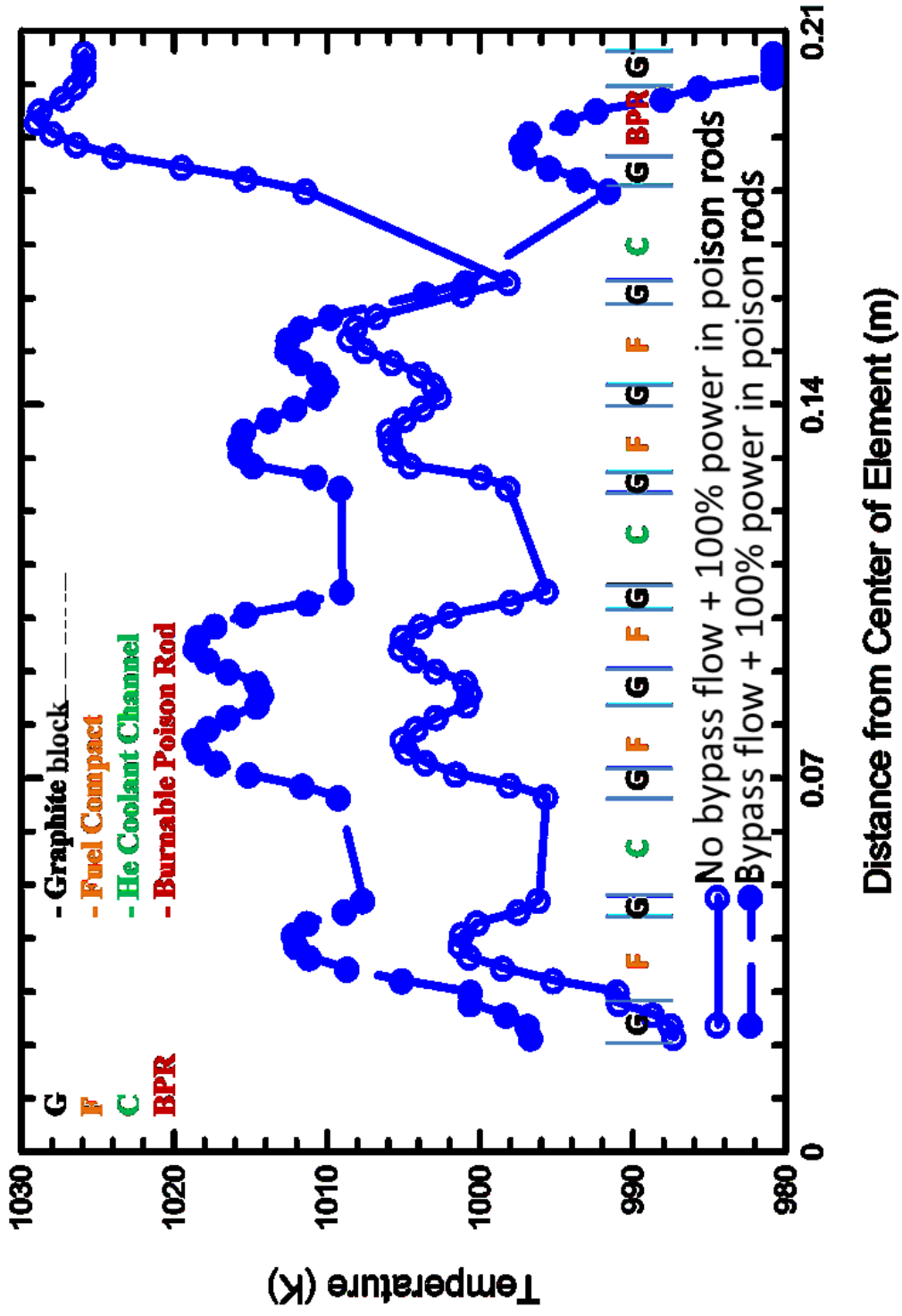

Figure 5.8 - Calculated radial temperature distributions along the 0 degree coordinate in fuel element with 100% power in burnable poison rods, with and without bypass flow (55 cm from top of element).

The heat generation in the corner burnable poison rods produces local hot spots, whose intensity depends on the assumed volumetric heat generation rate in these rods (5.7b – 5.7d). The local hot spots are clearly evident in Fig. 5.7b, in which the volumetric heat generation rate in the burnable poison rods is assumed the same as that of the fuel compacts. Although unrealistic, it provides a reference case for comparison with the results in Figs. 5.7c and 5.7d. In these figures the volumetric heat generation in the burnable poison rods is 50% and 25% of that in the fuel compacts, respectively. Compared to the results in Fig. 5.7a, with no helium bypass flow and 100% volumetric power generation in the burnable poison rods (Fig. 5.7b); the temperatures of the fuel element are lower in the center but much higher near the edge of the fuel element.

Decreasing the volumetric heat generation in the corner burnable poison rods to 50% and 25% of that in the fuel compacts changes the temperature in the interior of the fuel element by only a few degrees but noticeably decreases the intensity of the corner hot spots (Figs. 5.7c and 5.7d). As indicated earlier, the volumetric heat generation in the burnable poison rods during reactor nominal operation is likely to be 25% - 30% of that in the fuel compacts, for which the image in Fig. 5.7d is representative of the average fuel element in a prismatic VHTR core. To further examine the temperature fields in the fuel element with and without helium bypass flow and with different heat generation rates in the burnable poison rods, the calculated temperatures in the fuel element along the 0^o and 30^o coordinates (Figs. 5.1 and 5.7b) are compared in Figs. 5.8 – 5.10 and 5.11, respectively. The results in Fig. 5.8 show the effect of the helium bypass flow on the temperature distribution in a fuel element with burnable poison rods generating the same volumetric heat generation rate as the fuel compacts (100%).

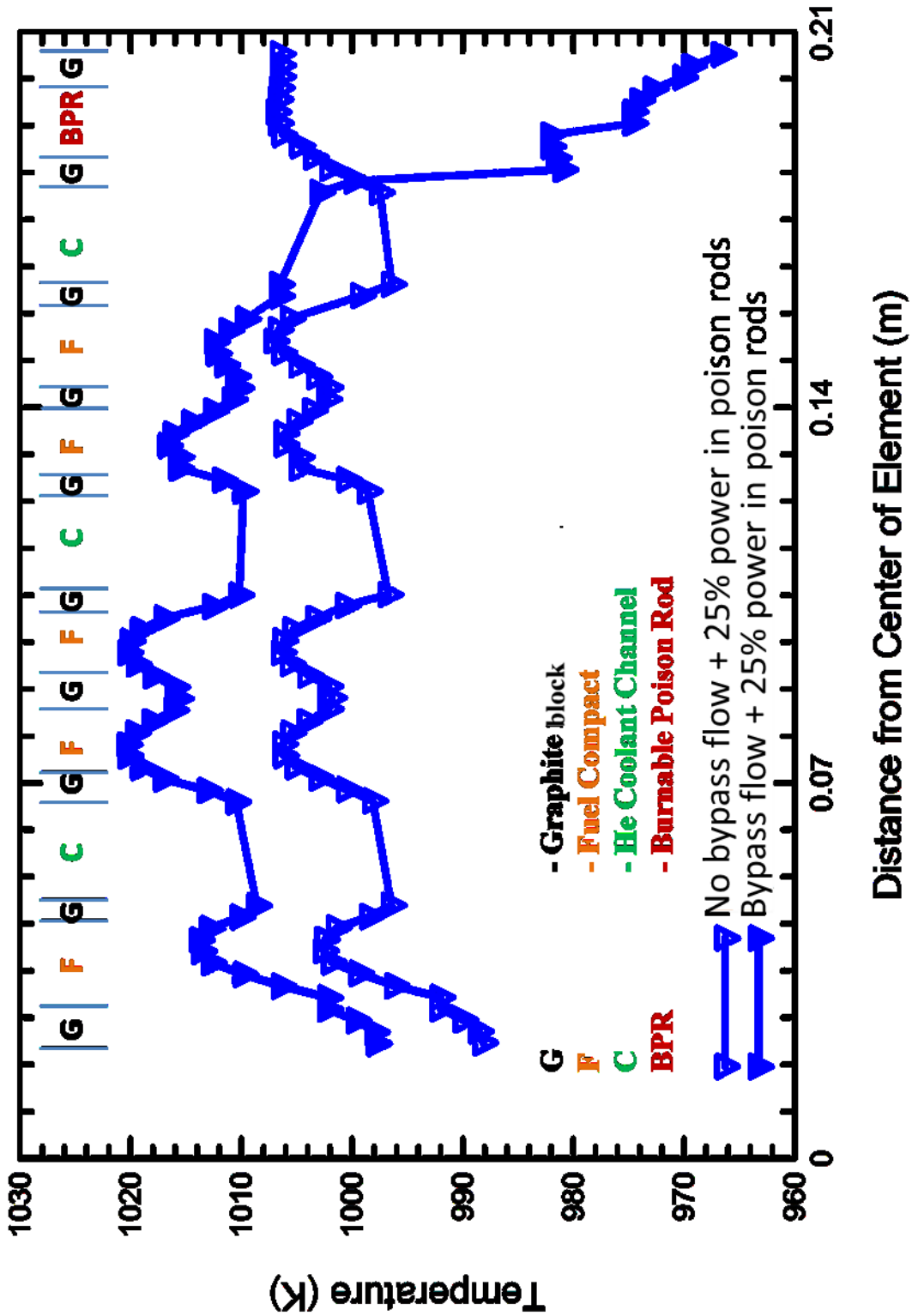

Figure 5.9 - Calculated radial temperature distributions along the 0 degree coordinate in fuel element with 25% power in burnable poison rods, with and without bypass flow (55 cm from top of element).

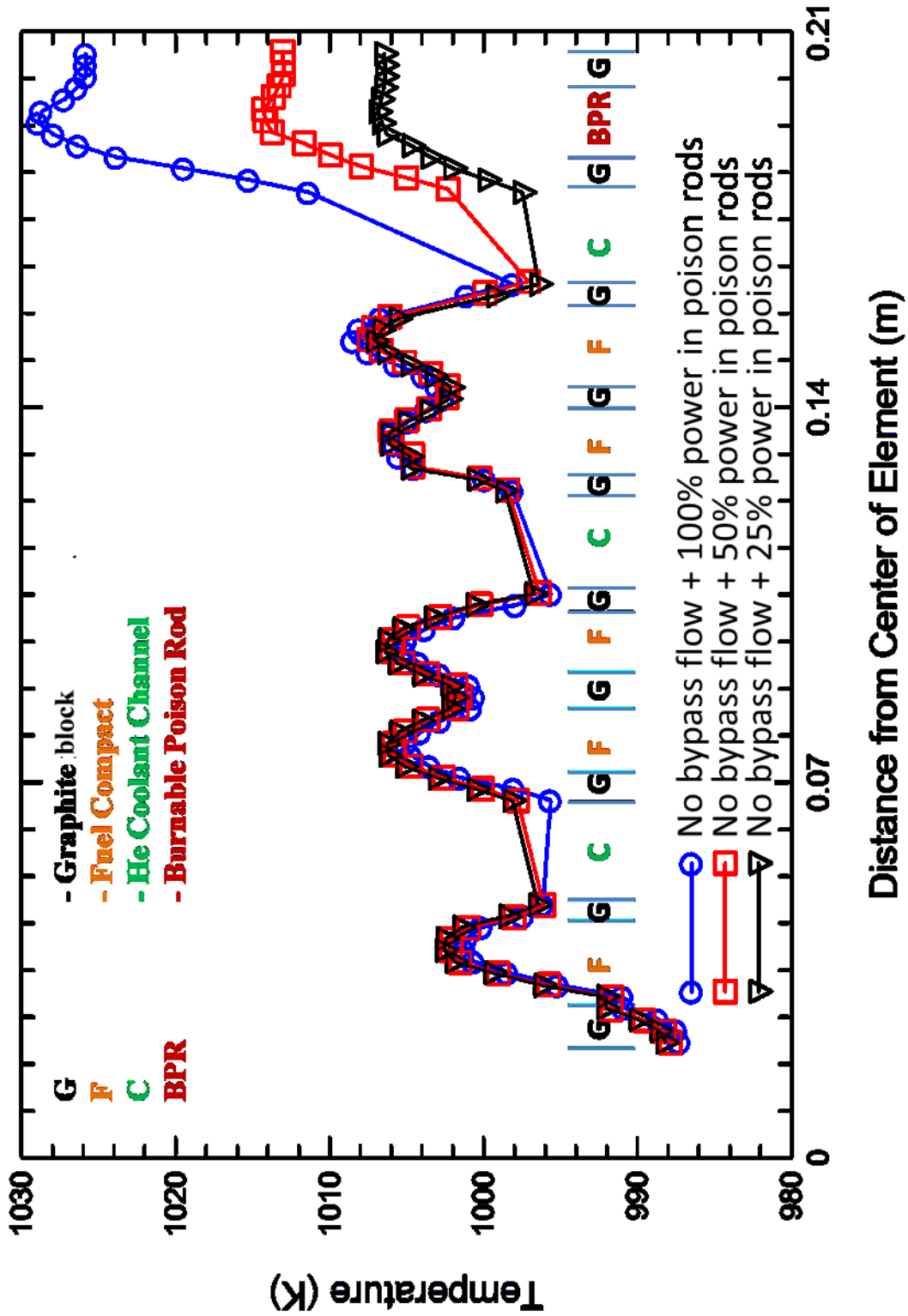

Figure 5.10 - Calculated radial temperatures along the 0 degree coordinate in fuel element without bypass flow and different power in the burnable poison rods (55 cm from top of element).

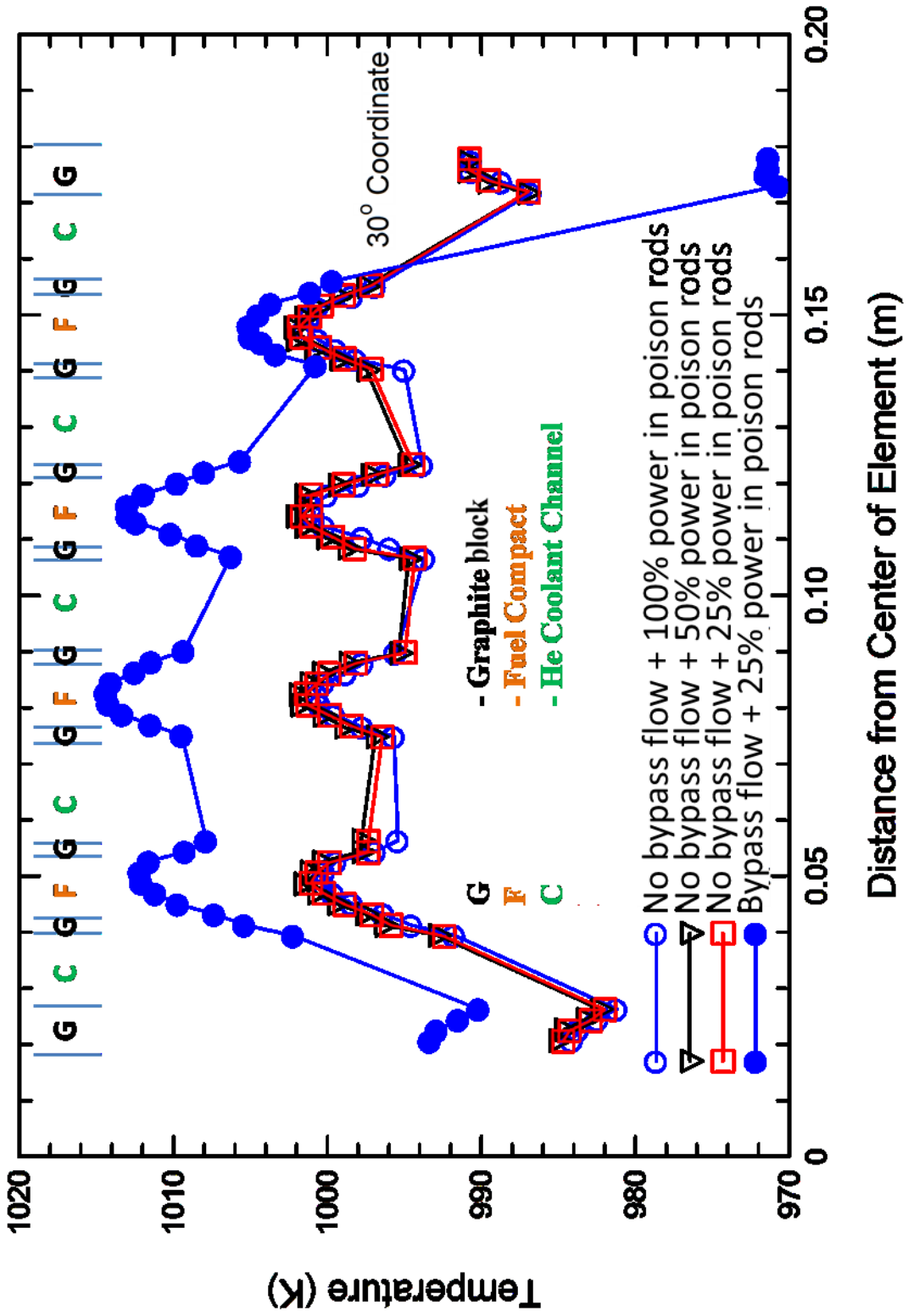

Figure 5.11 - Calculated temperature along the 30 degree coordinate in fuel element with and without bypass flow and different powers in the burnable poison rods (55 cm from top of element).

The helium bypass flow (filled circle symbols) increases the temperatures in most of the fuel element by ~ 10 – 15 K, while reducing the edge temperatures by as much as ~ 32 K, as compared to the same simulation with no bypass flow (void circle symbols). With a helium bypass flow, the maximum temperature near the center of the fuel element is 1018 K. Without a helium bypass flow, however, the temperature in most of the element is lower, except at the corner poison rod it peaks at 1029 K. In Figure 5.8, the temperature peaks within the fuel element correspond to the fuel compacts and the almost flat valleys correspond to the helium coolant channels. The peak temperatures near the edge of the fuel element without a helium bypass flow correspond to the corner burnable poison rods.

Figure 5.9 shows that reducing the volumetric power generation in the corner burnable poison rods (BPRs) to 25% of that in the fuel compact causes little change in the calculated temperatures within the majority of the fuel elements, but noticeably decreases the temperature of the corner burnable poison rods. This decrease in the BPR's temperature between the cases with and without helium bypass flow in Fig. 12 is 31 K, compared to 32 K in Fig. 5.8. The results in Fig. 5.9 show that the maximum temperature near the center of the fuel element with a helium bypass flow is 1021 K and that of the burnable poison rods is 1007 K. The latter is much lower than in Fig. 5.8, due to the lower heat generation rate in these rods. In general, decreasing the heat generation rate in the BPRs to what would be expected during nominal reactor operation (~ 25% – 30% of that in the fuel compacts) insignificantly changes the temperatures within most of the fuel element, except those of the BPRs and of the solid graphite in their vicinity. This is shown by the results in Fig. 5.10 for the fuel element with no helium bypass flow.

Decreasing the generated thermal power in the BPRs from 100% to 50% and 25% of that in the fuel compacts changes the average fuel element temperatures by only 1 – 2 K, but decreases that of the BPRs by 15 K and 22 K, respectively (Fig. 5.10). As indicated earlier, the temperature distributions presented in Figs. 5.8 – 5.10 are along the 0^o coordinate in the fuel element. The results in Fig. 5.11, however, are for the 30^o coordinate in the fuel element (Figs. 5.1 and 5.7b).

Figure 5.11 shows that the higher temperatures in the central region of the fuel element with helium bypass flow are even more prevalent. Without helium bypass flow, these temperatures decrease by 10 – 15 K, while varying the generated power in the BPRs has little effects on the temperature values and distribution in the fuel element. In general, attempting to reduce the interstitial gap width and hence, the helium bypass flow is desirable in terms of lowering the temperature and the differential thermal expansion of the fuel elements in a VHTR core. The next subsection investigates the effect of helium "bleed" flow through control rod channel on calculated temperatures in a fuel element, without a helium bypass flow.

5.3.3. Effect of helium flow through control rod channel

The thermal-hydraulics analysis results in this section are those calculated using both the simplified methodology as well as a full 3-D analysis of a fuel element without interstitial helium bypass flow (Figs. 5.12 and 5.13). The objective is to examine the effectiveness of the simplified methodology in which the flow through the coolant channels as well as is the control rod channel is 1-D, but thermally coupled to the 3-D conduction in the graphite and fuel compacts of the fuel element.

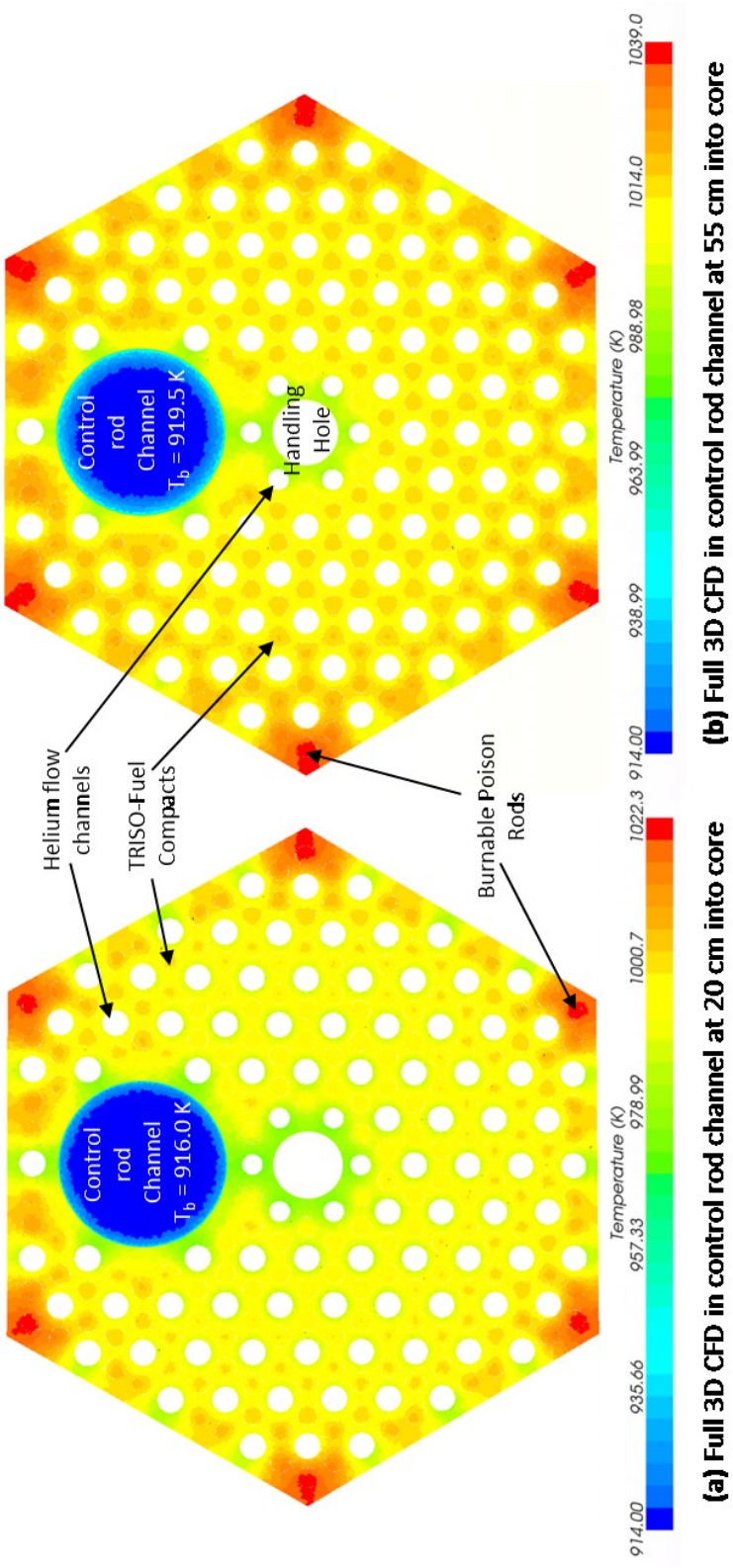

Figure 5.12 - Calculated temperatures using a full 3-D analysis of a prismatic fuel element with helium coolant bleed flow (3% of total) in the control rod channel (at 20 and 55 cm from entrance).

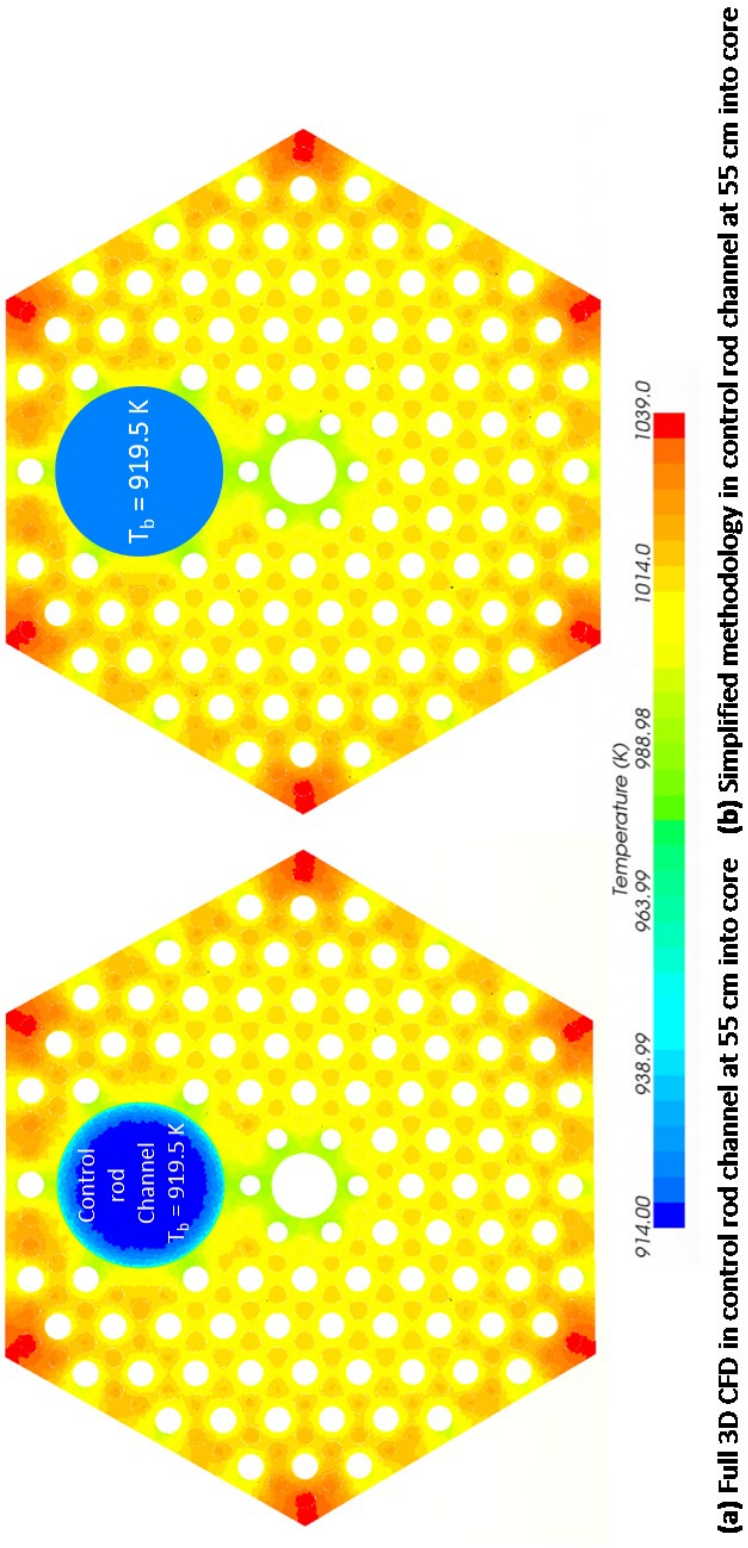

Figure 5.13 - Calculated temperatures using simplified methodology versus a full 3-D analysis of a prismatic fuel element with helium flow (3% of total) in control rod channel (at 55cm from entrance).

The helium flow rate in each of the 48 control rod channels in a prismatic VHTR core is 0.20625 kg/s, which totals 3% of the total helium flow rate into the reactor. Thus, 97% of the total helium coolant flows through the coolant channels of the core. The corresponding helium flow rate in each of the 1.5875 cm diameter, coolant channels is 0.02968 kg/s. Figures 5.12a and 5.12b compare the calculated temperature fields in a prismatic fuel element at two axial locations from the entrance (or top) 20 cm and 55 cm, respectively. In these figures, the analysis is performed using a full 3-D numerical simulation of the fuel element with helium flow through the control rod channel and the coolant channels, but with no helium bypass flow. In these calculations, the volumetric heat generation rate in the corner burnable poison rods is assumed the same as in the fuel compacts and the helium inlet temperature of 914 K is the same as in the coolant and the control rod channels. The axial heat generation rate in the fuel compacts is assumed uniform, since the height of the fuel element is $1/10^{th}$ of that of a VHTR active core.

The results in Figs. 5.12a and 5.12b show the growth of the thermal boundary layer and the increase in the local helium coolant bulk temperature in the control rod channel with axial elevation. These figures also show the calculated temperature contours in the thermal boundary layer within the control rod channel. The radial extent of the thermal boundary layer is limited to the region next to the channel wall, but does grow with axial distance as the flow progresses down the channel. Because of the high helium flow rate in the control rod channel, its bulk temperature is significantly lower than that in the surrounding helium coolant channels. At 55 cm from the fuel element entrance, the helium bulk temperature in the control rod channel is 919.5 K (Fig. 5.12b), versus 940.5 K in the surrounding coolant channels.

The simplified thermal-hydraulics analysis methodology calculates almost the same temperature distribution in the fuel element, and the same helium local bulk temperatures in the control rod and coolant channels, but provides no details on the growth as well as the temperature gradient in the thermal boundary layers in the control rod and the coolant channels. This thermal-hydraulics analysis methodology significantly reduces the number of the numerical mesh elements and the computation time. The results calculated using the simplified methodology (Fig. 5.13b) are compared with those obtained using a full 3-D analysis (Fig. 5.13a), at 55 cm from the entrance of the coolant channels in the fuel element. Note that Fig. 5.13a is the same as Fig. 5.12b.

In Fig. 5.13b, the helium flow in the control rod and helium coolant channels in the fuel element is simulated as 1-D, in conjunction with the forced convection correlations in Eqs. (4.6) and (4.9) for calculating the local heat transfer coefficient. The helium coolant flow in these channels is thermally coupled to the 3-D conduction in the graphite and fuel compacts in the fuel element and exits at the same bulk temperature as that calculated using the full 3-D analysis (928.35 K). Although no meshing is required in the control rod and coolant flow channels when using the simplified methodology, in the full 3-D analysis meshing the control rod channel (Fig. 5.13a) adds approximately 560,000 numerical mesh elements to the total used in the analysis with no helium flow in the control rod channel. In addition, the full 3-D simulation runs significantly slower than that with the simplified methodology.

A full simulation of the fuel element with helium flow in the control rod channel using the simplified methodology (Fig. 5.13b) took 2.5 hours to complete versus ~ 26 hours for the full 3-D simulation (Fig. 5.13a). However, the calculated temperatures in

Figs. 5.13a and 5.13b using both simulation methods are almost identical. The largest difference between the calculated maximum temperatures in the fuel element using the two methods is 0.3 K, and the temperature difference between Figs. 5.13a and 5.13b at the center of the element near the control rod channel is 0.12 K.

These results further confirm the effectiveness and accuracy of the simplified methodology for thermal-hydraulics analysis of the fuel element with the helium flow in the control rod channel. In the next subsection, the simplified methodology is used to perform the thermal-hydraulics analysis of a prismatic fuel element with helium flow in the control rod channel and helium bypass flow in a 5-mm wide interstitial gap. The results show the combined effect of the helium bleed flow in the control rod channel and through the interstitial gap on the calculated temperatures in the fuel element.

5.3.4. Fuel element analysis with helium bypass and flow in control rod channel

The results of the combined effect of the interstitial helium bypass flow and the helium flow through the control rod channel on the temperatures of the fuel element, shown in Fig. 5.14b at 55 cm from the entrance. These results are obtained using the simplified methodology for performing the thermal-hydraulics analysis of the fuel element. Note that Fig. 5.14a is the same as Fig. 5.13b with helium flow in the control rod channel, but without a helium bypass flow. In both figures, the volumetric heat generation rate in the corner burnable poison rods is assumed the same as that in the fuel compacts. The helium bypass flow cools the edges of the fuel element, including the poison rods, but raises temperatures in the central region of the element (Fig. 5.14b).

The peak temperature in the center region of the element in Fig. 5.14b is ~ 1030 K versus 1015 K in Fig. 5.14a without a helium bypass flow. In Fig. 5.14a, the edge

temperatures vary from 1005 K – 1018 K and those of the corner burnable poison rods peak at 1039 K. The helium bypass flow in Fig. 5.14b cools the edges of the fuel element to 975 K – 980 K and the burnable poison rods to ~ 1003 K. The 3-D simulation of the helium bypass flow in the 5-mm wide interstitial gap (Fig. 5.14b) increases the total number of the numerical mesh cells in the fuel element by an additional 2.75 million mesh cells, totaling 20 million cells. This prolonged the time to complete the calculations to ~ 48 hours, versus only ~ 2 hours in Fig. 5.14a without helium bypass flow.

The next section presents the results of the thermal-hydraulics analyses of a one element high (0.793 m) VHTR 1/6 core with and without helium flow in 5-mm wide interstitial gaps between the fuel elements and in the channels for the control rod elements. The modeled helium flow through the coolant and control rod channels is one-dimensional using the simplified methodology detailed earlier. The numerical meshing in the coolant channels is thus omitted, but the helium flow in the channels is coupled to 3-D heat conduction in the core's solid graphite moderator and fuel compacts. The helium flow in the interstitial gaps between the core fuel elements is modeled using full 3-D.

5.4 Thermal-hydraulics analysis of a one fuel element high VHTR 1/6 core

This subsection presents and discusses the results of thermal-hydraulics analyses of a one fuel element high (0.793 m) VHTR 1/6 core. The analyses are with and without helium bypass flows in interstitial gaps between fuel elements and bleed flow in the control rod channels (Fig. 5.15). The heat generation and conduction in the radial reflector graphite blocks insignificantly affect the temperature field in the active core region. Thus, the analyses include a single row of graphite blocks in the inner and outer radial reflectors.

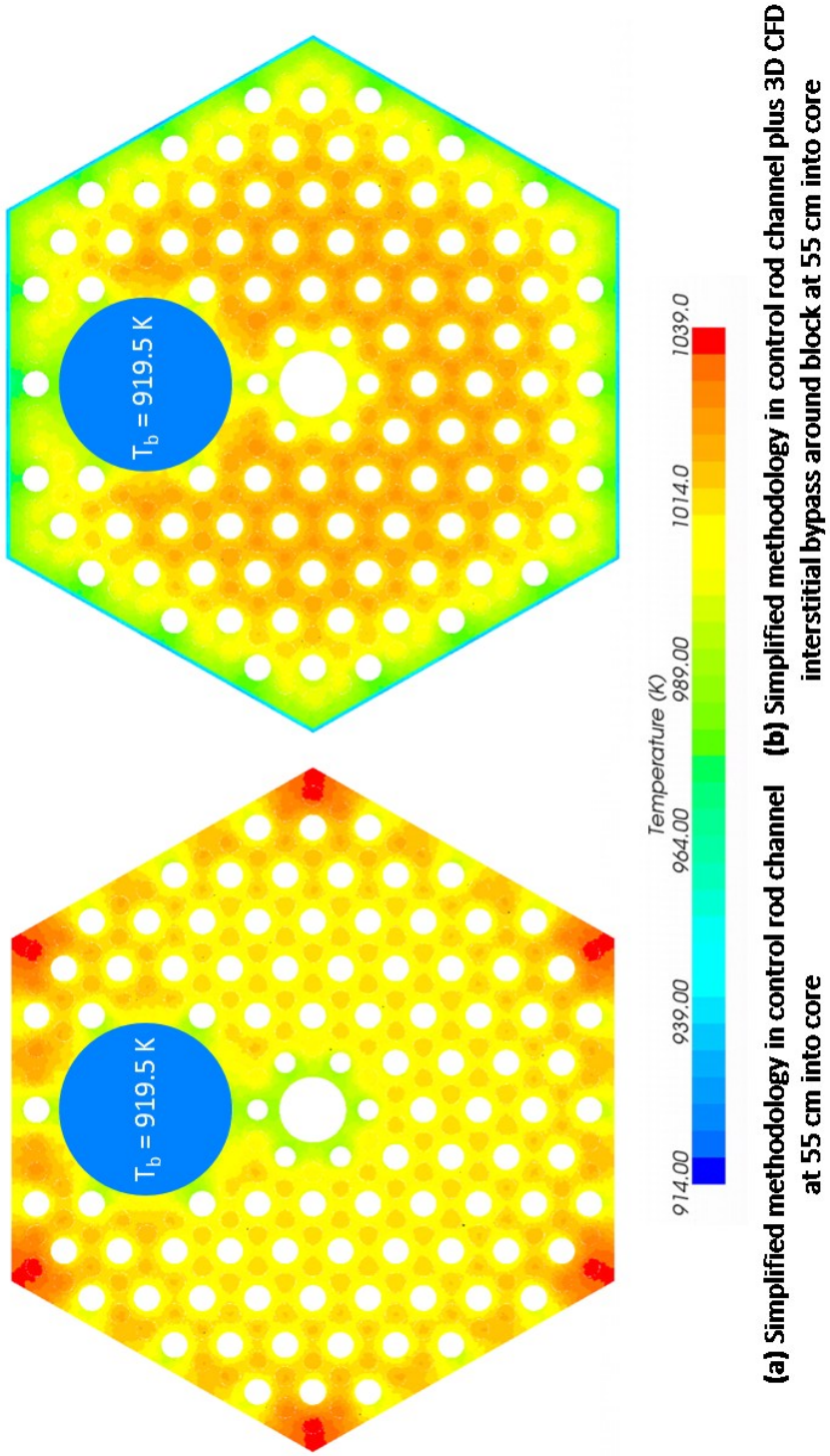

Figure 5.14 - Calculated temperatures using the simplified methodology of a prismatic fuel element with helium flow in the control rod channel and interstitial bypass flow (at 55 cm from entrance).

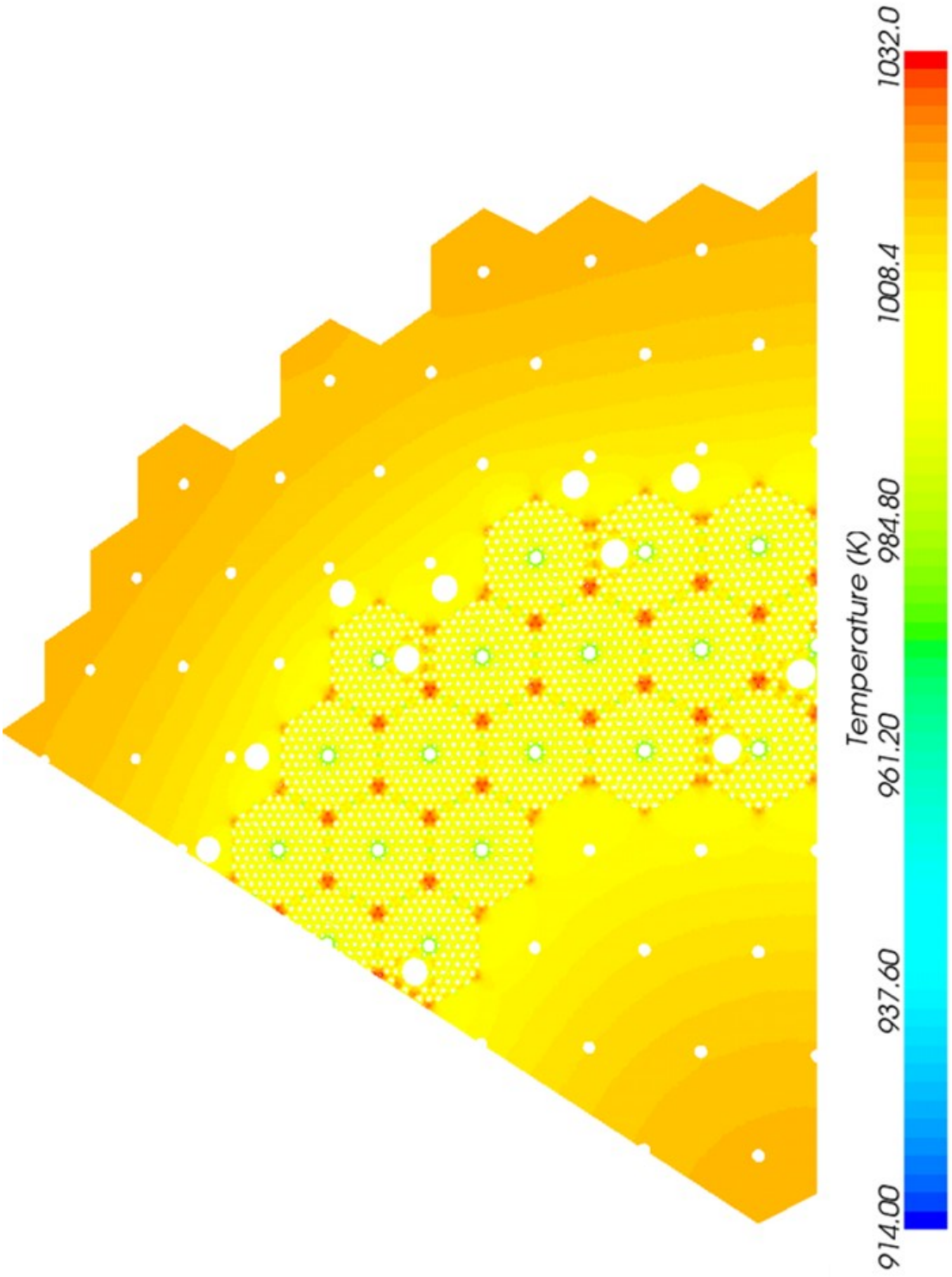

Figure 5.15 - Calculated temperature field for a one-fuel element (0.793 m) high, VHTR 1/6 core without helium bypass or bleed flow in control rod channels, 55 m from top of VHTR core.

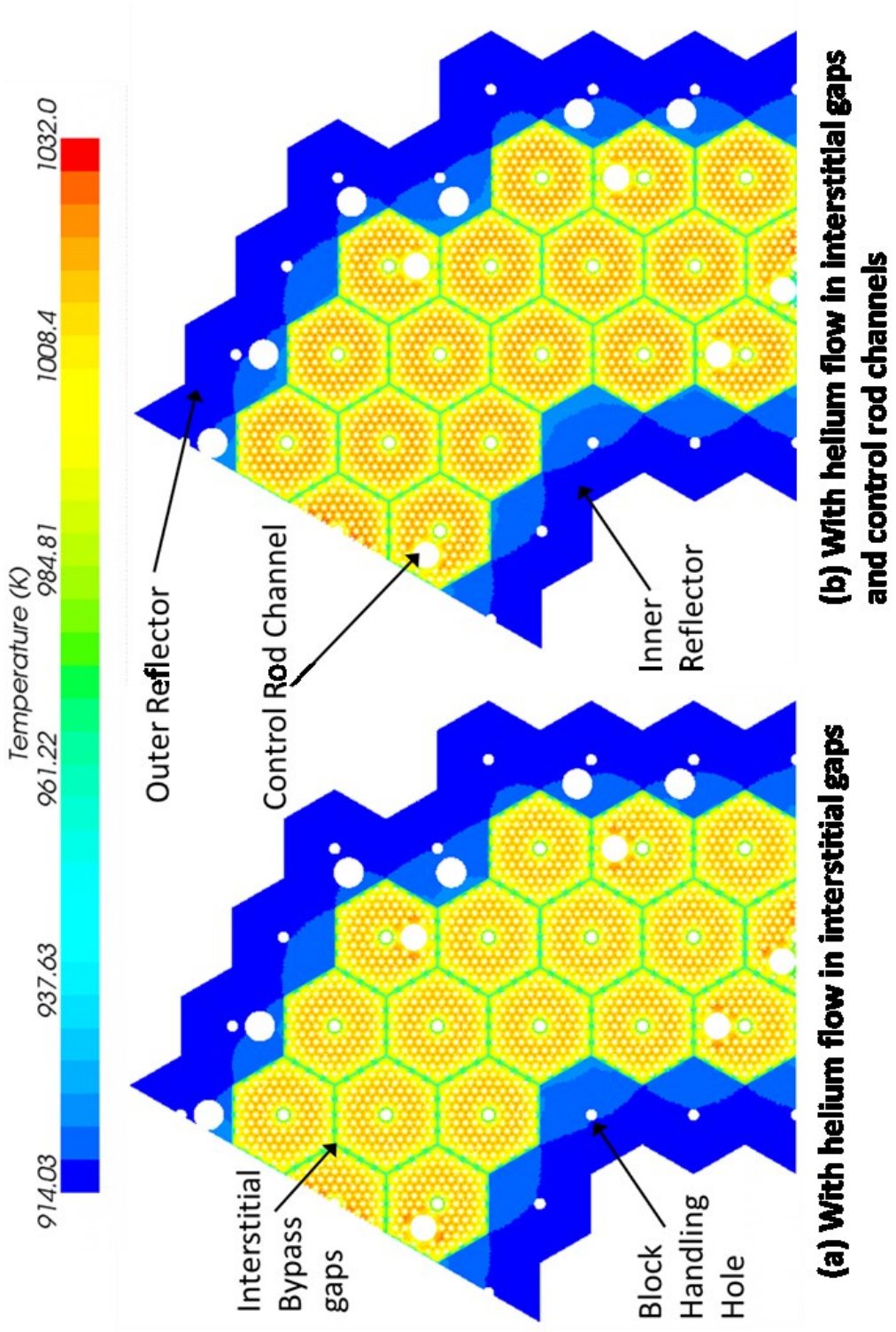

Figure 5.16 - Calculated temperature field for a one fuel element (0.793 m) high, VHTR 1/6 core with helium bypass flow and bleed flow in control rod channels, 0.55 m from the top of the core.

The objectives of the one-fuel element tall (0.793 m), VHTR 1/6 core thermal-hydraulics analyses are to further examine the effectiveness of the simplified methodology, to reduce the numerical meshing requirements and complete the calculations in a reasonable time. The performed thermal-hydraulics analyses in this section are for uniform axial and radial power profiles in the VHTR active core region, but the same helium inlet temperature (914.0 K) from the upper plenum, and same exit pressure (7.064 MPa). The helium bleed flow into the control rods channels is assumed 3% of the total entering the reactor (330 kg/s), while that flowing through the 5-mm wide interstitial gaps totals 10.67% (or 5.87 kg/s for the 1/6 core). Without flow in the control rod channels, the helium flow through the interstitial gaps increases to 11.0% of the total into the reactor.

The analysis performed in this section with helium bypass flow in the interstitial gaps and bleed flow in the control rods channels requires a large number of numerical mesh elements, totaling 109.9 million. They are broken down as follows: 21.0 M elements or cells in core fuel compacts; 638,000 cells in the corner burnable poison rods; 16.8 M cells in the graphite moderator of the fuel elements; 122,000 and 223,000 cells in the inner and outer radial reflector blocks; and 71.1 M cells in the interstitial bypass flow gap between the core fuel elements. Owing to the large number of the mesh elements used, particularly for modeling the 3-D helium flow in the interstitial gaps, calculations took 10 - 11 days to complete using the computer hardware discussed in Chapter 3. It is worth noting that the total number of mesh elements used in this analysis is comparable to that implemented in the next section for the thermal-hydraulics analysis of a full height (9.93 m) VHTR 1/6

core, including the 1.2 and 0.8 m top and bottom graphite reflectors. Such an analysis does include interstitial helium bypass flow or helium bleed flow in control rod channels.

The results in Figs. 5.15 and 5.16 highlight the effect of the interstitial helium bypass flow on the calculated temperatures in the reactor core, 0.55 m from the entrance (top). Fig. 5.15 clearly shows the hot spots at the locations of the burnable poison rods, in which the volumetric heat generation is assumed conservatively the same as that in the fuel compacts. The temperature of these rods peaks at 1032 K. The temperatures of radial graphite reflector blocks are 10 – 20 K hotter than the graphite in the core fuel elements (Fig. 5.15). This can be attributed to two effects: (a) the convective mixing of the developing helium flow in the entrance section of the coolant channels ($z/D \leq 25$), which increases the local heat transfer coefficient, thus enhancing the cooling of the fuel elements; and (b) the axial conduction that transfers heat from the bottom to the top of the reflector. The high thermal conductivity of graphite also stimulates radial heat conduction in the reflector (Figs. 5.15-5.18).

The heat transfer between the radial reflector blocks and the nearest fuel elements in the core is small, and insignificant with helium bypass flow through the interstitial gaps (Fig. 5.16). Such flow has an insulating effect that hinders heat transfer, not only among the core fuel elements but also to and from the surrounding graphite reflector blocks. Without helium bypass flow, the temperatures near the center of the core fuel elements (Fig. 5.15) are 20 – 40 K lower than those with helium bypass flow (Fig. 5.16a) due to the decrease in the helium flow rate in the core coolant channels. The helium bleed flow in the control rod channels also increases the temperature in the core fuel elements because it further decreases helium flow rate in the core coolant channels (Fig. 5.16b).

Figures 5.16a and 5.16b show the temperatures of the fuel compacts in the VHTR core, including those near the control rod channels. In Fig. 5.16a, it is clear that the temperatures of the fuel compacts in close vicinity to the control rod channels are higher than in the interior of the core fuel elements. The helium bleed flow in the control rod channels increases the temperatures within the core fuel elements by 2 – 3 K, except near the channels, where the temperatures decrease by 3 – 4 K (Fig. 5.16b). In both Figs. 5.16a and 5.16b, the temperatures in the rings of the radial graphite blocks adjacent to the annular core region remain low (914 – 935 K). The next subsection presents the results of the thermal-hydraulics analysis for full height VHTR 1/6 core without helium bypass flow nor bleed flow in the control rod channels, further examining the validity of the simplified analysis methodology.

5.5 Thermal-hydraulics analysis of a full height 1/6 core without bypass flow

The performed thermal-hydraulics analysis of a full height (9.93 m), prismatic VHTR 1/6 core without helium bypass flow or bleed flow in the control rods channels, used the simplified methodology for the operating conditions listed in Table 5.1, with both uniform and chopped-cosine axial power profiles and a uniform radial power profile. This analysis took approximately 72 – 108 hours of real time to complete using the computational hardware discussed in Chapter 3. Simulations using the 48 GB node ran significantly faster, likely due to a reduced reliance on the slower virtual memory. ANL (Pointer and Thomas, 2010) conducted similar runs of full 3-D thermal-hydraulics analysis for a full height VHTR 1/6 core, but with lower helium inlet temperature (784 K) and volumetric heat generation rate in the fuel compacts (33.59 MW/m^3). They used 24 cores of a 25.9 teraflop cluster and took over 300 hours of CPU time to complete. These

calculations also required an unknown amount of RAM, but in the authors' experience, it would have been an extensive amount.

The results of the performed thermal-hydraulics analysis of the full height VHTR 1/6 core are presented in Figs. 5.17 and 5.18. The inner and outer reflectors in a prismatic VHTR are made of the same IG-110 graphite as the fuel elements. This analysis is for a uniform volumetric heat generation in the fuel compacts, constant helium flow mass flux but different flow rates in the standard and smaller diameter coolant channels in the core, no helium bypass flow, and no helium flow in the control rod channels. Figures 5.17 and 5.18 show relatively uniform temperatures in the active core region, but hotspots at the corners of the core fuel elements where burnable poison control rods are located. This analysis is overly conservative, assuming that the poison rods experience the same volumetric heat generation rate as in the fuel compacts. In reality, the hot spots at the burnable poison rods locations (Fig. 5.7a) would not exist to the same extent because the volumetric heat generation in the poison rods would be lower, ~25% – 30% of that in the fuel compacts. It is notable that slightly smaller hot spots occur near the core's reserve shutdown channels, not cooled in this analysis (Fig. 5.17). The hot spots at the locations of the burnable poison rods in the core are only a concern under non-standard flow conditions and with unrealistically high volumetric heat generation rate in these rods.

The inevitable helium bypass flow through interstitial gaps between the core fuel elements and between these elements and the surrounding graphite assemblies of the radial reflector is likely to cool the edges of the fuel elements and alleviate the hot spots at the burnable poison rods' locations. This would occur at the expense of increasing the temperature in the interior of the core fuel elements. Based on the results discussed

earlier for a fuel element with and without helium bypass flow in Figs. 5.7 – 5.11, such an increase in the core fuel elements' temperatures could be as much as 30 K.

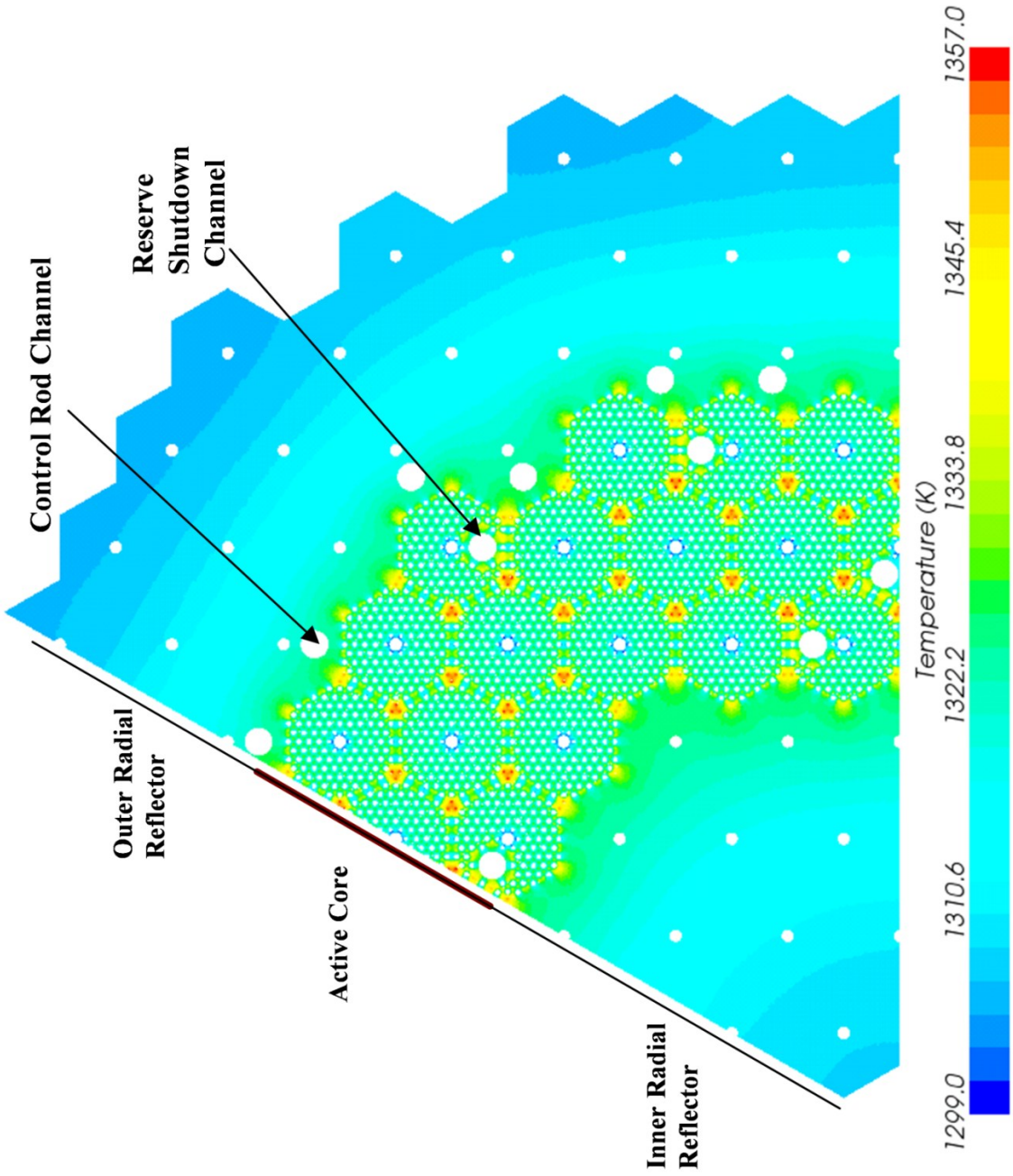

Figure 5.17 - Calculated radial temperatures field at core mid-plane in the thermal-hydraulics analysis of a full height, VHTR 1/6 core with constant volumetric heat generation in fuel compacts and no helium bypass flow.

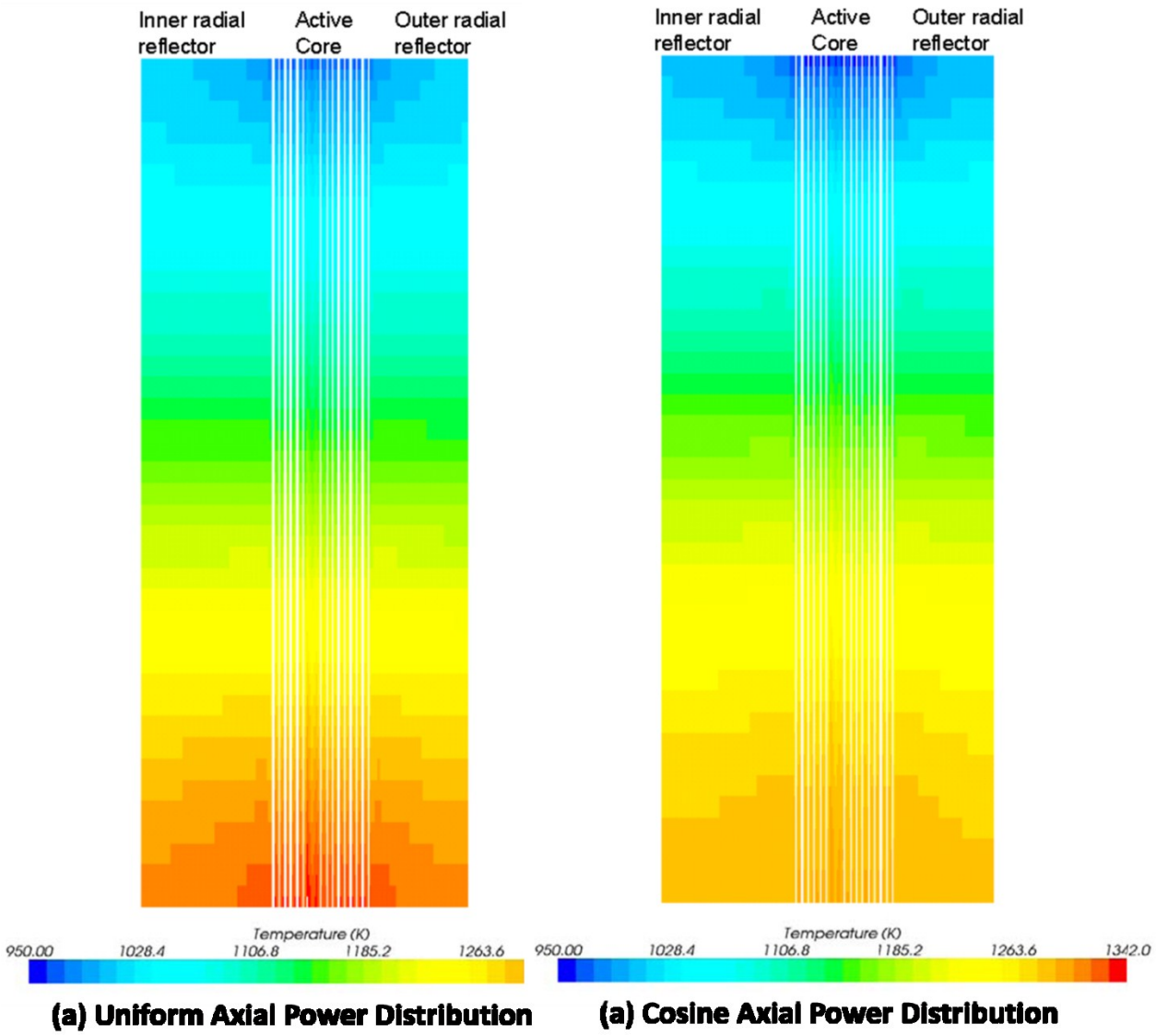

Figure 5.18 - Calculated axial temperature distributions in the thermal-hydraulics analysis of a full height VHTR 1/6 core with constant volumetric heat generation and no helium bypass flow.

The presented images of the calculated temperature fields of the VHTR core in Figs. 5.18a and 5.18b also show the axial delineation in the numerical meshing. The two figures are for the same total heat generation in the reactor core (600 MW_{th}), but different axial power profiles. With a uniform axial power profile, the hottest temperatures occur at the exit of the core (bottom of Fig. 5.18a). With a chopped-cosine axial power profile, however, (Fig. 5.18b) there are notable differences in the calculated axial temperature

distribution. The cosine power profile increases the temperatures in the axial middle section of the core by more than 50 K, but decreases the temperatures near the core exit (bottom of Fig. 5.18b).

This chapter investigated and demonstrated the effectiveness and accuracy of the developed simplified methodology for conducting thermal-hydraulics analyses of VHTR core and hexagonal fuel elements with and without helium flows through the control rod channels and in interstitial gaps. Results indicate this methodology is accurate and quicker than full 3-D CFD for performing thermal-hydraulic analyses for fuel elements and a VHTR 1/6 core both with helium bypass flow in interstitial gaps between fuel element and helium “bleed” flow through the control rod channels and without.

Chapter 6 - Summary and conclusions

This research developed an effective thermal-hydraulics analysis methodology that markedly reduces the numerical meshing requirements and computational time. The simplified thermal-hydraulics analysis methodology is an effective surrogate to a full 3-D analysis of VHTR fuel elements or a full core. It couples a 1-D convective flow and heat transfer of helium in the coolant channels to the full 3-D heat conduction in the graphite moderator and fuel compacts of the VHTR fuel elements. Besides the helium local bulk temperature in the channels, the local heat transfer coefficient is calculated using a Nusselt number correlation, developed and validated in this work. This methodology effectively decreases the total computation time and simplifies the meshing requirements with a negligible effect on the accuracy of the numerical results. In addition to omitting the numerical meshing in the coolant channels, it decreases the total computation time by a factor of ~33 – 40 with little effect on the calculated temperatures (< 5 K), compared to a full 3-D thermal-hydraulics analysis of a fuel element, without compromising the accuracy of the results.

The developed correlation accounts for the effect of entrance mixing, which increases the local heat transfer coefficient. The entrance region extends to ~ 25 times the channel diameter ($z/D \leq 25$). Beyond this entrance length, turbulent convection becomes fully developed and the local Nusselt number becomes independent of axial distance in the channel. The developed correlation is within $\pm$ 2% of the numerical results, including in the entrance mixing length. It compares favorably, to within 10%, with Taylor's correlation (based on high temperature hydrogen heat transfer, Taylor, 1967). For the local bulk temperature of the helium flow in the coolant channels, the developed Nusselt

number correlation calculates the local heat transfer coefficient. The calculated values are used, in conjunction with the calculated heat flow from the graphite to the VHTR coolant channels wall to determine the local wall surface temperature.

Performed are thermal-hydraulics analyses of a VHTR fuel element, with and without helium bypass flow in interstitial gaps (5 mm wide) and helium bleed flow in the control rod channels. Analyses are also performed of a one-fuel element tall VHTR 1/6 core, with and without helium bypass flow, and of a full height VHTR 1/6 core without helium bypass or bleed helium flow. These analyses that use the developed simplified methodology in the STAR-CCM+ commercial software package account for the changes in the properties of graphite, fuel compacts, and helium with temperature. The thermal-hydraulics analyses are for the same reactor thermal power (600 MWt_h) and inlet and exit temperatures of 914 K and 1263 K, using both uniform and chopped-cosine axial power profiles in the active reactor core. Although the axial thermal power profile slightly changes the local helium coolant bulk and channel wall temperatures, it insignificantly affects the local values of the heat transfer coefficient in the coolant channels.

A full 3-D thermal-hydraulics analysis of a single fuel element without a helium bypass flow took ~ 100 hours of real time to complete, versus only ~ 3 hours with the simplified methodology. The calculated temperature fields in the thermal-hydraulics analyses of a VHTR fuel element using the full 3-D and the simplified methodology are similar and the values are within a few degrees (< 4 K). The performed thermal-hydraulics analysis using the simplified methodology for the fuel element without helium bypass flow, but with helium flow in the control rod channel, took 2.5 hours to complete versus ~ 26 hours using a full 3-D simulation. The relatively high helium flow rate in the

control rod channels decreases the flow rate in the rest of the coolant channels of the VHTR core. The largest difference between the calculated maximum temperatures in the fuel element using the simplified methodology and the full 3-D simulation is 0.3 K, and the temperature difference near the control rod channel is 0.12 K.

The helium bypass flow in the interstitial gap between the core fuel elements has a beneficial effect on the hot spots at the corner burnable poison rods. Results show that the helium bypass flow in the 5-mm wide interstitial gap cools the edges of the fuel element, including the corner burnable poison rods, but raises the temperature in most of the central region of the fuel element. Even without bypass, the intensity of these hot spots dramatically decreases as the volumetric heat generation rate in the poison rods decreases to a level more akin to that expected during nominal reactor operation (~ 25% of that in the fuel compacts). When the assumed volumetric heat generation rate in the corner burnable poison rods is the same as in the fuel compacts, the helium bypass flow increases the temperatures in most of the fuel element by ~ 10 – 15 K, while reducing the edge temperatures by as much as ~ 32 K. With a helium bypass flow, the maximum temperature near the center of an average fuel element is 1018 K. Without a helium bypass flow, the temperature in most of the fuel element is lower except at the corner poison rods, where it peaks at 1029 K. Reducing the volumetric power generation rate in the corner burnable poison rods to 25% of that in a fuel compact has little change on the temperatures of the fuel element, but effectively decreases the poison rods temperature. The maximum temperature near the center of the fuel element with a helium bypass flow is 1021 K and that of the burnable poison rods is 1007 K. Decreasing the volumetric thermal power in the burnable poison rods from 100% to 25% of that in the fuel compacts

increases the temperature near the center of the fuel element by only ~ 1 – 2 K, but decreases that of the poison rods by as much as 22 K.

In general, it is desirable to decrease helium bypass flow in interstitial gaps between VHTR core fuel elements. Results show that the helium bypass flow cools the edges but increases the temperatures in most of the fuel elements, and hence the differential thermal expansion. The interstitial gaps are initially present because of the manufacturing tolerances of the prismatic fuel elements, but their width changes during reactor operation due to thermal expansion and graphite swelling by neutron irradiation. Thermal-hydraulics analyses are also performed for a one element high (0.793 m) and a full height (9.73 m) VHTR 1/6 core using the simplified methodology and uniform and chopped-cosine axial power profiles. In addition to the significant savings in the computation time and numerical meshing requirements, the results are reasonably accurate, further confirming the effectiveness of the simplified methodology for future use in thermal-hydraulics and safety analyses of prismatic VHTRs or HTGRs.

Chapter 7 - Recommendations for future work

Much like all research, results typically identify additional areas for future investigations. This work demonstrated the effectiveness of the developed methodology for thermal-hydraulics analyses of VHTRs and the developed turbulent convection correlation in the coolant channels, including the entrance effects. Suggestions for future expansion of this research are summarized below..

(a) ***Perform experimental verification of the developed Nusselt number correlation*****.** These experiments would effectively measure the changes in the heat transfer coefficient in the entrance section of the coolant channels and heat flux and local temperatures at the inner wall as well as those of the bulk gas flow in the channels.

(b) ***Expand the use of the simplified methodology to thermal-hydraulics analysis of a full height VHTR 1/6 core, with helium bypass flow and helium bleed flow in the control rod channels*****.** This requires more advanced computation hardware, as compared to that used in the present research**,** and could quantify the benefits in term of decreasing the numerical meshing requirements**,** memory requirements and total CPU time to complete the calculations. One refinement that is relatively simple to implement is the radial power profile in the core, which this work assumes it uniform. Adding this profile to the CFD model is straightforward. The radial profile depends on fuel loading and the operational period. In addition, a given radial profile may not simply be a function of radius, but also of angle to some extent. This complicates the implementation of such a profile. This non-uniform radial behavior might also be present in coolant distributions. Effectively implementing a more specific coolant distribution is another improvement that could be made to the current work. It assumes that coolant flow in all core channels

of the same size is the same, reasonable but not entirely true. Chapter 5 demonstrated that in a given single block, the difference in the helium flow rate in any given channel compared to the average flow rate can differ by approximately 3 percent. This, in conjunction with the potential increase in the temperature gradients resulting from a radial power profile, could change the results of the thermal-hydraulics analysis.

(c) ***Investigate impact of failure modes on the temperatures of a full height 1/6 core.*** Another potential avenue for future research involves investigating different failure modes. The simplest of these involves examining the effect of coolant channel blockages, much like Tak et al. (2010), for example by reducing the convective heat transfer coefficient to zero in some channels. While the investigation of unintended flow blockages or impediments has benefits to the safety analysis of a VHTR, further examining other lesser explored failure modes may also prove valuable.

(d) ***Study the impact of VHTR operation life on the thermal conductivity of the graphite moderator and fuel compacts.*** Because the thermal conductivity of graphite (here, IG-110) is a strong function of irradiation dose, it might have significant effects on the heat transfer and peak temperatures within the graphite. Additional simulations run with different thermal conductivity functions could have significantly different results.

List of Appendices

Appendix A - Materials properties

Materials choices are an important consideration for the VHTR, given the very high temperatures in the reactor and the relatively complex effect of radiation on these materials, particularly the graphite moderator in the core and the steel reactor vessel. In HTGRs, serious considerations have been paid to the materials comprising the reactor; this fact remains true, as the temperatures for VHTRs have increased (Beck et al., 2010). The CFD code used in this work, STAR-CCM+, does not include most materials properties of interest, so it is important to import into the code a qualified set of temperature-dependent properties.

The bulk material in the VHTRs is nuclear graphite moderator in the annular core, surrounding radial inner outer reflector and the top and bottom reflector as well as the massive support columns in the lower plenum (see Figs. 2.7-2.9). There are several types of nuclear graphite considered by the reactor developers in different countries. In this work, the Japanese manufactured IG-110 nuclear graphite is used (Nightingale et al., 1962 and Ishiyama, 1996). The properties used in the present analyses are of un-irradiated graphite. The changes in the graphite properties, such as the heat capacity and thermal conductivity could affect the results of the analyses presented in this work, which is a topic for future follow-on research. Table A.1 lists the properties of the un-irradiated IG-110 nuclear graphite used in this work. The helium properties in the temperature regime of interest in the VHTR core (Tournier and El-Genk, 2008) are also listed in Table A.1. Figures A.1 and A.2 present the correlations and data for the specific heat and thermal conductivity of the solid materials in the VHTR core.

Table A.1 - Materials properties used in the present analyses of the VHTR core and fuel elements (temperature T in K).

Material Property	Material	Value or Correlation
density, ρ (kg/m^3)	IG-110 Graphite (block properties)	1740
specific heat, C_p (J/kg-K)*		$6.05\text{x}10^{-7}\,T^3 - 0.00269\,T^2 + 4.19\,T - 294$
thermal conductivity, k (W/m-K)**		$-13.2+2.50\text{x}10^4/(T+268)^{0.78}$
density, ρ (kg/m^3)	Composite Fuel (fuel properties), based on reported properties for IG-110 (Ishiyama et al., 1996, Nightingale et al., 1962) and UCO (IAEA, 2006)	1650
specific heat, C_p (J/kg-K), for 300<T<2000 K		$3.11\text{x}10^{-7}\,T^3 - 0.00155\,T^2 + 2.73\,T - 82.4$
thermal conductivity, k (W/m-K), for 300<T<1400 K		$8.5 + 7.68\text{x}10^4 / (T+268)^{0.995}$
density, ρ (kg/m^3)	Helium (coolant properties), (Tournier and El-Genk, 2008)	P/RgT
specific heat, C_p (J/kg-K)		5197.6
thermal conductivity, k (W/m-K)		0.000258 T + 0.103388
dynamic viscosity, μ (uPa-s)		0.03319 T + 13.0744

* Best fit of the data reported by Nightingale et al. (1962) for temperatures from 300 to 2000 K

**Best fit of the data reported by Ishiyama et al. (1996) for temperatures from 300 K to 1400 K

The material properties for the fuel compacts prove to be rather more complex. The fuel compact consists of TRISO particles are dispersed in a graphite matrix, and thus, effective properties for this heterogeneous mixture are needed. There are a number of approaches that could be used to model the properties this matrix of coated fuel particles and graphite. The expression for the specific heat, relatively straightforward, is obtained based on the mass fractions of the different materials on the fuel compacts. Barring irregularities in the arrangement of the fuel particles within the graphite matrix, this work assumes the fuel particles are uniformly dispersed in the graphite matrix with a packing fraction of 0.289 (MacDonald et al., 2003. The specific heat of the fuel compact is the summation of the mass fractions of each of the components times their individual specific heat. In Table A-1, the specific heat of each component (UCO, SiC, pyrolytic graphite in the TRISO particle and the IG-110 making up the graphite matrix) as a function of temperature are compiled and then multiplied by the relative mass fractions to determine the specific heat of the fuel compacts. A best fit polynomial of that data are obtained for use in STAR-CCM+, as the code requires that specific heat be either a constant or a polynomial function of temperature. The polynomials in Fig. A.1 are those of the specific heat as a function of temperature for both the fuel compacts and the un-irradiated IG-110 graphite.

For the thermal conductivity of the fuel compacts, Maxwell's derivation for widely dispersed spheres (Eq. A.1) in an otherwise homogenous material is used (Leung and Dooley, 2002). Rayleigh's derivation, which involves additional corrective terms in the denominator, is more appropriate in the case densely packed spheres, but even in cases

where the spheres nearly touch, its effect is minimal. Thus, the Maxwell's, less complicated equation, is used instead (Leung and Dooley, 2002), as:

$$\frac{k_{eff}}{k_0} = 1 + \frac{3\varphi}{\left(\frac{k_1+2k_0}{k_1-k_0}\right)-\varphi} \qquad \text{(A.1)}$$

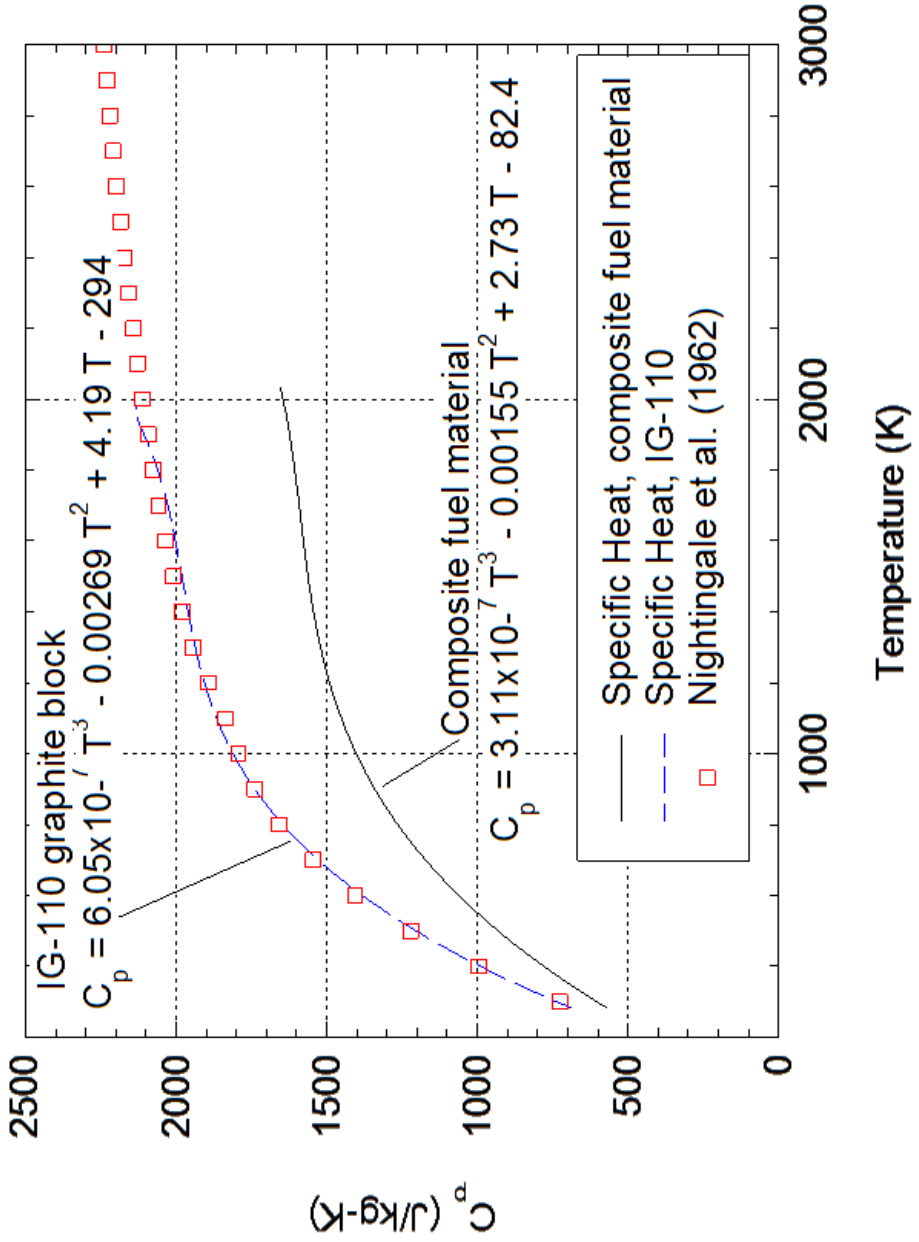

Figure A.1 - Specific heats for fuel compacts and un-irradiated IG-110 nuclear graphite as functions of temperature.

In Eq. A.1, k_{eff} is the effective thermal conductivity of the fuel compact, k_n is the thermal conductivity of material n, 0 being the graphite matrix, and φ is the volume fraction of the coated fuel microspheres.

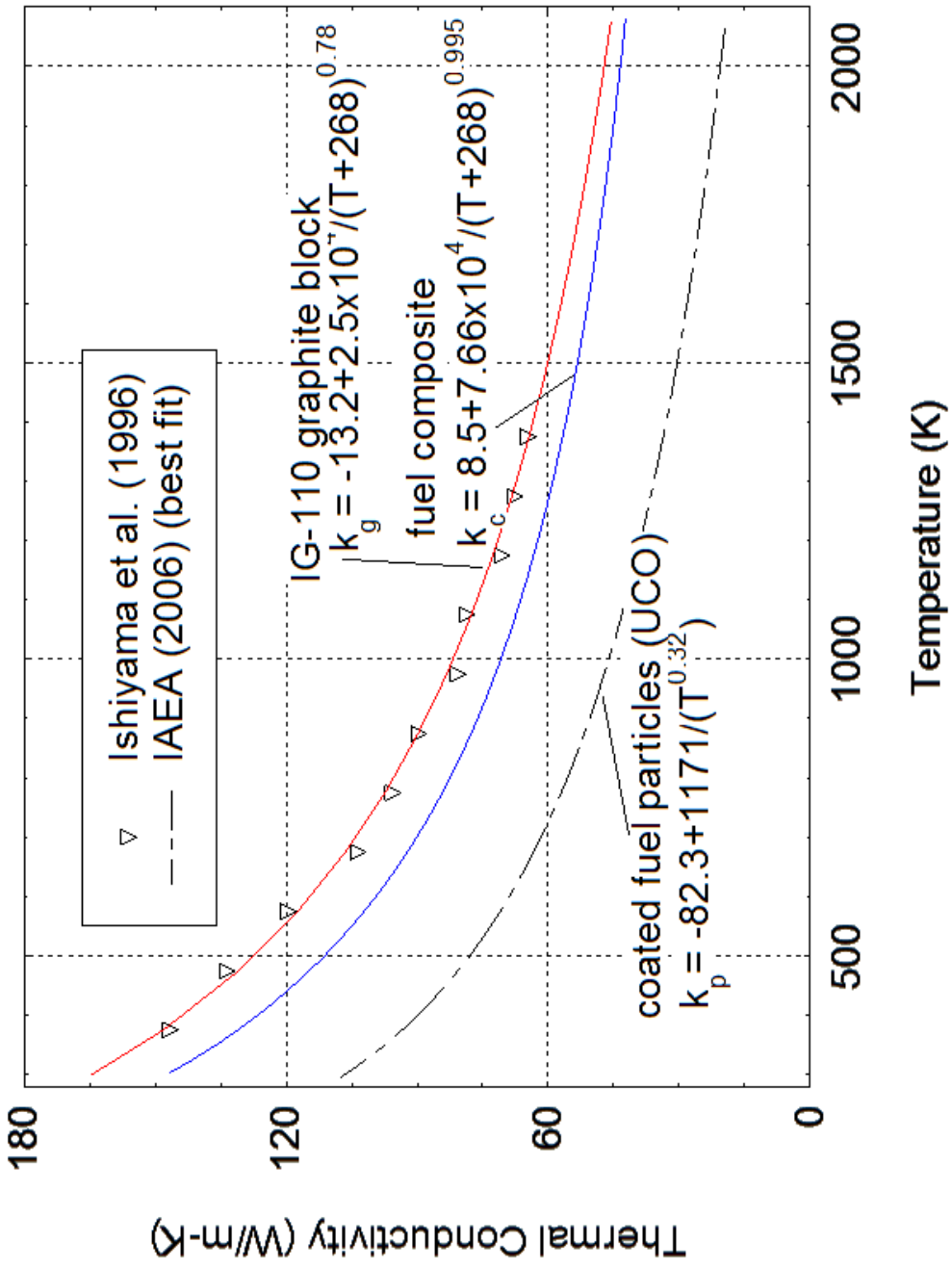

Figure A.2 - Thermal conductivities coated fuel particles and un-irradiated IG-110 as functions of temperature.

The graphite matrix in the fuel compact is IG-110. The thermal conductivity of the fuel compact requires the effective thermal conductivity of the TRISO fuel microsphere. Eq. A.1 is applied first to obtaining thermal conductivity of the coated fuel particles by simulated each coating layer as a sphere embedded within the homogenous matrix of graphite and spheres represented the other coating layers. Eq. A.1 is them used to obtain the average thermal conductivity of the fuel compact as a homogenous matrix of IG-110 nuclear graphite with dispersed coated fuel particles. The effect of the fuel microspheres on the average thermal conductivity of the coated fuel particle, as compared to that of the IG-110 nuclear graphite can be seen in Fig. A.2. The developed expression for the average thermal conductivity of the fuel compact as a function of temperature is listed in Table A.1.

Appendix B - Choice of turbulence models in thermal-hydraulics analysis

Computational Fluid Dynamics (CFD) codes use a variety of methods to solve for and model fluid flows, most of which are based on the Navier-Stokes equations. Flow in this work is turbulent, so direct solutions of the Navier-Stokes equations are not ideal. As a finite volume solver, STAR-CCM+, the code of choice for this work, has a limited supply of options available to model turbulent flows. The code package does not come equipped with the ability to solve high Reynolds number flows via direct numerical simulation (understandably so, as even moderate Reynolds number flows can be difficult to solve without vast computing resources using direct solution over all possible values of the Navier-Stokes equations).

STAR-CCM+ uses the Reynolds-Averaged Navier-Stokes (RANS) approach with a variety of different implementations in order to resolve turbulent flows (CD-adapco, 2012). The code package also includes Large Eddy Simulation (LES) and Detached Eddy Simulation (DES), but special allowances are made in order to use these models (namely additional computational costs along with additional user inputs). Choosing which of the implementations available is appropriate is an important task when modeling simulations in STAR-CCM+ as each has its own quirks and appropriate applications. STAR-CCM+ employs four distinct RANS solvers, each with its own set of sub-models namely (CD-adapco, 2012): (a) K-epsilon; (b) K-omega, (c) Spalart-Allmaras; and (d) Reynolds Stress Turbulence.

The k-epsilon model, a modification of the Navier-Stokes equation, uses two eddy expressions for two transport variables (k and ε). The k variable is representative of turbulent kinetic energy transport, while ε is representative of the dissipation of turbulent kinetic energy. The standard model uses differential equations (B.1) and (B.2) for k and ε, and equation (B.3) relates the two together (Jones and Launder, 1972; Launder and Sharma, 1974):

$$\frac{\partial \rho k}{\partial t} + \frac{\partial}{\partial x_j}\left[\rho u_j \frac{\partial k}{\partial x_j} - \left(\mu + \frac{\mu_t}{\sigma_k}\right)\frac{\partial k}{\partial x_j}\right] = \tau_{ij} S_{ij} - \rho\varepsilon + \varphi_k \ , \tag{B.1}$$

$$\frac{\partial \rho \varepsilon}{\partial t} + \frac{\partial}{\partial x_j}\left[\rho u_j \varepsilon - \left(\mu + \frac{\mu_t}{\sigma_\varepsilon}\right)\frac{\partial \varepsilon}{\partial x_j}\right] = c_{\varepsilon 1}\frac{\varepsilon}{k}\tau_{ij} S_{ij} - c_{\varepsilon 2} f_2 \rho \frac{\varepsilon^2}{k} + \varphi_\varepsilon \ . \tag{B.2}$$

In these equations, τ_{ij} are the Reynolds stresses, functions of the eddy viscosity, μ_t. It contains the primary relationship between k and ε:

$$\mu_t = c_\mu f_\mu \rho k^2 / \varepsilon \ , \tag{B.3}$$

where the velocity scale is on the order $k^{1/2}$ and the length scale is of the order $k^{3/2} / \varepsilon$. C and σ values with subscripts represent constants in use (as determined by the code package; these defaults can be changed but it is not recommended), f-subscripts symbolizes wall damping functions, and φ-subscripts are explicit wall terms (Bardina et al., 1997). The above equations adequately describe the standard two-layer k-ε turbulence model, which has been in use in finite volume solvers since proposed by Launder and Sharma (1974). This model is not the default recommended in STAR-CCM+. Instead, the code package uses a "realizable" two-layer model (one-layer models are not considered in this discussion, as they are generally more limited than two-layer models). This model implements a different equation for ε (B.4), and treats c_μ as a function of flow and

relative turbulence properties as opposed to a constant (B.5) (Alfonsi, 2009; Shih, 1994; Lien, 1998).

$$\rho \frac{D\varepsilon}{Dt} = \frac{\delta}{\delta x_j}\left[\left(\mu + \frac{\mu_t}{\sigma_\varepsilon}\right)\frac{\delta \varepsilon}{\delta x_j}\right] + \rho C_1 S\varepsilon - \rho C_2 \frac{\varepsilon^2}{k+\sqrt{\upsilon\varepsilon}} + C_{1\varepsilon}\frac{\varepsilon}{k}C_{3\varepsilon}G_b \ , \tag{B.4}$$

$$c_\mu = \frac{1}{A_0 + A_S U^* \frac{k}{\epsilon}} . \tag{B.5}$$

In general, the realizable *k*-ε model is perceived to be the better of the two (at worst, the model should produce results as accurate as the standard model), and thus should be used when employing the *k*-ε model (Alfonsi, 2009; Bakker, 2005). The changes to the realizable *k*-ε model from the standard model help resolve wall effects better, and as such provide better data from the wall itself if the simulation is concerned with such effects (as this one is). Both realizable and standard models also have a one-layer approach, but this is by definition more limited than the two-layer implementation, and thus ignored for the purposes of this work.

The other sub-model of note available in STAR-CCM+ is the V2F *k*-ε model. It is generally intended for low Reynolds number turbulent flows and is therefore of little use to our system. The model does not use wall damping functions f, and as such is somewhat less effective for highly turbulent effects near the wall. This model was explored for an application to a system very similar to this by Pointer and Thomas (2010); their results indicated that the realizable two-layer *k*-ε model was the preferred model of choice for this simulation (they did not explore *k*-ω models in detail to the best of the author's knowledge).

Another *k*-ε model exists (not included in STAR-CCM+), the Renormalization Group Method (RNG). This model adds an additional term in the ε equation to account for the interaction between dissipation and mean shear (Bakker, 2005). It also makes allowances for changes in the turbulent Prandtl number and effective viscosity (less constants), which improves simulation fidelity for transitional flows, as well as heat and mass transfer from the wall (highly applicable to this simulation). The realizable *k*-ε method provides many of the same benefits as this model while addressing some jet and swirl effects, though the RNG model is thought to do a better job of resolving some transitional flows (Bakker, 2005).

Generally, *k*-ε models are the default models when turbulence is accounted for in finite volume solvers, and a great deal of work has been done using variants on the model (indeed, the default turbulence model in STAR-CCM+ is the realizable two-layer *k*-ε). The *k*-ε model gives good results for flows with small pressure gradients, and is relatively insensitive to effects propagating from free-stream turbulence (Bardina et al., 1997). As such, it does a good job at capturing effects near walls (again, given a small pressure gradient in the direction normal to the wall), but does so at the cost of an increased mesh refinement. It is only valid for fully turbulent flows – if the flow approaches the transition region, the results begin to become invalid. *k*-ε models also struggle with swirling (not applicable here, LES simulations should be used for these), separation effects, and non-circular ducts (Bakker, 2005) (not applicable to most flows in the core, but if bypass flow is to be modeled, this effect must be taken into consideration).

Conversely, the *k*-ω model is not as widely applied in finite volume systems. *k*-ω models come in two primary sub-models: the standard one, and the shear stress transport model, which blends the *k*-ω and *k*-ε models.

Similar to the *k*-ε model, the *k*-ω model is a two equation eddy viscosity model. As before, the *k* variable is representative of the turbulent kinetic energy transport, while in this case the second variable, ω, represents the specific dissipation rate of turbulent kinetic energy, and accounts for the turbulent frequency of the system.

The transport equations for k and ω differ slightly from those of the *k*-ε model (Wilcox, 1993). As before, there are a number of constants in the equations (α, β's, and σ's are all constants), and the Reynolds stresses are a function of eddy viscosity μ_t (B.6):

$$\mu_t = \rho k/\omega \tag{B.6}$$

The standard *k*-ω model is not recommended for most applications, since while it can be fairly accurate, it tends to incorporate a fair amount of uncertainty into results due to the nature of the ω variable in the free stream (values can get very large away from the wall) (Bardina, 1997). As such, the unmodified *k*-ω model sees very little use aside from some specialized cases, none of which applies to pipe flow.

The shear stress transport (SST) *k*-ω model, on the other hand, can be applied to much more varying systems and vies with the realizable *k*-ε two-layer model for general finite volume use. Each has advantages and disadvantages that make them more applicable to specific systems. The SST *k*-ω model uses the same *k* equation, but adds a blend function F1 to the ω equation in order to emulate having both ω and ε present. It

also uses a forcing function on the eddy viscosity (B.7) to limit large swings in the values away from the wall (Menter, 1994a, 1994b):

$$\mu_t = \frac{\rho k}{\omega} / (\max\left(1 \,||\, \frac{\Omega F_2}{a_1 \omega}\right)) \quad . \tag{B.7}$$

Note that Ω is the vorticity and F_2 is a function of wall distance. The changes in the ω equation act to transform the equation into the *k*-ω model near the wall and the *k*-ε model away from the wall in free stream areas.

One interesting addition to the SST *k*-ω model is an additional formulation for the transition model (namely near the boundary layer of certain walls). While not important for the formulation of this model, this does have some impact on other systems. For all the models in STAR-CCM+ except SST *k*-ω, the only available option for emulating transition in turbulent flow near a boundary is the turbulence suppression model, where a distance from a wall is specified and turbulence is ignored at the wall up to that specified distance from the wall. In the *k*-ω model, a second transition approach is available: the Gamma ReTheta transition model. This model uses a correlation to force transition in a dynamic region near the boundary layer, with a distance based on local variables and the free stream Reynolds number, much like a standard engineering correlation (CD-adapco, 2012). Some prior knowledge about the flow is needed to make use of this, and so the turbulence suppression is most often used, but this specification can be of use for certain flow regimes.

The basic *k*-ω model is of very little use outside specialized corner cases. The SST *k*-ω model, though, bears investigation as a model of use for this work. The equations are well refined, and the model retains the positive characteristics from the *k*-ω model (wall

flow) while still keeping fidelity in the free stream by incorporating the *k*-ε model. Based on the views of some experts (Bakker, 2005), the realizable k-ε model tends to be the more widely used of the two.

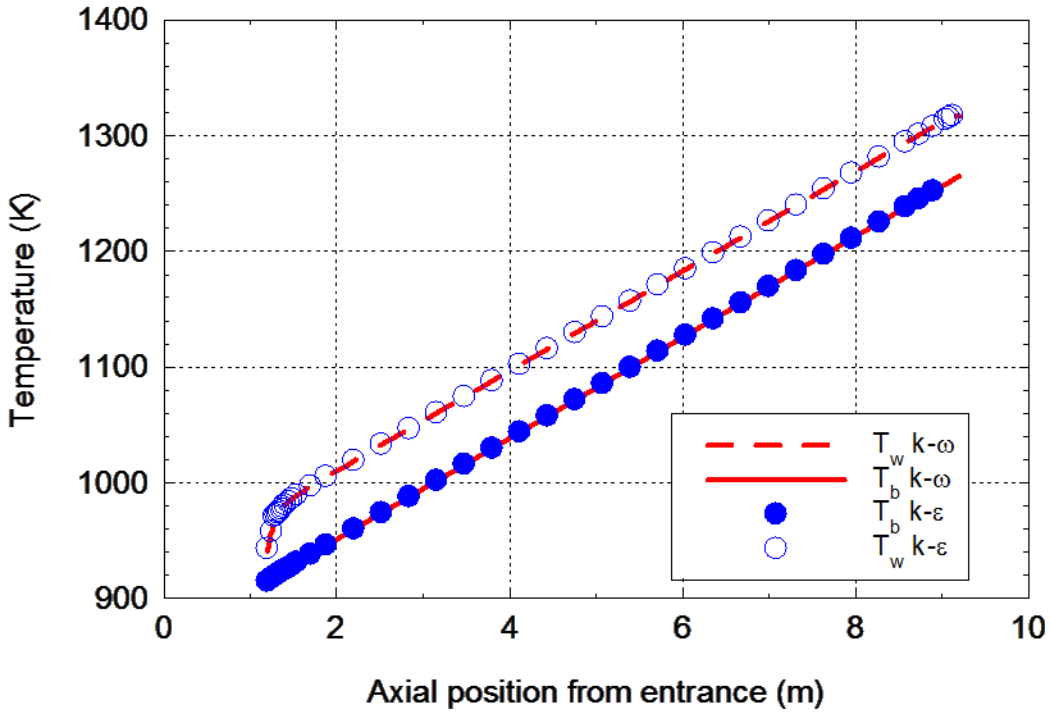

Figure B.1 - Effect of turbulence model on the calculated temperature distribution in the single channel module.

This work compared the effect of the *k*-ε and *k*-ω models in order to determine their effect on the simulation. Although the research done by Pointer and Thomas (2010) and Sato et al. (2010) indicates that the *k*-ε model is better suited for this sort of work, no appreciable difference (< 2%) was found between the two models, as is apparent in Fig. B.1. Nevertheless, the *k*-ε model was chosen as the basis for this work based on the familiarity with this model for channel flow combined with the recommendations noted (Pointer and Thomas, 2010; Sato et al., 2010).

The Spallart-Allmaras turbulence model, in contrast with the k-ε and k-ω models, is a one equation eddy model. The equation directly accounts for the transport of turbulent kinetic energy, and introduces terms to adjust for the production and dissipation of the turbulent kinetic energy (Spalart, 1992). The model does an acceptable job of resolving well-defined, wall-bounded flows, but struggles with flows that separate, flows where free shear is present, and flows where the amount of turbulence rapidly decays or increases (i.e. entrance/exit regions) (Bardina, 1997; Bakker, 2005). As such, the model is not of a great deal of use for the present modeling of the VHTR core considering the need to resolve the entrance effects.

The Reynolds Stress turbulence model has not been studied in detail in this work, due to issues with incompatibility with the current system in STAR-CCM+. This model is studied as an application to a system that is highly similar to one by investigated by Pointer and Thomas (2010). They found that the wall layer treatment in this model predicted a higher thermal resistance in the boundary later than the other models, causing much higher temperatures in the solid, and thus discarded this model as solution for this simulation. It is a significantly more complex model that uses seven equations instead of two to resolve turbulence in the flow. As such, this model is much more suited for modeling highly complex flows (swirling, rotation, separation), but incurs a high cost in computational requirements.

References

Alfonsi, G., 2009, Reynolds-Averaged Navier-Stokes Equations for Turbulence Modeling, *Applied Mechanics Reviews*, Vol. 62, pp. 1-20.

Bakker, A., 2005, Turbulence Models, *Applied Computational Fluid Dynamics*, Lecture 10, URL: www.bakker.org, 2005, Accessed June 2011.

Bardina, J. E., Huang, P. G., Coakley, T. J. 1997,Turbulence Modeling Validation, Testing, and Development, NASA Tech. Memo. 110446, Ames Research Center.

Beck, J. M., Garcia, C. B., Pincock, L. F., 2010, High Temperature Gas-Cooled Reactors Lessons Learned Applicable to the Next Generation Nuclear Plant, Idaho National Laboratory Report INL/EXT-10-19329.

Becker, S., Laurien E., 2003, Three-dimensional numerical simulation of flow and heat transport in high-temperature nuclear reactors, *Nuclear Engineering and Design*, Volume 222, Issues 2–3, pp. 189-201.

Carbajo, J., Qualls, A., and McDuffee, J., 2008, Comparison of RELAP5-3-D/ATHENA And ANSYS/FLOTRAN Thermal-Hydraulic Results, American Nuclear Society: 2008 Annual Meeting "Nuclear Science and Technology: Now Arriving on Main Street," June 8–12, 2008, Anaheim, California. *Trans. Am. Nucl. Soc*., vol. 98, pp. 457–459.

CD-adapco, (2010-2012), STAR-CCM+ Releases 5.04, 6.02, 6.04, 7.04 (user's manual), URL: http://www.cd-adapco.com/products/star_ccm_plus/.

Copinger, D.A., Moses, D.L., 2004, Fort Saint Vrain Gas Cooled Reactor Operational Experience. Oak Ridge National Laboratory Report ORNL/TM-2003/223.

Dittus, F. W. and Boelter, L. M. K., 1930, Heat Transfer in Automobile Radiators of Tubular Type, *University of California – Berkeley Publications in Engineering*, vol. 2, pp. 443 - 461.

El-Genk M. S. and Tournier, J.-M., 2008, Noble Gas Binary Mixtures for Gas-Cooled Reactor Power Plants, *J. Nuclear Engineering and Design*, vol. 238, pp. 1353 – 1372.

El-Genk, M. S. and Tournier, J.-M., 2009, Performance Analyses of VHTR Plants with Direct and Indirect Closed Brayton Cycles, *Progress in Nuclear Energy*, vol. 51, pp. 526 – 542.

El-Genk, M. S. and Tournier, J.-M., 2010, Effects of Working Fluid and Shaft Rotation Speed on the Performance of HTR Plants and the Size of CBC Turbo-Machine, *J. Nuclear Engineering and Design*, vol. 239, pp. 1811 – 1827.

Elder, R, Allen, R., 2009, Nuclear heat for hydrogen production: Coupling a very high/high temperature reactor to a hydrogen production plant, *Progress in Nuclear Energy*, vol. 51, pp. 500-525.

Fujimoto, N., Fujikawa, S., Hayashi, H., Nakazawa, T., Iyoku, T., Kawasaki, K., 2004, Present Status of HTTR Project – Achievement of 950 ° C of reactor outlet coolant temperature, *Proceedings of the 2nd International Topical Meeting on High Temperature Reactor Technology,* Beijing, China, September 22-24, 2004, Paper # A07.

General Atomics, 1996, Gas Turbine-Modular Helium Reactor (GT-MHR) Conceptual Design Description Report, General Atomics Report GA-910720, San Diego, CA.

Huang, Z., Wang, J. and Li, J., 2004, Study on the Thermodynamic Cycle of HTR-10GT, *Proceedings of the 2nd International Topical Meeting on High Temperature Reactor Technology (HTR2004)*, Beijing, China, September 22 – 24, 2004, Paper # D01.

IAEA, 2001, Current Status and Future Development of Modular High Temperature Gas Cooled Reactor Technology, Technical Report: IAEA-TECDOC-1198, International Atomic Energy Agency, Vienna, Austria,.

IAEA, 2006, Thermophysical Properties Database of Materials for Light Water Reactors and Heavy Water Reactors, Technical Report: IAEA-TECDOC-1496, International Atomic Energy Agency, Vienna, Austria.

Idaho National Laboratory, 2011a, Basis for NGNP Reactor Design Down-Selection, INL report INL/EXT-10-19565.

Idaho National Laboratory, 2011b, NGNP Project, 2011 Status and Path Forward, INL report INL/EXT-11-23907.

Idaho National Laboratory, 2012, RELAP5-3D Manuals, URL: http://www.inel.gov/relap5/r5manuals.htm, last accessed November 2012.

Ishiyama, S, T.D. Burchell, J.P. Strizak and M. Eto., 1996, The Effect of High Fluence Neutron Irradiation on the Properties of Fine-Grained Isotropic Nuclear Graphite, *Journal of Nuclear Materials*, vol. 230, pp. 1-7.

Johnson, G.A., 2008, Power conversion system evaluation for the next generation nuclear plant (NGNP), *Proc. International Congress on Advances in Nuclear Power Plants (ICAPP 08)*, Anaheim, CA, 8–12 June 2008, Paper # 8253, American Nuclear Society.

Johnson, R. W., 2009, CFD Investigation of Experimental Data Proposed to be a Validation Data Set, in *Proceedings ICONE #17*, Brussels, Belgium, June 12-16, 2009, paper # 75604,.

Jones, W. P., and Launder, B. E., 1972, The Prediction of Laminarization with a Two-Equation Model of Turbulence, *International Journal of Heat and Mass Transfer*, vol. 15, pp. 301-314.

Kiryushin, A. I., Kodochigov, N. G., Kouzavkov, N. G., Ponomarev-Stepnoi, N. N., Gloushkov, E. S. and Grebennik, V. N., 1997, Project of the GT-MHR High-Temperature Helium Reactor with Gas Turbine, *J. Nuclear Engineering and Design*, vol. 173, pp. 119 - 129.

LaBar, M. P., Shenoy, A. S., Simon, W. A. and Campbell, E. M., 2004, The Gas-Turbine Modular Helium Reactor, *J. Nuclear Future*, vol. 43, pp. 165 – 175.

Launder, B. E., and Sharma, B. I., 1974, Application of the Energy Dissipation Model of Turbulence to the Calculation of Flow Near a Spinning Disc, *Letters in Heat and Mass Transfer*, vol. 1, pp. 131-138.

Lee, C. H., Zhong, Z., Taiwo, T. A., Yang, W. S., Smith, M. A. and Palmiotti, G., 2006, Status of Reactor Physics Activities on Cross Section Generation and Functionalization for the Prismatic Very High Temperature Reactor, and Development of Spatially-Heterogeneous Codes, Technical Report: ANL-GenIV-075, Argonne National Laboratory, Chicago, IL.

Leung, S and Dooley, N., 2002, Effective Thermal Conductivity of Composite Solids, URL: http://www.owlnet.rice.edu/~ceng402/proj02/sleung/finalproject.htm, Accessed Sept 2010.

Lien, L.S., Kalitzin, G., 1998, and Durbin, P. A., RANS modeling for compressible and transitional flows, *Center for Turbulence Research - Proceedings of the Summer Program*.

MacDonald, P.E., Sterbentz, J.W., Sant, R.L., Bayless, P.D., Schultz, R.R., Gougar, H.D., Moore, R.L., Ougouag, A.M. and Terry, W.K., 2003, NGNP Preliminary Point Design – Results of Initial Neutronics and Thermal-Hydraulic Assessments during FY-03, Technical Report: INEEL/EXT-03-00870 Rev. 1, Idaho National Engineering and Environmental Laboratory.

MacDonald, P.E., Bayless, P.D., Gougar, H.D., Moore, R.L., Ougouag, A.M., Sant, R. L., Sterbentz, J.W., and Terry, W. K., 2004, The Next Generation Nuclear Plant – Insights Gained from the INEEL Point Design Studies, *Proceedings ICAPP '04* Pittsburgh, PA, June 13-17, 2004, Paper # 4305.

Matzner, D., 2004, PBMR Project Status and the Way Ahead, 2nd International Topical Meeting on High Temperature Reactor Technology, Beijing, China, September 22-24, 2004, Paper #A04,.

McEligot, D. M., Magee, P. M. and Leppert, G., 1965, Effect of Large Temperature Gradient on Convective Heat Transfer: the Downstream Region, *J. Heat Transfer*, vol. 87, pp. 67 – 76.

Menter, F. R., 1994a, Two-Equation Eddy Viscosity Turbulence Models for Engineering Applications, *AIAA J.*, vol. 32, pp. 1299-1310.

Menter, F. R., and Rumsey, L. C., 1994b, Assessment of Two-Equation Turbulence Models for Transonic Flows, 25th AIAA Fluid Dynamics Conference, Colorado Springs, Colo., June 20-23, 1994, AIAA Paper 94-2343.

Minshall, P.C., Wickham, A.J., 2001, The Description of Wigner Energy and its Release From Windscale Pile Graphite for Application to Waste Packaging and Disposal, *Proceedings of IAEA Technical committee meeting on nuclear graphite waste management*, IAEA.

Murphy, B.D., 2004, ORIGEN-ARP Cross-Section Libraries for Magnox, Advanced Gas-Cooled, and VVER Reactor Designs, Oak Ridge National Laboratory Report ORNL/TM-2003/263, pp. 2-10.

Nightingale, R. E., Yoshikawa, H.H. and Losty, H.H.W., 1962, Nuclear Graphite, Ed. R.E. Nightingale, Academic Press, New York, Chp, 6, pp. 117-194.

Pointer, W. D. and Thomas, J. W., 2010, Steady-State, Whole-Core Prismatic VHTR Simulation Including Core Bypass, *Proceedings ICAPP '10*, San Diego, CA, June 13-17, 2010 Paper # 10310, American Nuclear Society.

Sakaba, N., Kasahara, S., Onuki, K., and Kunitomi, K., 2007, Conceptual design of hydrogen production system with thermochemical water-splitting iodine-sulfur process utilizing heat from the high-temperature gas-cooled reactor HTTR, *International J. of Hydrogen Energy*, vol. 32, pp. 4160-4169.

Sato, H., Johnson, R. and Schultz, R., 2010, Computational fluid dynamic analysis of core bypass flow phenomena in a prismatic VHTR, *Annals of Nuclear Energy*, vol. 37, pp. 1172 – 1185.

Schultz, R. R., Nigg, D. W., Ougouag, A. M., Terry, W. K., Wolf, J. R., Gougar, H. D., Johnson, G. W., McEligot, D. M., McGreery, G. E., Johnson, R. W., Sterbentz, J. W., MacDonald, P. E., Taiwo, T. A., Wei, T. Y. C., Yang, W. S., Vilim, R. B., Pointer, W. D. and Khalil, H. S., 2004, *Next Generation Nuclear Plant-Design Methods Development and Validation Research and Development Program Plan,* Technical Report: INEEL/EXT-04-02293 Rev. 0, Idaho National Engineering and Environmental Laboratory.

Schultz, R. R., Kim, M-H., Vilim, R., Park, C. G., and Hassan, Y., 2012, Experimental and Analytic Study on the Core Bypass Flow in a Very High Temperature Reactor, Idaho National Laboratory report INL/EXT-12-24603.

Seider, E. N. and Tate, G. E., 1936, Heat Transfer and Pressure Drop of Liquids in Tubes, *Ind. Eng. Chem.*, vol. 28, pp. 1429 - 1435.

Shih, T.-H., Liou, W.W., Shabbir, A., Yang, Z. and Zhu, J., 1994, A New *k*- Eddy Viscosity Model for High Reynolds Number Turbulent Flows -Model Development and Validation, NASA TM 106721.

Shiozawa, S., S. Fujikawa, T. Iyoku, K. Kunitomi and Y. Tachibana., 2004, Overview of HTTR Design Features, *Nuclear Engineering and Design*, vol. 233, pp. 11 – 21.

Solidworks, 2006, Solidworks version SP 4.1, URL: www.solidworks.com/.

Southworth, F. H., MacDonald, P. E., Harrell, D. J., Shaber, E. L., Park, C. V., Holbrook, M. R., and Petti, D. A., 2003, The Next Generation Nuclear Power Plant (NGNP) Project, INEEL/CON-03-01150.

Spalart, P. R., and Allmaras, S. R., 1992, A One-Equation Turbulence Model for Aerodynamic Flows, AIAA 30nd Aerospace Sciences Meeting & Exhibit, Reno, NV, 1992, AIAA Paper 92-0439.

Tak, N. I., Kim, M. H. and Lim, H. S., 2008, Numerical Investigation of a Heat Transfer within the Prismatic Fuel Assembly of a Very High Temperature Reactor, *Annals Nuclear Energy*, vol. 35, pp. 1892 - 1899.

Tak, N. I., Kim, M. H. and Lim, H. S., 2010, A Practical Method for Thermal Analysis and Design of Prismatic Fuel Blocks, in *Proceedings ICAPP '10*, San Diego, CA, June 13-17, 2010, paper # 10362, American Nuclear Society.

Taylor, M. F., 1967, Correlation of Local Heat-Transfer Coefficients for Single-Phase Turbulent Flow of Hydrogen in Tubes with Temperature Ratios to 23, Technical Report: TN D-4332, NASA Lewis Research Center, Cleveland, Ohio.

Tournier, J.-M., P. and El-Genk, M. S., 2008, Properties of Helium Nitrogen and He-N_2 Binary Gas Mixtures, *J. Thermophysics and Heat Transfer*, vol. 22, pp. 442 – 456.

Tournier, J.-M., P., and El-Genk, M. S., 2009, Axial Flow, Multi-Stage Turbine and Compressor Models, *Energy Conversion and Management*, vol. 51, pp. 16 – 29.

Travis, B.W. and El-Genk, M.S., 2012, Numerical simulation and turbulent convection heat transfer correlation for coolant channels in a VHTR, *J. Heat Transfer Engineering,* vol. 34, pp. 1-14.

Wilcox, D. C., 1993, Turbulence Modeling for CFD, DCW Industries, Inc., La Cafiada, California.

Zhang, Z. and Yu, S., 2002, Future HTGR Developments in China after the Criticality of the HTR-10, *Nuclear Engineering and Design,* vol. 218, pp. 249–257.

Zhang, Z., Wu, Z., Sun, Y., 2006, and Li, F., Design aspects of the Chinese modular high-temperature gas-cooled reactor HTR-PM, *Nuclear Engineering and Design*, vol. 236, pp. 485–490.

Zhu S., Tang Y., Xiao K., and Zhang Z., 2008, Coupling of Modular High-Temperature Gas-Cooled Reactor with Supercritical Rankine Cycle, *Science and Technology of Nuclear Installations*, vol. 2008.